Faculdade de Engenharia da Universidade do Porto
Mestrado Integrado em Bioengenharia

Biomechanical Study of Age-related Changes of the Pelvic Floor Ligaments

by

Rita Luísa Rocha Martins

Master's Dissertation

Preliminary Version

Supervisor:
Pedro Alexandre Lopes de Sousa Martins
Post Doctoral Researcher at IDMEC - Pólo FEUP

Co-Supervisor:
Renato Manuel Natal Jorge
Associate Professor, Faculty of Engineering, University of Porto

July 2014

A todos os P's da minha vida.

"Só é difícil para quem não sabe.
E só não sabe quem não quer saber."

José Rocha

Agradecimentos

Não poderia terminar o meu mestrado sem deixar uma última palavra de agradecimento a quem para aqui me direccionou, a quem por aqui me guiou e a quem permitiu que chegasse (inteira) ao final da estrada.

Começando pelo fim, quero agradecer ao meu orientador, Pedro Martins, por toda a orientação e esforço que tornaram este trabalho possível e, acima de tudo, desafiante. Ao meu co-orientador, Professor Doutor Renato Natal, toda a disponibilidade e ajuda durante estes últimos meses. À delegação Norte do Instituto Nacional de Medicina Legal, I. P., por disponibilizar os meios necessários à realização deste trabalho. Quero também agraceder ao Instituto de Engenharia Mecânica (IDMEC) pelas instalações e pela forma carinhosa como me receberam.

Aos meus amigos, aqueles com quem pude sempre contar, quero dizer, do fundo do meu coração, Obrigada! Por todos os momentos que tornaram este percurso mais fácil e divertido, por todos os momentos que o tornaram tão único e especial. Aos rapazes que nada fazem e às meninas que fazem tudo. Às biológicas, às biomédicas, às "INESCAS", às do "DEQ" e aos biotecos, o meu mais sincero Obrigada, sem vocês não teria sido a mesma coisa!

Ao Paulo, obrigada por mudares a minha vida! Por todo o apoio e desapoio que tão bem sabes distinguir e por nunca teres desistido, mesmo quando eu já não acreditava. Obrigada por me conheceres tão bem ou melhor que eu.

E, finalmente, à minha família. Todos, desde o mais pequeno ao mais sábio. À Alice, pelo seu sorriso que me ilumina de força, ao meu irmão Pedro e à Ana pela lufada de ar fresco que trazem sempre. À minha prima Inês, companheira de vida e viagem, à Raquel, que é como se fosse da família. Aos meus primos Rodrigo, Ricardo, Rafael, João, Tico, Joana, Teresa, Miguel, Nuno, Marta e Clara, pelas nossas aventuras. À Luna, Magali, Farrusco e especialmente ao Tobias, por todos os passeios para desanuviar e parvoíces. Aos meus tios Nuno, Dadinha, Gi, Romeu, Zé, Tó, Né e Novais, pela música, doces, cinemas, festas e bolos. Aos avós Zéquita e Olguinha, Rosa e Quim por serem a minha inspiração e o meu orgulho. E finalmente, à minha mãe e ao meu pai, por serem as pessoas mais fortes que conheço, por ultrapassarem tudo e me desafiarem constantemente para chegar onde cheguei. Obrigada pela vossa exigência e pelo vosso carinho incondicional que juntos fizeram de mim aquilo que sou e fizeram querer ser sempre mais.

Abstract

The pelvic floor is the lower closure of the abdominal cavity with the functionality to support visceral organs and maintain their proper physiology. Pelvic floor disorders are common health issues among aging women. The process of aging affects the pelvic ligaments, compromising these structures, responsible for the maintenance of pelvic support. The collagen content and conformation may change, jeopardizing the ligaments' strength. A weakened ligament can lead to urinary incontinence or pelvic organ prolapse, whose common treatments are corrective surgeries.

Through the years, the knowledge about mechanical properties of tissues has been increasing, allowing to know the materials' behavior when submitted to specific loading conditions. Constitutive equations are responsible to mathematically describe these behaviors.

The aim of this study was to understand the mechanical changes that the round and uterosacral ligaments of the pelvic floor undergo through the aging process, and to propose a material model with age-influenced parameters, to describe those changes.

The ligaments studied revealed a dissimilar age-affected behavior. While the round ligament tensile strength and tangent modulus increased as age progresses, the uterosacral ligament mechanical properties did not show significant differences. In accordance with other studies (Rivaux et al., 2013; Martins et al., 2013), a higher rigidity was observed for the uterosacral ligament, which implies its importance in the pelvic floor maintenance.

Using Weiss modified material model, proposed by Martins et al. (2010), it was possible to mimic these tissues' behavior under uniaxial longitudinal tensile stress, using an optimization (Martins et al., 2010) and a manual process. Both processes were suitable for material parameters' estimation.

It was possible to establish a relationship between the material parameters obtained and aging for the round ligament, in accordance with the mechanical properties. The uterosacral ligament specimens demonstrated inherent material constants that did not change with age.

These knowledges allowed a better understanding of the influence of age in the pelvic support. An improvement of the parameters' estimation process, for Weiss modified material model, enabled accurate simulations of these ligaments' behavior under tension. Using the mechanical models and the optimization strategies proposed, future simulations could help the prediction of pelvic floor disorders.

Contents

List of Figures

List of Tables

Nomenclature

α_i	Dimensionless constants of the strain-energy function
$\boldsymbol{\chi}$	Motion of a body $\mathcal{B}$
$\boldsymbol{\lambda}_{\mathbf{a}_0}$	Stretch vector
$\boldsymbol{\sigma}$	Cauchy stress tensor
ϵ	Normalized mean square root error
λ	Stretch ratio
$\lambda^{ultimate}$	Ultimate stretch
λ_i	Principal stretches or experimental stretch
$\mathbb{E}^3$	Euclidean space
$\mathcal{B}$	A body
P	Particle of a body $\mathcal{B}$
X, x	Points of the reference Ω_0 and deformed Ω configurations, respectively, of the body $\mathcal{B}$
μ	Shear modulus
Ω	Deformed configuration of a body $\mathcal{B}$
Ω_0	Reference configuration of a body $\mathcal{B}$
Ψ	Strain-energy function
σ^{max}	Maximum stress or Tensile strength
σ^{yield}	Yield strength
σ_i	Experimental stress
$\mathbf{m}$	Fiber direction on the deformed configuration
$\mathbf{m}_0$	Fiber direction on the reference configuration
ε	Material deformation or engineering strain
$\varepsilon^{ultimate}$	Ultimate strain

ε_i	Experimental strain at time t_i
A_i	Cross-sectional area at time t_i
d	Displacement
E_S	Secant modulus or S modulus
E_T	Tangent modulus or T modulus
I_i	Principal invariants of the Cauchy-Green tensor
J	Jacobian determinant
l	Current length
l_0	Initial length
$O(\vec{C})$	Objective function
p, q	Lagrange multipliers
Q	Function of the components of the right Cauchy-Green tensor
R^2	Correlation coefficient
O	Origin of the coordinate system
$\mathbf{b}$	Left Cauchy-Green tensor
$\mathbf{C}$	Right Cauchy-Green tensor
$\mathbf{E}$	Green-Lagrange strain tensor
$\mathbf{e}$	Eulerian or Almansi strain tensor
$\mathbf{F}$	Deformation gradient
$\mathbf{I}$	Second-order unit tensor or identity
$\mathbf{P}$	First Piola-Kirchhoff stress tensor
$\mathbf{S}$	Second Piola-Kirchhoff stress tensor
$\mathbf{T}$	First Piola-Kirchhoff traction vector
$\mathbf{t}$	Cauchy traction vector
$\mathbf{u}$	Displacement vector
$\mathbf{X}$, $\mathbf{x}$	Position vectors of X and x

Chapter 1

Introduction

Female pelvic floor (Figure 1.1) is a complex unit involved in multiple functions that extend beyond the sole support of pelvic organs. The pelvic floor musculature has two major functions: to provide support or act as a floor for the abdominal viscera, including the rectum, and to provide a constrictor or continence mechanism to the urethral, anal, and vaginal orifices (in females). Pelvic floor consists of several muscles, all fundamental for the support and function of female pelvic structures (Mannella et al., 2013).

Pelvic connective tissues are structured into a fascial sheet which covers the pelvic floor muscles and forms ligaments, connecting pelvic organs to the bony pelvis. During evolution, human female pelvis has undergone significant enlargement and structural changes to allow the delivery of fetuses with increasing head diameters, upright standing and walking. Thus, connections of fascial structures to the pelvic sidewalls have progressively grown, suggesting a central role in the stabilization of the pelvic viscera of connective tissue (Chen, 2007; Mannella et al., 2013).

As it has been mentioned in several studies (Ashton-Miller and DeLancey, 2007; Woodfield et al., 2010; Mannella et al., 2013), failure of one of the functional and structural elements of the pelvic floor complex, e.g. the levator ani muscles, results in increased mechanical load on other components (connective tissue and smooth muscle), which will eventually fail, as well. On the other side, connective tissue abnormalities and smooth muscle alterations may represent the leading event in the development of prolapse, or other pathologies (Mannella et al., 2013).

Pelvic floor disorders include urinary incontinence, pelvic organ prolapse (POP), fecal incontinence, and other sensory and emptying abnormalities of the lower urinary and gastrointestinal

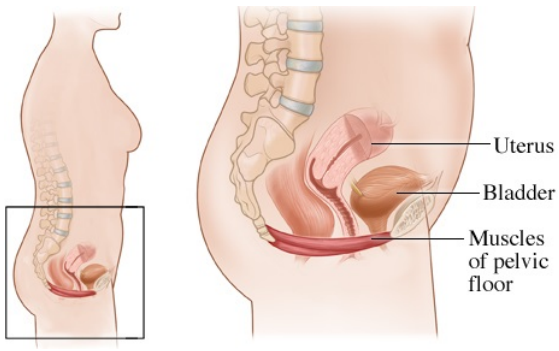

Figure 1.1: Female pelvic cavity.

tracts (MacLennan et al., 2000; Nygaard et al., 2008; Mannella et al., 2013). These pathologies affect a substantial proportion of women and increase with age (Strohbehn, 1998; Berman et al., 2000; Chen, 2007; Nygaard et al., 2008; de Araujo et al., 2009; Woodfield et al., 2010). Urinary incontinence affects between 17% and 45% of adult women and it is estimated that 0.4% to 17% of adult ambulatory women are faecally incontinent with an increasing prevalence with advancing age. Similarly, POP is a common condition accounting for about 20% of major gynecological surgery in developed countries (MacLennan et al., 2000).

Therefore, pelvic floor laxity depends on muscle injury and progressive pelvic floor weakening as a result of connective tissue degradation, pelvic denervation and devascularization and anatomic modifications. All of this determines a decline in mechanical strength and a dyssynergy of pelvic floor function, predisposing to prolapse (Mannella et al., 2013).

Aging is an universal, decremental and intrinsic process which should be considered innate to our genetic design, not pathological. The rate of aging is highly individual and depends on many factors including genetics, lifestyle and former disease processes (Kannus et al., 2005). Changes of body composition are common features of aging (Liu et al., 2013) and various functions of the body gradually deteriorate (Kannus et al., 2005). It has been shown that aging induces structural changes to capsular, fascial and ligamentous structures, mainly to the elastic and collagen fibers (Barros et al., 2002).

Because of the high prevalence of pelvic floor disorders in women, an understanding of the complex anatomy responsible for maintaining normal support is important (Strohbehn, 1998). Given that, with aging, connective tissues and fascia of the pelvic floor may lose strength (Goepel, 2008), there is a need to fully realize the mechanical changes that the pelvic floor ligaments undergo in the female life span.

The quantification and measurement of the relevant health variables has become a more important activity and the modeling and simulation of the physiological processes and healing strategies have become widespread activities in health related research.(Woo et al., 1999). Models have been found to be the best tools for the analysis of physical and mechanical problems associated with biological structures. These models can characterize the biomechanical behavior of the tissues by means of constitutive laws (Cowin and Doty, 2007).

The lack of information regarding the pelvic floor ligaments age-related changes makes this an important subject of study. Therefore, the aim of this work is to understand the changes in the mechanical behavior of pelvic floor ligaments (round and uterosacral) with aging and to model those changes by optimizing the constitutive laws' parameters.

Chapter 2

State of the Art

2.1 Pelvic Floor

2.1.1 Introduction

The pelvic floor is a complex inter-related structure of muscles, ligaments and fascia with multiple functions. These functions concern support of visceral organs, maintaining continence, facilitating micturition and evacuation as well as forming part of the birth canal (Strohbehn, 1998; Stoker, 2009; Petros, 2010; Scheiner et al., 2010; Santoro et al., 2010; Orlandi and Ferlosio, 2014). This multi functional unit has connections to the bony pelvis, to organs and to the extensive fibro-elastic network in the fat-containing anatomical spaces (Stoker, 2009; Orlandi and Ferlosio, 2014).

The pelvic floor as the lower closure of the abdominal cavity has to withstand the abdominal pressure (Scheiner et al., 2010). Pregnancy and vaginal delivery damage the pelvic floor directly, chronic stress like cough, heavy lifting, or obesity leads to a chronic overstraining of the pelvic floor. Aging, structural changes, and possibly estrogen deficiency have also a negative impact on its structures (Scheiner et al., 2010).

Although there is good anatomical knowledge of the region, the neurological and biomechanical functions of the pelvic floor are not well understood and knowledge of these is continuously evolving. Consequently, correct assessment of pelvic floor anatomy is essential to understand the pathogenesis and surgical correction of pelvic disturbances (Orlandi and Ferlosio, 2014).

2.1.2 Anatomy

This chapter contextualizes the pelvic cavity and was based on the work of Standring (2008) and Drake et al. (2009).

2.1.2.1 Pelvis

The bones of the pelvis consist of the right and left pelvic bones (hips), the sacrum, and the coccyx. Each pelvic bone is formed by three elements: the ilium, pubis and ischium (Herschorn, 2004). The lumbosacral joints are reinforced by strong ligaments: the iliolumbar and the lumbosacral ligaments. The sacro-iliac joints transmit forces from the lower limbs to the vertebral column. The joint surfaces have an irregular contour and interlock to resist movement. Each sacro iliac joint is stabilized by three ligaments:

- anterior sacro-iliac ligament, which is a thickening of the fibrous membrane of the joint capsule, and runs anteriorly and inferiorly to the joint.
- interosseous sacro-iliac ligament, which is the largest, strongest ligament of the three, is positioned immediately posterosuperior to the joint and attaches to adjacent expansive roughened areas on the ilium and sacrum, thereby filling the gap between the two bones
- posterior sacro-iliac ligament, which covers the interosseous sacro-iliac ligament.

The pubic symphysis lies anteriorly between the adjacent surfaces of the pubic bones. The joint is surrounded by interwoven layers of collagen fibers and the two major ligaments associated with it are superior and inferior pubic ligament.

2.1.2.2 True pelvis

The true pelvis is a bowl-shaped structure formed by the pelvic bones, the ligaments which interconnect these bones and the muscles which line their inner surfaces. It has an inlet, a wall, and an outlet (Figure 2.1). The inlet is open, whereas the pelvic floor closes the outlet and separates the pelvic cavity (above) from the perineum (below).

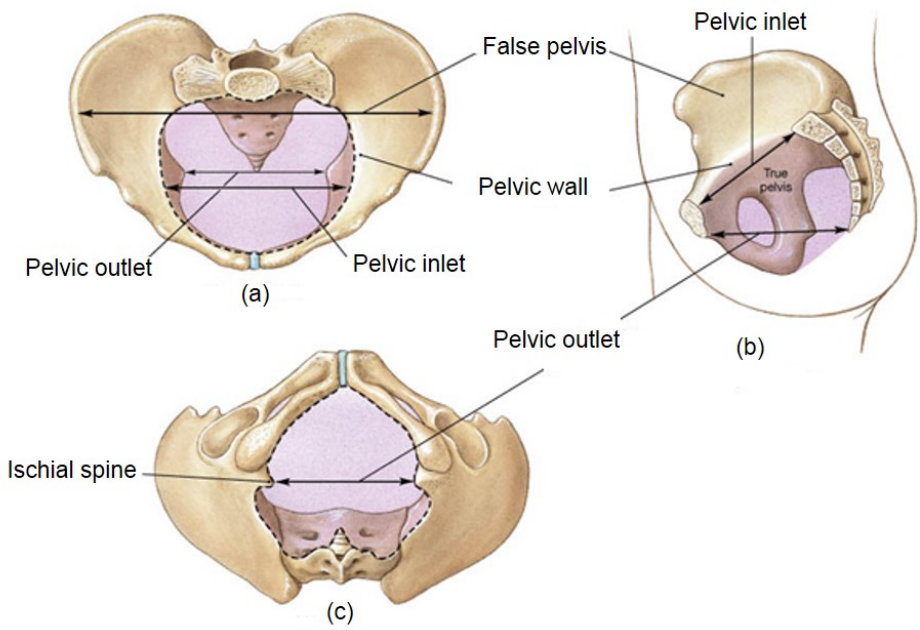

Figure 2.1: Division of the true pelvis. a) Superior view. b) Lateral view. c) Inferior view. Adapted from Droual.

The pelvis has two basins: the major (or greater) pelvis and the minor (or lesser) pelvis. The abdominal viscera occupies the major pelvis; the minor pelvis is the narrower continuation of the major pelvis inferiorly. The female pelvis has a wider diameter and a more circular shape than the male (Herschorn, 2004). Numerous projections and contours provide attachment sites for ligaments, muscles, and fascial layers.

Pelvic inlet

The pelvic inlet is the circular opening between the abdominal cavity and the pelvic cavity through which structures traverse. It is completely surrounded by bones and joints. A wider inlet facilitates head engagement and parturition (Herschorn, 2004).

Pelvic wall

The walls of the pelvis consist of the sacrum, the coccyx, the pelvic bones inferior to the linea terminalis (oblique line on the medial surface of the bone), two ligaments, and two muscles. The pelvic organs rely on their connective tissue attachments to the pelvic walls, and support from the levator ani muscles that are under neuronal control from the peripheral and central nervous systems (Santoro et al., 2010). The pelvic viscera include parts of the gastrointestinal system, the urinary system and the reproductive system.

Ligaments

The sacrospinous and sacrotuberous ligaments are major components of the lateral pelvic walls that help define the apertures between the pelvic cavity and adjacent regions through which structures pass. The smaller of the two, the sacrospinous ligament lies inferiorly to the sacrotuberous ligament. These triangular ligaments stabilize the sacrum on the pelvic bones by resisting the upward tilting of the inferior aspect of the sacrum.

Muscles

The wall of the pelvis, as previous mentioned, consist of two muscles: the obturator internus and the piriformis. These muscles are considered as primarily muscles of the lower limb.

The obturator internus forms a large part of the anterolateral wall of the pelvic cavity. This muscle together with the piriformis is responsible for lateral rotation of the extended hip joint and abduction of flexed hip. A large part of the posterolateral wall of the pelvic cavity is formed by the piriformis.

Apertures

Each lateral pelvic wall has three major apertures through which structures pass between the pelvic cavity and other regions: the obturator canal, the greater sciatic foramen and the lesser sciatic foramen. The greater sciatic foramen is a major route of communication between the pelvic cavity and the lower limb.

Pelvic outlet

The pelvic outlet is diamond shaped, with the anterior part of the diamond defined predominantly by bone and the posterior part mainly by ligaments. In the mid line anteriorly, the boundary of the pelvic outlet is the pubic symphysis. Together, the elements on both sides form the pubic arch. A wider outlet predisposes to subsequent pelvic floor weakness (Herschorn, 2004). Terminal parts of the urinary and gastrointestinal tracts and the vagina pass through the pelvic outlet. The area enclosed by the boundaries of the pelvic outlet and below the pelvic floor is the perineum.

2.1.2.3 Pelvic floor

The pelvic floor consists of several components lying between the peritoneum and the vulvar skin (Santoro et al., 2010). Although often thought of as a single muscular layer, the pelvic floor is constituted by four principal layers: endopelvic fascia, the pelvic diaphragm (commonly referred to as levator plate), the perineal membrane (urogenital diaphragm) and the superficial transverse

perineii (from superior to inferior) (Stoker, 2009; Santoro et al., 2010).

Endopelvic fascia

The endopelvic fascia is an adventitial layer of a dense, fibrous connective tissue, covered by parietal peritoneum on top of the pelvic diaphragm and visceral structures. This fascia is important for passive support of visceral organs and has expansible properties. It has attachments to the tendinous arcs (arcus tendineus levator ani and the arcus tendineus fascia pelvis) at the pelvic side wall (Ashton-Miller and DeLancey, 2007; Stoker, 2009). The fascia extending from the cervix to the pelvic sidewall is termed by the parametrium and superiorly it forms the cardinal and uterosacral ligaments (Woodfield et al., 2010)

Pelvic diaphragm

The pelvic diaphragm is the muscular part of the pelvic floor, which serves as the principal support of the pelvic viscera as well as partition between the pelvic cavity and the perineum (Figure 2.2). The pelvic diaphragm surrounds and is pierced by the urethra, vagina, and rectum (Wester and Brubaker, 1998). Shaped like a bowl or funnel and attached superiorly to the pelvic walls, it consists of the levator ani and the coccygeus muscles. The constant muscle tone of these muscles constituted by type I striated muscle fibers prevents the ligaments from becoming overstretched and damaged by constant tension (Barber, 2005; Stoker, 2009; Woodfield et al., 2010).

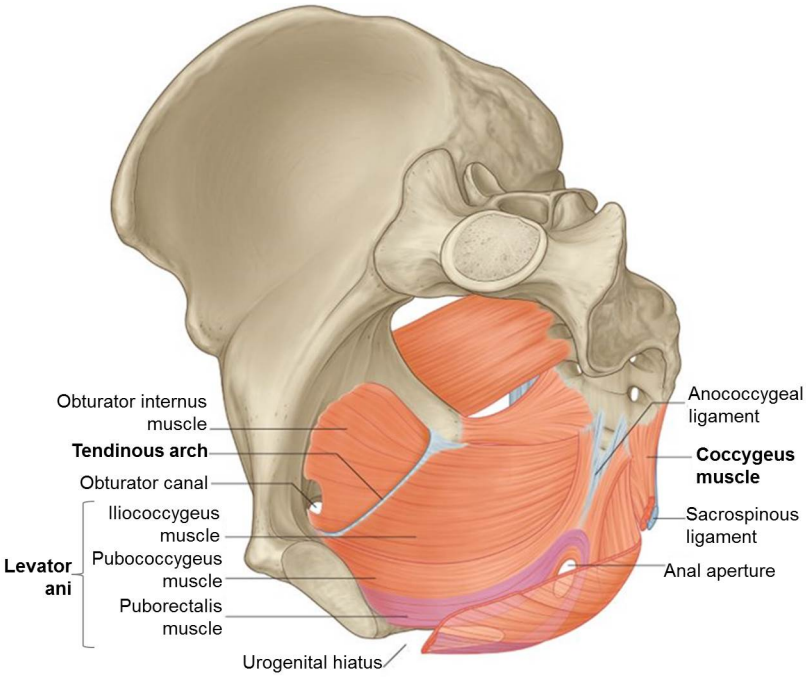

Figure 2.2: Pelvic diaphragm, lateral view. Adapted from Drake et al. (2009)

The levator ani muscle, as can be seen in Figure 2.2, is formed by the ischiococcygeus, iliococcygeus and pubococcygeus. These muscles can be identified as separate parts by their origin, direction and contribute to the formation of the pelvic floor. They play an integral role in urinary,

defecatory and sexual function (Barber, 2005). The pubococcygeus is often subdivided into separate parts according to the pelvic viscera to which they relate (puboperinealis, puboprostaticus or pubovaginalis, puboanalis, puborectalis). The last four are sometimes collectively referred to as pubovisceralis. During vaginal delivery the levator ani muscle is substantially stretched and injury may occur, often near the pubic bone insertion.

The two coccygeus muscles form the posterior part of the pelvic diaphragm, as shown in Figure 2.2. The sacrospinous ligament is at the posterior edge of the muscles and is fused with them. The proportions of the muscular and ligamentous parts may vary. The coccygeus is not part of the levator ani, having a different function: apart from supporting pelvic viscera, it pulls coccyx forward after defecation.

Perineal membrane

The perineal membrane (Figure 2.3a) is a thick fascial structure attached to the bony framework of the pubic arch (Stoker, 2009). It is related to a thin space above called the deep perineal pouch (deep perineal space), which contains a layer of skeletal muscle and various neurovascular elements and is opened above. These structures in the perineal pouch (Figure 2.3b) toguether with the parts of perineal membrane, contribute to the pelvic floor and support elements of the urogenital system in the pelvic cavity, even though the perineal membrane and deep perineal pouch are usually considered parts of the perineum. The perineal membrane and adjacent pubic arch provide attachment for the roots of the external genitalia and the muscles associated with them.

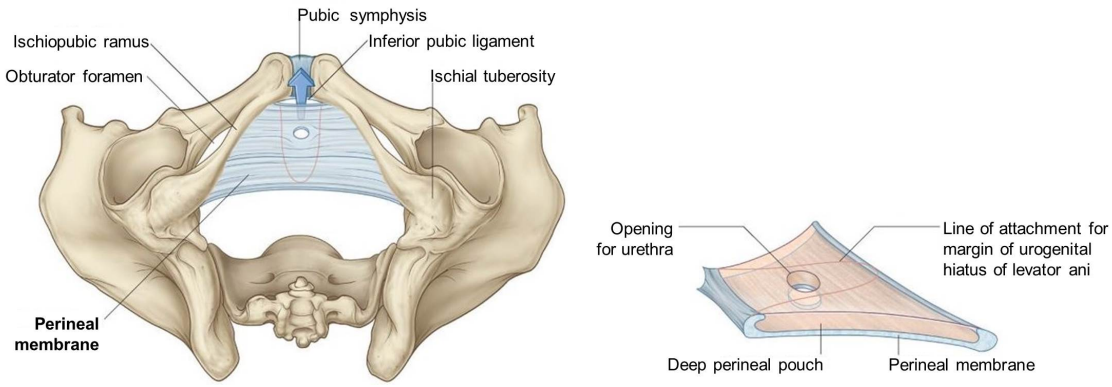

(a) Inferior view **(b)** Superolateral view

Figure 2.3: Perineal membrane and deep perioneal pouch. Adapted from Drake et al. (2009)

The perineal body is an important connective tissue structure into which muscles of the pelvic floor and the perineum attach. In men, this structure is a central point sometimes named the central perineal tendon. In women, the imbrication of the muscle fibers is more pronounced and therefore described as the perineal body (Stoker, 2009).

Superficial transverse perineii

The superficial transverse perineii, the bulbospongiosus and the ischiocavernosus, are the external genital muscles and form the most superficial component of the pelvic floor. The superficial transverse perineii has a supportive function whereas the bulbospongiosus and the ischiocavernosus play a role in sexual function (Stoker, 2009).

2.1.2.4 Fascia

The fascia in the pelvic cavity lines the pelvic walls, surrounds the bases of the pelvic viscera, and forms sheaths around blood vessels and nerves that course medially from the pelvic walls to reach the viscera in the mid line. The pelvic fascia is a continuation of the extraperitoneal connective tissue layer found in the abdomen. It may be conveniently divided into the parietal pelvic fascia, which mainly forms the coverings of the pelvic muscles, and the visceral pelvic fascia, which forms the coverings of the pelvic viscera and their vessels and nerves.

In women (Figure 2.4a), condensations of fascia form ligaments that extend from the cervix to the anterior (pubocervical ligament), lateral (transverse cervical or cardinal ligament), and posterior (uterosacral ligament) pelvic walls. These ligaments, together with the perineal membrane, the levator ani muscles, and the perineal body, are thought to stabilize the uterus in the pelvic cavity. The most important of these ligaments are the transverse cervical (cardinal ligaments or ligaments of Mackenrodt), which extend laterally from each side of the cervix and vaginal vault to the related pelvic wall. The uterosacral ligament complex is composed by recto-uterine folds containing fibrous tissue and smooth muscle, suspending the uterus and upper vagina. It serves to maintain vaginal length and keep the vaginal axis nearly horizontal in a standing woman so that it can be supported by the levator plate (Barber, 2005).

In men (Figure 2.4b), a condensation of fascia around the anterior and lateral region of the prostate (prostatic fascia) contains and surrounds the prostatic plexus of veins and is continuous posteriorly with the rectovesical septum, which separates the posterior surface of the prostate and base of the bladder from the rectum.

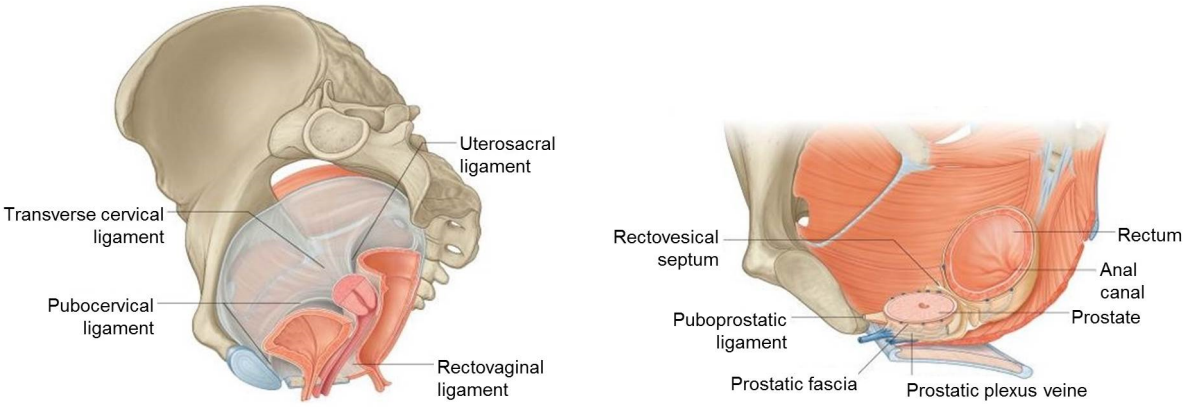

(a) In women **(b)** In men

Figure 2.4: Pelvic fascia. Adapted from Drake et al. (2009)

2.1.2.5 Peritoneum

The peritoneum of the pelvis is a continuity at the pelvic inlet with the peritoneum of the abdomen. In the pelvis, the peritoneum drapes over the pelvic viscera in the mid line, forming pouches between adjacent viscera and folds, and ligaments between viscera and pelvic walls.

The broad ligament is a sheet-like fold of peritoneum oriented in the coronal plane that runs from the lateral pelvic wall to the uterus, and encloses the uterine tube in its superior margin and suspends the ovary from its posterior aspect (Figure 2.5). The ligament of the ovary and round

ligament (Figure 2.5) of the uterus are enclosed within the parts of the broad ligament related to the ovary and uterus, respectively. The broad ligament has three parts:

- the mesometrium, the largest part of the broad ligament, which extends from the pelvic floor to the ovarian ligament and uterine body. It contains the ovarian vessels and nerves lying within the fibrous suspensory ligament of the ovary. The mesometrium also encloses the proximal part of the round ligament of the uterus, as well as smooth muscle and loose connective tissue;
- the mesosalpinx, the most superior part of the broad ligament, which suspends the uterine tube in the pelvic cavity and its attached posteroinferiorly to the mesovarium. Superior and laterally it is attached to the suspensory ligament of the ovary and medially it is attached to the ovarian ligament; and
- the mesovarium, a posterior extension of the broad ligament, which attaches to the ovary.

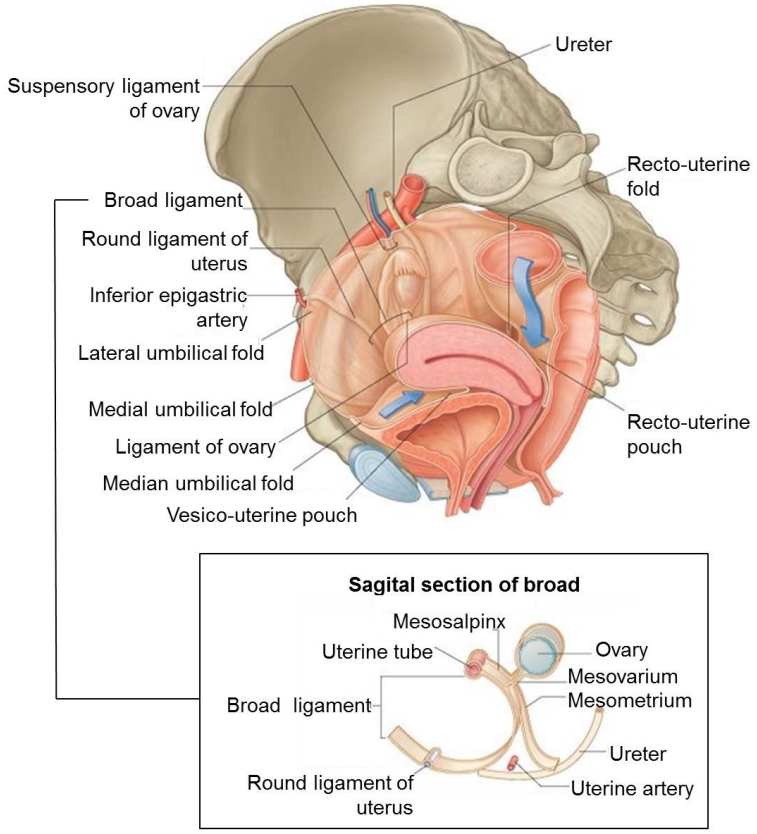

Figure 2.5: Peritoneum in the pelvis of women. Adapted from Drake et al. (2009)

The ovary ligament is a fibromuscular band of tissue, which courses medially in the margin of the mesovarium to the uterus and then continues anterolaterally as the round ligament of uterus. The round ligaments of uterus are narrow, somewhat flattened bands 10–12 cm long, which passes over the pelvic inlet. Near the uterus, the round ligament contains a considerable amount of

smooth muscle but this gradually diminishes and the terminal portion is purely fibrous. The round ligament contains blood vessels, nerves and lymphatics. Both the ligament of ovary and the round ligament of uterus are remnants of the gubernaculum, which attaches the gonad to the labioscrotal swellings in the embryo.

2.1.3 Physiology

A normal pelvic floor function can be viewed as a balanced, interrelated system composed of muscle, connective tissue and nerve components, with connective tissue being the most vulnerable to damage. The pelvic floor organs (urethra, vagina and rectum) have no inherent form, structure or strength. These are created by the synergistic action of ligaments, fascia and muscles (Petros, 2010).

Physiologically, the muscles of the pelvic floor differ from most other skeletal muscles. They demonstrate constant electrophysiologic activity except during voiding, defecation, and Valsalva maneuver. This property enables them to maintain tone, even during times of rest, providing primary support to the pelvic contents. Optimal urinary and colorectal storage and elimination depend on complex structural and functional integrity of the pelvic floor (Wester and Brubaker, 1998; Strohbehn, 1998).

The normal baseline activity of the levator ani muscle keeps the urogenital hiatus closed by compressing the vagina, urethra, and rectum against the pubic bone, the pelvic floor and organs in a cephalic direction. This constant action eliminates any opening within the pelvic floor through which prolapse could occur (Ashton-Miller and DeLancey, 2007). When voluntarily contracted, the pubovisceral and the puborectalis muscles of the levator ani pull the pelvic organs anteriorly against the pubic bone, constricting the pelvic organs closed (Wester and Brubaker, 1998; Ashton-Miller and DeLancey, 2007). By definition, the levators elevate the anus anteriorly, forming the anorectal angle that is critical in maintaining fecal continence (Wester and Brubaker, 1998; Hall, 2010). Maximal contraction of the mid and dorsal ilioccyggeus muscles elevates the central region of the posterior pelvic floor (Ashton-Miller and DeLancey, 2007). Defecation signals entering the spinal cord initiate several effects such as contraction of the abdominal wall muscles to force the fecal contents of the colon downward and at the same time cause the pelvic floor to relax downward and pull outward on the anal ring to evaginate the feces (Hall, 2010).

The levator ani muscles play an important role in protecting the pelvic connective tissues from excess load. If the ligaments and fascia within the pelvis were subjected to the continuous stress imposed on the pelvic floor by the great force of abdominal pressure, they would stretch. The constant tonic activity of the pelvic floor muscles closes the urogenital hiatus and carries the weight of the abdominal and pelvic organs, hereby preventing constant strain on the ligaments and fascia within the pelvis (Ashton-Miller and DeLancey, 2007; Hall, 2010).

The posterior vaginal wall is supported by connections between the vagina, the bony pelvis, and the levator ani muscles. As shown in Figure 2.6a, the lower one-third of the vagina (level 3) is fused with the perineal body. Its connection with the perineal membrane on either side prevents downward descent of the rectum in this region. In the mid vagina (level 2), the wall is connected to the inside of the levator ani muscles by sheets of endopelvic fascia, preventing the ventral movement of the vagina during increases in abdominal pressure. In the upper one-third (level 1), the vaginal wall is connected laterally and posteriorly by the cardinal and vaginal portion of the uterosacral ligament. In this region (Figure 2.6b) there is a single attachment to the vagina, and a separate system for the anterior vaginal walls does not exist. Therefore, when abdominal pressure forces the vaginal wall downward towards the introitus, attachments between the posterior vagina and the levator ani muscles prevent this downward movement. The lateral connections of the mid vagina hold this portion in place and prevent a mid vaginal posterior prolapse from occurring.

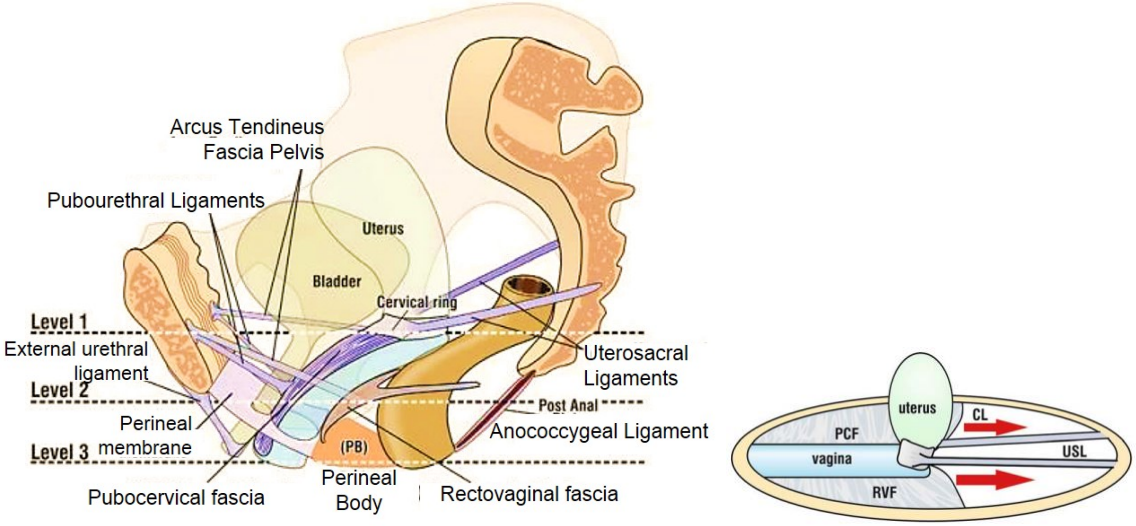

(a) Sagittal section **(b)** Level 1

Figure 2.6: Scheme of the main connective tissue structures of the pelvis. PCF= pubocervical fascia; RVF=rectivaginal fascia; CL= cardinal ligament; USL= uterosacral ligament. Adapted from Petros (2010).

The multiple connections of the perineal body to the levator ani muscles and the pelvic sidewall prevent a low posterior prolapse from descending downward through the opening of the vagina (the urogenital hiatus and the levator ani muscles) (Ashton-Miller and DeLancey, 2007).

The interaction between the pelvic floor muscles and the supportive ligaments is critical to pelvic organ support. As long as the levator ani muscles function to properly maintain closure of the genital hiatus, the ligaments and fascial structures supporting the pelvic organs are under minimal tension. The fascia simply act to stabilize the organs in their position above the levator ani muscles. When the pelvic floor muscles relax or are damaged, the pelvic floor opens and the vagina lies between the zones of high abdominal pressure and low atmospheric pressure outside the body. In this situation it must be held in place by the suspensory ligaments (Ashton-Miller and DeLancey, 2007).

2.1.4 Pathologies

As aforementioned, the main functions of the pelvic floor are to provide support of the pelvic organs and to prevent incontinence by promoting voluntary closure of the urethral and anal sphincters. Adequate pelvic floor muscle function is a necessary component for bowel and bladder control (Wester and Brubaker, 1998; Strohbehn, 1998; Rosenbaum, 2007; Chen, 2007; de Araujo et al., 2009).

Pelvic floor disorders such as pelvic organ prolapse (POP), urinary incontinence and fecal incontinence affect a large number of women (Bump and Norton, 1998; Chen, 2007; Abramowitch et al., 2009; Woodfield et al., 2010). Although, the development of these disorders is often a complex and multi factorial process. Weakness and/or tears of the structures that support the pelvic organs (i.e., the pelvic fascia, ligaments, and levator ani muscles) variably contribute to increased pelvic organ mobility, to prolapse, and, ultimately, to a variety of symptoms ranging from pelvic pain

and pressure to urinary and fecal incontinence or retention, and defecatory dysfunction. There are numerous risk factors for developing a pelvic floor disorder. Additional risk factors include but are not limited to increasing age, parity, prior pelvic surgeries, and chronic increased intra abdominal pressure (Scheiner et al., 2010; Woodfield et al., 2010).

Voluntary storage of urine and enteric contents occurs despite sudden changes in abdomino-pelvic pressures that accompany daily activities such as laughing, sneezing, coughing, positional changes, walking, bending, and standing (Strohbehn, 1998). Loss of fascial and ligamentous support to the urethra and bladder can allow urethral hypermobility and ultimately bladder prolapse, cystocele. Patients may present feelings of a vaginal bulge. Hypermobility of the urethra also frequently leads to stress urinary incontinence and kinking at the vesico-urethral junction can result in urinary retention (Woodfield et al., 2010).

Abnormalities of the pubocervical fascia, parametrium, paracolpium, or uterosacral ligaments allow mobility and descent of the uterus, cervix, or vaginal cuff, creating a sensation of vaginal bulge, and may contribute to voiding and defecatory dysfunction. (Woodfield et al., 2010). The fascia stabilizes the organs in their position above the levator ani muscles. When the pelvic floor muscles relax or are damaged, the pelvic floor opens and the vagina must be held in place by the suspensory ligaments (see Figure 2.6). Although the ligaments can sustain these loads for short periods of time, if the pelvic muscles do not close the pelvic floor, then the connective tissue will stretch and may eventually fail, resulting in pelvic organ prolapse. Furthermore, if the fibers of the vagina that connect one side with the other of the perineal membrane rupture, then the bowel may protrude downward resulting in a posterior vaginal wall prolapse. Defects in the support at the level of the perineal body most frequently occur during vaginal delivery and are the most common type of posterior vaginal wall support problem (Ashton-Miller and DeLancey, 2007; Woodfield et al., 2010).

Defects of the recto-vaginal fascia allow the descent of peritoneal contents between the vagina and rectum as well as bulging of the rectal wall, which can again create a swelling sensation, and be a cause of either fecal incontinence or obstructive defecation. Rectal bulges are also referred to as rectoceles. Atrophy or defects of the levator ani muscle can result in a pelvic diaphragm that is unable to compensate for weakened fascia and ligaments, and ultimately lead to global descent of the pelvic organs and urinary or defecatory dysfunction (Woodfield et al., 2010).

The attachment of the levator ani muscles into the perineal body is important and damage to this part of the muscle during delivery is one of the irreparable injuries to pelvic floor. It is likely that this muscular damage is an important factor associated with recurrence of pelvic organ prolapse after initial surgical repair (Ashton-Miller and DeLancey, 2007). In women with normal pelvic statics, smooth muscle fibers in the anterior vaginal wall are organized in tight bundles orientated in circular and longitudinal order. In comparison, in women with POP, the vaginal muscularity presents a decline of overall smooth muscle amount, fewer, smaller and disorganized bundles (Mannella et al., 2013).

Moreover, Liu et al. (2006) studies also raised the possibility that a failure of elastic fiber homeostasis on pelvic floor ligaments, either due to genetic predisposition or advancing age, could underlie the etiology of pelvic floor dysfunction in women. Liapis et al. (2001) and Gabriel et al. (2005) researches found a likely correlation between a severe reduction in the quantity of collagen type III of the pubocervical ligament with the development of urinary incontinence, while genital prolapse appears to have a statistically significant association with moderate reduction of collagen type III of the uterosacral ligament.

Chen (2007) concluded that the aging process plays a negative role in either function or structure of the pelvic floor in women. It may add to the deterioration of a pre-existing pelvic floor dysfunction during the lifespan of a woman or interact with other potential predisposing factors, such as parity and mode delivery, menopausal estrogen deficiency, high body mass index, previ-

ous pelvic surgery, and co morbidity including diabetes mellitus, hypertension and poor cognitive function, to cause major pelvic floor failure.

2.2 The Pelvic Ligaments

2.2.1 Histology

Ligaments are mainly constituted by fibers of type I collagen and are dense, often parallel-oriented, tissues. Generally, these tissues consist of approximately 20% cellular material and about 80% extracellular material (Woo et al., 1999; Natali et al., 2008); the extracellular material is further subdivided into about 30% solids and 70% water. These extracellular solids are collagen, the ground substance, and a small amount of elastin (Woo et al., 1999; Weiss et al., 2005). Elastin is a protein fiber extremely flexible that behaves much in the same way as rubber (Natali et al., 2008). The collagen content is generally over 75% (Woo et al., 1999) and those fibers are stiff and form the main tensile load-bearing components in the tissues. The amorphous matrix or ground substance in which fibers are embedded is a viscous gel composed of water, proteoglycans (PGs), and other glycoproteins (Weiss et al., 2005; Natali et al., 2008).

Regarding the pelvic ligaments, those are unlike the ligaments from other body regions. These are thickenings of retro-peritoneal fascia and consist primarily of blood and lymphatic vessels, nerves and fatty connective tissue (Raizada and Mittal, 2008). Extra cellular matrix (ECM) is a complex mixture of long chain proteins, including collagen, elastin and proteoglycans. It is maintained by fibroblasts (mesenchymally derived connective tissue cells) through the secretion of proteases and growth factors, which modulate the synthesis and breakdown of the structural fibers (Chen and Yeh, 2011). The ground substance consists of non-collagenous glycoproteins, proteoglycans and hyaluronan (Goepel, 2008; Kerkhof et al., 2009). In addition, these tissues contain a significant amount of smooth muscle cells. However, the quantity, type and organization of collagen, elastin and smooth muscles cells vary within the different tissues (Kerkhof et al., 2009).

Type I collagen assembles, via collagen molecules, into collagen fibrils which are long filamentous structures that aggregate to form collagen fibers (Provenzano et al., 2006). The fibrillar component is thought to contribute the most to the biomechanical behavior of these tissues. The quantity and quality of collagen and elastin are regulated through a precise equilibrium between synthesis, maturation and degradation (Kerkhof et al., 2009). Collagen I fibers are universally present and are flexible offering great resistance to tension (strength), while collagen III is predominant in tissues that require increased flexibility and distension and that are subjected to periodic stress (Kerkhof et al., 2009; Chen and Yeh, 2011). It is the primary collagen subtype in vagina and supportive tissues.

Structurally, collagen has an S shaped fibril (Figure 2.7). Once the curves are straightened out by distension, collagen acts as a rigid rod, preventing further distension. At this point, any force applied is transmitted directly. Thus, the distensibility of a tissue depends entirely on the configuration of these collagen fibrils (Petros, 2010). Furthermore, the specific orientation of collagen fibers determines the characteristic anisotropic response of soft tissue. Because collagen elements are characterized by significantly higher stiffness than ground substance, they are largely responsible for the tensile behavior of soft connective tissue. In contrast, because of the high length-thickness ratio characteristic of collagen elements, when compressive loads are applied, the behavior of the tissue is mainly determined by the ground substance and its interactions with the fibrous network (Natali et al., 2008).

An increase in collagen III and V decreases the mechanical strength of connective tissue by decreasing fiber size. It is generally agreed that a higher I/III ratio in the ligaments is indicative of greater strength, whereas a lower ratio may result in tissue laxity.

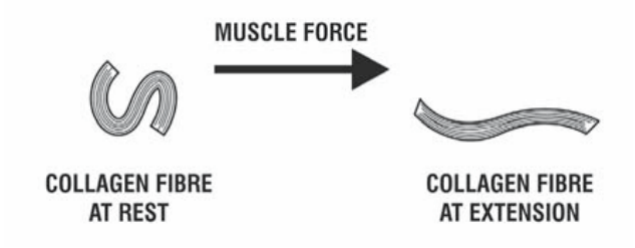

Figure 2.7: Collagen fiber at rest and during extension. From Petros (2010)

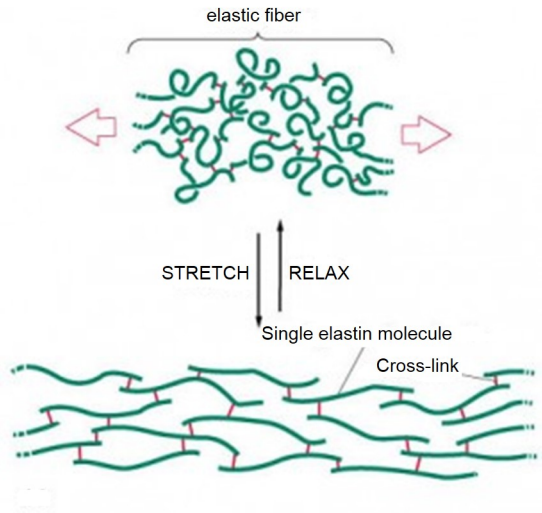

Figure 2.8: Behavior of the elastic fibers in stretch and relaxation periods. Adapted from Emily (2009).

The mechanical properties of tissues are also dependent on the proportion of elastin, an insoluble polymer that allows the tissue to stretch and return to its original shape without energy input, as represented in Figure 2.8. This property of resilience is presumed important for reproductive tissues. It accommodates the enormous expansion in pregnancy and involution after parturition (Kerkhof et al., 2009).

Kerkhof et al. (2009) found that histological changes in the connective tissue of uterine ligaments associated with pelvic relaxation include significantly decreased fibroblast content (cellularity) and an increase in collagen fibers. Connective tissue is a living structure, which undergoes remodeling in response to various factors or stress. In case of wound, ligaments are healed by collagen scarring and after the healing process they will be elongated, with lack of elasticity and strength. Although the amount of collagen within the connective tissues responsible for pelvic support appears to be increased in women with genital prolapse, this is most probably weaker type III collagen produced by genetically defective fibroblasts. This situation may be the key factor that leads to pelvic support disorders (Kökçü et al., 2002).

2.2.2 Aging phenomena

Aging affects the human body in several different ways by means of the blood, bones and skin constituents. During lifetime, all organs and muscles undergo changes that may compromise the body's health and strength. The cells become less efficient and less able to replace damaged materials and, at the same time, the tissues stiffen (Cerami et al., 1987). Therefore, the process of aging is a universal, decremental, and intrinsic process which should be considered innate to our genetic design, not pathological (Kannus et al., 2005).

Ligaments have time- and history-dependent viscoelastic properties that arise from the interaction of water with the ground substance matrix and the inherent viscoelasticity of the solid phase (Weiss et al., 2005). Therefore, the mechanical behavior of the ligaments is determined by the properties and quantity of the components and their interactions.

During maturation (up to 20 years of age) the number and quality of collagen cross-links increases, resulting in increased tensile strength of the ligaments (Woo et al., 1999). After maturation, as aging progresses, collagen reaches a plateau with respect to its mechanical properties, after which the tensile strength and stiffness of the tissue begin to decrease. The collagen content of ligaments also decreases during aging, contributing to a gradual decline in their mechanical properties (strength, stiffness, and ability to withstand deformation) (Woo et al., 1999). According to Natali et al. (2008), the main consequences of aging are reflected in a modification of the collagen conformation, with a decrease in the diameter of the collagen fibers and a change in their typical configuration (Woo et al., 1999).

In younger women, the S shaped collagen (Figure 2.7) of the pelvic ligaments easily extends. In older women, the increased inter and intramolecular cross-bonding of the collagen stiffens the S and so the tissue may shrink. Age-related loss of elastin may cause tissues to ′droop′ due to the effect of gravity realigning the collagen fibrils, as demonstrated in Figure 2.9. When the ligaments are young, the elastic fibers shrink the ligament to its original shape. When these fibers disappear with age, the ligament becomes loose and the pelvic organs drop. Though the individual collagen fibrils strengthen up to 400% with age, the total tensile strength of the urogenital tissues decreases to about 60% (Petros, 2010).

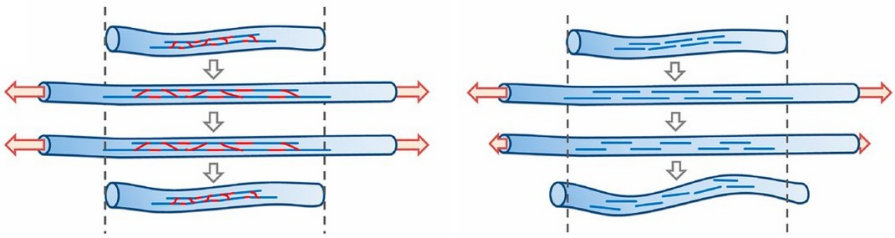

(a) Younger ligament. **(b)** Older ligament.

Figure 2.9: Behavior of younger and older ligaments when subjected to a stretch. Blue lines - collagen fibers; red lines - elastic fibers. Adapted from Münster et al. (2013).

Several studies demonstrated that significant reductions in strength and stiffness of ligament units occur with advancing age to a greater degree than expected. A summary of these studies conclusions can be consulted in Table 2.1.

Iida et al. (2002) findings suggest, as aforementioned, that aging influences the quality of the ligament, leading to a decrease in ligament strength. It appears to be due to hypertrophy of the ligaments that the ultimate load does not decrease parallel to age with some tissues. Barros et al.

Table 2.1: Review of the human ligaments' age-related changes studies.

Study	Tissue analysed	Findings
Iida et al. (2002)	Supraspinous and interspinous ligaments at L4–5 level	Significant negative correlation between age and tensile strength and elastic modulus and no correlation with ultimate load
Barros et al. (2002)	Cervical interspinous ligaments	The greater number of fragmented and degenerated elastic fibers in the dense connective tissue of the older ligaments promotes a loss of the normal compliance. Aging induces a disappearance of oxytalan fibers, which are responsible for tissue resistance
Weiss et al. (2005)	Medial collateral ligament of the knee joint	Small but significant increases in the effective modulus/dynamic stiffness of ligaments with increasing rate of loading.
Tinelli et al. (2010)	Uterosacral ligaments	Tissue denervation and devascularization, anatomic alterations, and increased degradation of collagen. A reduction in protein content and estrogens.

(2002) concluded that collagen and elastin composition or its structural arrangement is altered with age, jeopardizing tissue compliance. Tinelli et al. (2010) suggested that aging lead to a decrease in mechanical strength and predispose an individual to prolapse. The results of Weiss et al. (2005) support the conclusions of previous studies.

Differences in the strength of various pelvic ligaments were hypothesized by Martins et al. (2013) and Rivaux et al. (2013). The last one observed a non-linear stress-strain relationship and a hyperelastic mechanical behavior of the tissues. Both studies mentioned that the uterosacral ligaments were the most rigid (higher stiffness), whether at a low or high deformation, while the round ligament was more rigid than the broad ligament. Martins et al. (2013), by measuring mechanical parameters that are able to characterize a state of uniaxial tension, also referred that the uterosacral ligaments have a higher maximum stress compared to the round ligament. These results are in accordance with clinical data, as the round ligaments do not have a role in supporting the pelvic organs, whereas the uterosacral ligaments represent an important part of the pelvic support system and establishes the level one support of the cervix and the upper vagina (Figure 2.6a).

However, there is lack of information regarding the pelvic ligaments aging phenomena. As it is well known, different tissues may have different reactions to this phenomena, being extremely important to fill this gap.

2.2.3 Mechanical properties

The mechanical properties of ligaments depend strongly upon the properties of the collagen fibers, but also on the arrangement and proportion of its constituents, particularly the collagen and the elastin, as described in the previous section 2.2.1.

As aforementioned, ligaments have time- and history-dependent viscoelastic properties that arise from both the inherent viscoelasticity of the solid phase and the interaction of water with the ground substance matrix (Weiss et al., 2005; Cowin and Doty, 2007). A viscoelastic material

is characterized by hysteresis phenomenon: the loading and unloading curves do not coincide (Holzapfel, 2002). The variation of ligament stress-strain behavior with strain rate is another indicator of the viscoelastic nature of the tissue. Cowin and Doty (2007) mentioned that differences in stress relaxation and creep behavior are due to progressive recruitment of collagen fibers during creep.

Isotropic versus anisotropic behavior is a manifestation of internal symmetries in the microstructure of the material. Isotropy implies that the material response to an applied load, relative to a prescribed configuration, is independent of the direction of the loading. If this is not verified, the material is considered anisotropic which might be transversely isotropic or orthotropic. By transversely isotropic it is meant that material behavior is the same in all directions transverse (i.e., perpendicular) to a single preferred direction within the material. Orthotropic, on the other hand, implies that the material has three orthogonal preferred directions. Thus, if one applies equivalent loads in each of the three directions, each response will differ (Humphrey, 2002).

Ligaments are highly anisotropic because of their strongly unidirectionally oriented fibrous structure. Collagen provides the primary resistance to tensile loading but offers negligible resistance to compression. These tissues also offer little resistance to bending (Cowin and Doty, 2007). The simplest representation of a material anisotropy is transverse isotropy, for which the stress at a material point depends both on the deformation gradient and the fiber orientation. According to Weiss et al. (1996), this symmetry class provides an excellent framework for constitutive model development for tissues, such as ligaments.

Material inhomogeneities are present within individual ligaments. The homogeneity depends upon whether the material internal constituents are assumed to be uniform on a continuum scale. Cowin and Doty (2007) summarized that variations in collagen concentration along the ligaments' length correspond to variations in ultimate modulus, ultimate stress and strain energy density. Material inhomogeneities are believed to be especially common near the insertion sites. However, in the process of building constitutive relations for these tissues, the ligaments are considered homogeneous for mathematical simplification (Cowin and Doty, 2007).

In previous studies (Weiss et al., 1996; Martins et al., 2006, 2010), this tissues' behavior is many times represented as hyperelastic, incompressible and transversely isotropic, since it simulates the nonlinear behavior of its mechanical properties. It is common to consider the material behavior as a result of both isotropic and anisotropic components, by adding a modified tensor that characterizes the anisotropic nature of particular soft tissues (the mechanical response in the fiber direction) to the isotropic tensor.

2.3 Kinematics of a continuum

2.3.1 Introduction

Kinematics is the study of the motion and deformation of a point, body or system regardless of the cause (Holzapfel, 2002). The continuum theory implies that a body is indefinitely divisible. Therefore, one accepts the idea of an infinitesimal volume of materials referred to as a particle in the continuum, and in every neighborhood of a particle there are always neighbor particles. The continuum mechanics studies the response of materials to different loading conditions (Lai et al., 2009).

2.3.2 Motion

A certain deformable body $\mathcal{B}$ and a particle $\mathsf{P} \in \mathcal{B}$ is shown in Figure 2.10, in the three-dimensional Euclidean space $\mathbb{E}^3$ at a given instant of time t. As it moves in space from one instant of time

to another, it occupies a continuous sequence of geometrical regions denoted by Ω_0,...,Ω. At the initial time $t = t_0 = 0$, the region Ω_0 with the point X is referred to the initial configuration or reference (undeformed) configuration of $\mathcal{B}$. At this time, the point X has the position of a particle $\mathsf{P} \in \mathcal{B}$ at $t = 0$, and P may be identified by the referential position vector $\mathbf{X}$ of point X relative to the fixed origin O.

When the configuration Ω_0 moves to a new region Ω it continues occupied by the continuum body $\mathcal{B}$ at a subsequent time $t > 0$. Ω is called the current or deformed configuration in which the typical point X of the reference configuration is now related to a point x. The position vector $\mathbf{x}$ gives the coordinates of x, associated with the particle $\mathsf{P} \in \mathcal{B}$ at time t.

The map $\mathbf{X} = \boldsymbol{\kappa}_0(\mathsf{P}, t)$ is a one-to-one correspondence between $\mathsf{P} \in \mathcal{B}$ and the point $\mathbf{X} \in \Omega_0$, whereas the $\boldsymbol{\kappa}$ act on $\mathcal{B}$ to produce the region Ω at time t through the map $\mathbf{x} = \boldsymbol{\kappa}(\mathsf{P}, t)$. The position vectors of X and x are defined by $\mathbf{X} = X_A \mathbf{E}_A$ and $\mathbf{x} = x_a \mathbf{e}_a$ with $X_A, A = 1, 2, 3$ the referential coordinates and $x_a, a = 1, 2, 3$ as the current coordinates. From this point forward, the following notation will be used:

- uppercase letters are used to denote scalar, vector and tensor quantities in the reference configuration and lowercase letters are referred to quantities in the current configuration;
- zero index implies the reference configuration;
- lowercase, bold-face letters are used for vectors whereas uppercase, bold-face letters correspond to second-order tensors.

The motion of the body $\mathcal{B}$ from the reference configuration Ω_0 to the current configuration Ω can be mapped by $\boldsymbol{\chi}$, since it corresponds to the vector field that specifies the place $\mathbf{x}$ of $\mathbf{X}$ for all fixed t. The parametric Equation 2.1 determines successive positions $\mathbf{x}$ of a typical particle P in space.

$$\mathbf{x} = \boldsymbol{\chi}(\mathbf{X}, t) \quad , \qquad x_a = \chi_a(X_1, X_2, X_3, t) \tag{2.1}$$

The inverse motion $\boldsymbol{\chi}^{-1}$, for a given time t carries points located at Ω to points in the reference

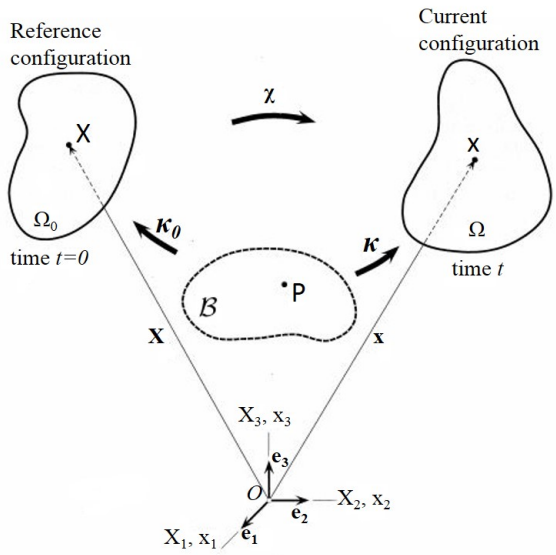

Figure 2.10: Configuration and motion of a continuum body. From Holzapfel (2002).

configuration Ω_0.

$$\mathbf{X} = \boldsymbol{\chi}^{-1}(\mathbf{x}, t) \quad , \qquad X_A = \chi_A^{-1}(x_1, x_2, x_3, t) \tag{2.2}$$

A motion $\boldsymbol{\chi}$ of a body $\mathcal{B}$ will normally change its shape, position and orientation. A shape-altered body is called deformable and the deformation $\boldsymbol{\chi}$ and inverse deformation $\boldsymbol{\chi}^{-1}$ is a motion independent of time.

2.3.3 Material and spatial derivatives

A material description regards the independent variables ($\mathbf{X}$, t) , i.e. the referential position $\mathbf{X}$ with the material coordinates $X_A, A = 1, 2, 3$, and the time t, whereas in a spatial description the independent variables are ($\mathbf{x}$, t), i.e. the current position $\mathbf{x}$ with the spatial coordinates $x_a, a = 1, 2, 3$, and the time t. To each one can be associated a motion $\boldsymbol{\chi}$ described as $\mathcal{F} = \mathcal{F}(\mathbf{X}, t)$ and $f = f(\mathbf{x}, t)$, respectively.

A material time derivative of a smooth material description $\mathcal{F}(\mathbf{X}, t)$ is described by $D\mathcal{F}(\mathbf{X}, t)/Dt$ or $\dot{\mathcal{F}}(\mathbf{X}, t)$. This is a derivative of $\mathcal{F}$ with respect to time t, holding $\mathbf{X}$ fixed.

$$\dot{\mathcal{F}}(\mathbf{X}, t) = \frac{D\mathcal{F}(\mathbf{X}, t)}{Dt} = \left(\frac{\partial \mathcal{F}(\mathbf{X}, t)}{\partial t}\right)_{\mathbf{X}} \quad , \qquad \dot{\mathcal{F}}(X_A, t) = \left(\frac{\partial \mathcal{F}(X_A, t)}{\partial t}\right)_{X_A} \tag{2.3}$$

The material gradient of a material description $\mathrm{Grad}\mathcal{F}(\mathbf{X}, t)$ can be obtained by deriving $\mathcal{F}$ relative to the referential position $\mathbf{X}$, (X_A), at a fixed time t.

$$\mathrm{Grad}\mathcal{F}(\mathbf{X}, t) = \frac{\partial \mathcal{F}(\mathbf{X}, t)}{\partial \mathbf{X}} \tag{2.4}$$

On the other hand, the spatial time derivative of a smooth spatial field $f(\mathbf{x}, t)$ is the derivative of f with respect to time t, holding the current position $\mathbf{x}$ fixed (Equation 2.5) and the spatial gradient $\mathrm{grad}f$ is the derivative of f with respect to the current position $\mathbf{x}$, (x_a), at a fixed time t (Equation 2.6).

$$f(\mathbf{x}, t) = \frac{\partial f(\mathbf{x}, t)}{\partial t} \tag{2.5}$$

$$\mathrm{grad}f(\mathbf{x}, t) = \frac{\partial f(\mathbf{x}, t)}{\partial \mathbf{x}} \tag{2.6}$$

2.3.4 Deformation gradient

To measure the deformation motion $\boldsymbol{\chi}$ of a continuum body $\mathcal{B}$ from the reference configuration Ω_0 to the current configuration Ω it is used the deformation gradient $\mathbf{F}$. It maps elemental vectors of the reference configuration to elemental vectors in the spatial configuration.

$$\mathrm{d}\mathbf{x} = \mathbf{F}(\mathbf{X}, t)\mathrm{d}\mathbf{X} \quad \text{or} \quad \mathrm{d}x_a = F_{aA}\mathrm{d}X_A \tag{2.7}$$

Equation 2.8 defines this gradient.

$$\mathbf{F}(\mathbf{X}, t) = \frac{\partial \boldsymbol{\chi}(\mathbf{X}, t)}{\partial \mathbf{X}} = \mathrm{Grad}\mathbf{x}(\mathbf{X}, t) \quad \text{or} \quad F_{aA} = \frac{\partial \chi_a}{\partial X_A} = \mathrm{Grad}_{X_A} x_a \tag{2.8}$$

In general, $\mathbf{F}$ has nine components for all t, characterizing the behavior of motion in the neighborhood of a point.

$$[\mathbf{F}] = \begin{bmatrix} \frac{\partial x_1}{\partial X_1} & \frac{\partial x_1}{\partial X_2} & \frac{\partial x_1}{\partial X_3} \\ \frac{\partial x_2}{\partial X_1} & \frac{\partial x_2}{\partial X_2} & \frac{\partial x_2}{\partial X_3} \\ \frac{\partial x_3}{\partial X_1} & \frac{\partial x_3}{\partial X_2} & \frac{\partial x_3}{\partial X_3} \end{bmatrix} \tag{2.9}$$

To preserve $\mathcal{B}$ during the deformation, the local transformation (Equation 2.7) has to be one-to-one, therefore $\mathbf{F}$ cannot be singular. Being J the Jacobian determinant, $J = \det\mathbf{F} \neq 0$ relation is necessary. Also, to avoid the body's loss of volume $J > 0$. These conditions confirm the existence of an inverse of $\mathbf{F}$. The inverse of the deformation gradient $\mathbf{F}^{-1}$ obtains the elemental vectors of the reference configuration from the deformed configuration.

$$\mathbf{F}^{-1}(\mathbf{x}, t) = \frac{\partial \boldsymbol{\chi}^{-1}(\mathbf{x}, t)}{\partial \mathbf{x}} = \mathrm{grad}\mathbf{X}(\mathbf{x}, t) \quad \text{or} \quad F^{-1}_{Aa} = \frac{\partial \chi^{-1}_A}{\partial x_a} = \mathrm{grad}_{x_a} X_A \tag{2.10}$$

with the mapping of each point obtained through

$$d\mathbf{X} = \mathbf{F}^{-1} d\mathbf{x} \tag{2.11}$$

If there is no motion $\mathbf{F} = \mathbf{I}$ (where $\mathbf{I}$ is a second-order unit tensor called identity) and $\mathbf{x} = \mathbf{X}$ and, consequently, $J = 1$.

The displacement of any point can be defined using the displacement vector $\mathbf{u}$.

$$\mathbf{u} = \mathbf{x} - \mathbf{X} \Leftrightarrow \mathbf{x} = \mathbf{X} + \mathbf{u} \tag{2.12}$$

This leads $\mathbf{F}$ to Equation 2.13.

$$\mathbf{F} = \frac{\partial}{\partial \mathbf{X}}(\mathbf{X} + \mathbf{u}) = \frac{\partial \mathbf{X}}{\partial \mathbf{X}} + \frac{\partial \mathbf{u}}{\partial \mathbf{X}} = \mathbf{I} + \frac{\partial \mathbf{u}}{\partial \mathbf{X}} \tag{2.13}$$

2.3.5 Strain tensors

The strain tensors compute the change in length between two neighboring points in a certain configuration of a continuum body. The motion and deformation of $\mathcal{B}$ from the reference Ω_0 to the current configuration Ω can be determined in terms of second-order strain tensors. Considering two elemental vectors $d\mathbf{X}_1$ and $d\mathbf{X}_2$ of the reference configuration there is a tensor able to relate them, as they deform to $d\mathbf{x}_1$ and $d\mathbf{x}_2$ in the current configuration.

$$d\mathbf{x}_1 \cdot d\mathbf{x}_2 = d\mathbf{X}_1 \cdot \mathbf{C} d\mathbf{X}_2 \tag{2.14}$$

$\mathbf{C}$ is the right Cauchy-Green deformation tensor, that can be given in terms of the deformation gradient as in Equation 2.15. Since $\mathbf{C}$ is symmetric at each $\mathbf{X} \in \Omega_0$, Equation 2.16 is necessarily valid.

$$\mathbf{C} = \mathbf{F}^T\mathbf{F} \quad \text{or} \quad C_{AB} = F_{aA}F_{aB} \tag{2.15}$$

$$\mathbf{C} = \mathbf{F}^T\mathbf{F} = (\mathbf{F}^T\mathbf{F})^T = \mathbf{C}^T \tag{2.16}$$

At the initial state, when $\mathbf{F} = \mathbf{I} \Rightarrow \mathbf{C} = \mathbf{I}$ meaning that the initial strain is not zero. The principal invariants of the right Cauchy-Green tensor $\mathbf{C}$ are defined by

$$\begin{aligned} I_1 &= tr(\mathbf{C}) \\ I_2 &= \tfrac{1}{2}(tr(\mathbf{C})^2 - tr(\mathbf{C}^2)) \\ I_3 &= det(\mathbf{C}) \end{aligned} \tag{2.17}$$

The inverse scalar product can be obtained via left Cauchy-Green tensor $\mathbf{b}$ (Equation 2.18) defined by Equation 2.19.

$$d\mathbf{X}_1 \cdot d\mathbf{X}_2 = d\mathbf{x}_1 \cdot \mathbf{b}^{-1} d\mathbf{x}_2 \tag{2.18}$$

$$\mathbf{b} = \mathbf{F}\mathbf{F}^T \tag{2.19}$$

From Equations 2.14 and 2.18, respectively, it is noted that the tensor $\mathbf{C}$ operates in the material vectors $d\mathbf{X}_1$ and $d\mathbf{X}_2$ and, consequently, called material tensor quantity, whereas the tensor $\mathbf{b}^{-1}$ operates in the spatial vectors $d\mathbf{x}_1$ and $d\mathbf{x}_2$ and, therefore, both $\mathbf{b}$ and $\mathbf{b}^{-1}$ are spatial tensor quantities.

The stretch vector $\boldsymbol{\lambda}_{\mathbf{a}_0}$ (Equation 2.20) measures how much the unit vector $\mathbf{a}_0$, with origin at the point $\mathbf{X}$ and direction of the material line element, has stretched.

$$\boldsymbol{\lambda}_{\mathbf{a}_0}(\mathbf{X}, t) = \mathbf{F}(\mathbf{X}, t)\mathbf{a}_0 \tag{2.20}$$

Generally, the stretch or stretch ratio λ is defined by

$$\lambda = \frac{l_0 - l}{l_0} + 1 = 1 + \varepsilon \tag{2.21}$$

with ε the material deformation or engineering strain, l and l_0 the original and deformed lengths, respectively. When $\lambda > 1$, $\lambda = 1$ or $\lambda < 1$, the line element is extended, unstretched of compressed, respectively. The square root of λ is computed according to

$$\lambda^2 = \boldsymbol{\lambda}_{\mathbf{a_0}} \cdot \boldsymbol{\lambda}_{\mathbf{a_0}} = \mathbf{F}\mathbf{a}_0 \cdot \mathbf{F}\mathbf{a}_0 = \mathbf{a}_0 \cdot \mathbf{F}^T\mathbf{F}\mathbf{a}_0 = \mathbf{a}_0 \cdot \mathbf{C}\mathbf{a}_0 \tag{2.22}$$

relating the stretch with the right Cauchy-Green strain tensor.

The difference between the scalar product of the spatial and material vectors is found to be

$$\frac{1}{2}(d\mathbf{x}_1 \cdot d\mathbf{x}_2 - d\mathbf{X}_1 \cdot d\mathbf{X}_2) = d\mathbf{X}_1 \cdot \mathbf{E} d\mathbf{X}_2 \tag{2.23}$$

where $\mathbf{E}$ is the Green-Lagrange strain tensor defined by the following equation.

$$\mathbf{E} = \frac{1}{2}(\mathbf{F}^T\mathbf{F} - 1) = \frac{1}{2}(\mathbf{C} - 1) \quad \text{or} \quad E_{AB} = \frac{1}{2}(F_{iA}F_{iB} - \delta_{AB}) \tag{2.24}$$

Contrary to $\mathbf{C}$, the Green-Lagrange deformation tensor is zero for the reference configuration.

Alternatively, the Eulerian or Almansi strain tensor $\mathbf{e}$ is

$$\mathbf{e} = \frac{1}{2}(1 - \mathbf{b}^{-1}) \tag{2.25}$$

thus, it can relate the elemental vectors through

$$\frac{1}{2}(d\mathbf{x}_1 \cdot d\mathbf{x}_2 - d\mathbf{X}_1 \cdot d\mathbf{X}_2) = d\mathbf{x}_1 \cdot \mathbf{e} d\mathbf{x}_2 \tag{2.26}$$

With Equation 2.25, the relation between the Eulerian or Almansi strain tensor $\mathbf{e}$ and the Green-Lagrange strain tensor $\mathbf{E}$ can be obtained.

$$\mathbf{E} = \mathbf{F}^T\mathbf{e}\mathbf{F} \tag{2.27}$$

2.4 Stress

2.4.1 Introduction

Motion and deformation, as aforementioned, give rise to interactions between the material and the neighboring material in the interior part of the body (Holzapfel, 2002). A consequence of these interactions is stress and this section will focus on its concept and on the properties of traction vectors and stress tensors.

2.4.2 Traction vectors and stress tensors

A continuum deformable body $\mathcal{B}$ occupying an arbitrary region Ω of the physical space, with boundary surface $\partial\Omega$, at time t is shown in Figure 2.11. It is postulated that arbitrary forces act on the whole of the boundary surface (external forces), and on an imaginary surface within the interior of that body (internal forces) in some distributed manner.

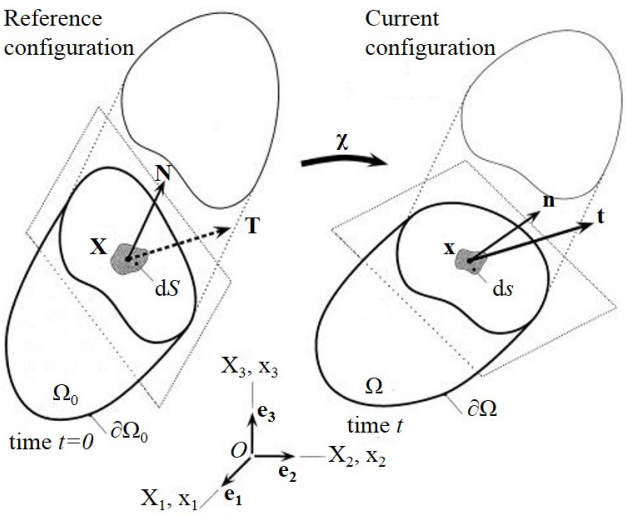

Figure 2.11: Traction vectors acting on infinitesimal surface elements with outward unit normals. From Holzapfel (2002).

Considering that the body $\mathcal{B}$ was cut by a plane surface which passes a given point $\mathbf{x} \in \Omega$ related to $\mathbf{X} \in \Omega_0$ with spatial coordinates x_a and X_a at a time t, respectively, there is a unit vector $\mathbf{n}$ at $\mathbf{x}$ and $\mathbf{N}$ at $\mathbf{X}$, that are directed along the outward normal to an infinitesimal spatial surface element, $\mathrm{d}s \in \partial\Omega$ and $\mathrm{d}S \in \partial\Omega_0$, respectively. The infinitesimal resultant force acting on a surface element is denoted as $\mathrm{d}\mathbf{f}$ and calculated from

$$\mathrm{d}\mathbf{f} = \mathbf{t}\mathrm{d}s = \mathbf{T}\mathrm{d}S \tag{2.28}$$

with $\mathbf{t} = \mathbf{t}(\mathbf{x}, t, \mathbf{n})$ and $\mathbf{T} = \mathbf{T}(\mathbf{X}, t, \mathbf{N})$. $\mathbf{t}$ represents the Cauchy traction vector and $\mathbf{T}$ is the first Piola-Kirchhoff traction vector. They measure the force per unit surface area defined in the current and reference configuration, respectively. The vectors $\mathbf{t}$ and $\mathbf{T}$ are called surface tractions that act across the surface elements $\mathrm{d}s$ and $\mathrm{d}S$, with respective normals $\mathbf{n}$ and $\mathbf{N}$.

According to the Cauchy's stress theorem there are unique second-order tensor fields $\boldsymbol{\sigma}$ and $\mathbf{P}$ so that

$$\begin{aligned} \mathbf{t} = (\mathbf{x}, t, \mathbf{n})s = \boldsymbol{\sigma}(\mathbf{x}, t)\mathbf{n} \qquad &\text{or} \qquad t_a = \sigma_{ab} n_b \\ \mathbf{T} = (\mathbf{X}, t, \mathbf{N}) = \mathbf{P}(\mathbf{X}, t)\mathbf{N} \qquad &\text{or} \qquad T_a = P_a A N_A \end{aligned} \tag{2.29}$$

where $\boldsymbol{\sigma}$ is the Cauchy stress tensor and $\mathbf{P}$ characterizes the first Piola Kirchhoff stress tensor. For computational purposes, is convenient to use the matrix notation to represent this theorem.

$$[\mathbf{t}] = [\boldsymbol{\sigma}][\mathbf{n}] \tag{2.30}$$

$$[\mathbf{t}] = \begin{bmatrix} t_1 \\ t_2 \\ t_3 \end{bmatrix} \quad , \quad [\boldsymbol{\sigma}] = \begin{bmatrix} \sigma_{11} & \sigma_{12} & \sigma_{13} \\ \sigma_{21} & \sigma_{22} & \sigma_{23} \\ \sigma_{31} & \sigma_{32} & \sigma_{33} \end{bmatrix} \quad , \quad [\mathbf{n}] = \begin{bmatrix} n_1 \\ n_2 \\ n_3 \end{bmatrix}$$

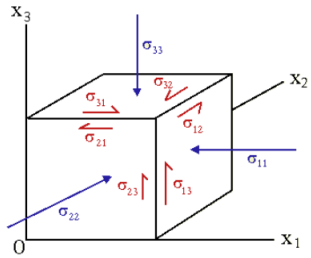

Finally, $\boldsymbol{\sigma}$ and $\mathbf{P}$ can be related through the following transformation.

$$\begin{aligned} \mathbf{t}(\mathbf{x}, t, \mathbf{n})\mathrm{d}s &= \mathbf{T}(\mathbf{X}, t, \mathbf{N})\mathrm{d}S \\ \boldsymbol{\sigma}(\mathbf{x}, t)\mathbf{n}\mathrm{d}s &= \mathbf{P}(\mathbf{X}, t)\mathbf{N}\mathrm{d}S \end{aligned} \tag{2.31}$$

Then, $\mathbf{P}$ can be written in terms of $\boldsymbol{\sigma}$, with Piola transformation, giving the stress measured on a surface element of the reference configuration.

$$\mathbf{P} = J\boldsymbol{\sigma}\mathbf{F}^{-\mathrm{T}} \quad \text{or} \quad P_{aA} = J\sigma_{ab}F^{-1}_{Ab} \tag{2.32}$$

The symmetric Cauchy stress tensor results in the constitutive Equation 2.33, which necessarily implies Equation 2.34.

$$\boldsymbol{\sigma} = J^{-1}\mathbf{P}\mathbf{F}^{\mathrm{T}} = \boldsymbol{\sigma}^{\mathrm{T}} \quad \text{or} \quad \sigma_{ab} = J^{-1}P_{aA}F_{bA} = \sigma_{ba} \tag{2.33}$$

$$\mathbf{P}\mathbf{F}^{\mathrm{T}} = \mathbf{F}\mathbf{P}^{\mathrm{T}} \tag{2.34}$$

2.5 Constitutive Laws

2.5.1 Introduction

Equations that characterize the physical properties of a system's material are called constitutive equations or constitutive laws (Fung, 1993; Cowin and Doty, 2007). Each material has a different constitutive equation to describe each of its physical properties.

Constitutive equations are unlike conservation principles (mass, momentum, angular momentum, energy, etc). The last ones must hold for all materials while constitutive equations only hold for a particular property of a specific material (Cowin and Doty, 2007). It is the aim of constitutive theories to develop mathematical models for representing the real behavior of matter (Holzapfel, 2002).

As Humphrey (2002) mentioned, it is important to assemble the theoretical knowledge previously referred with the mechanical classification of the material concerned. The constitutive equations interrelate the stress components and the strain components within a non-linear regime (Holzapfel, 2002).

2.5.2 Hiperelasticity

2.5.2.1 General remarks

Hyperelastic materials or Green-elastic materials, such as rubbers, or soft tissues, postulate the existence of a Helmholtz free-energy function Ψ, which is defined per unit reference volume, rather than per unit mass. The Helmholtz free-energy function is many times stated as strain-energy function or stored-energy function (Holzapfel, 2002). These materials demonstrate a non-linear elastic behavior, therefore hyperelasticity provides means of modeling their stress-strain curves. For homogeneous materials, the strain-energy function Ψ depends only upon the deformation gradient $\mathbf{F}$ (recall section 2.3.4), as described in Equation 2.35. For so-called heterogeneous materials Ψ will depend additionally upon the position of a point in the medium, Equation 2.36 (Holzapfel, 2002).

$$\Psi = \Psi(\mathbf{F}) \tag{2.35}$$

$$\Psi = \Psi(\mathbf{F}, \mathbf{X}) \tag{2.36}$$

A hyperelastic material is defined as a subclass of an elastic material, whose response functions can be described by means of the first Piola-Kirchhoff stress tensor $\mathbf{P}$ and second-order Piola Kirchhoff stress $\mathbf{S}$. These second-order tensors define the stress field in terms of the right Cauchy-Green deformation tensor $\mathbf{C}$ and the Green-Lagrange strain tensor $\mathbf{E}$ (recall section 2.3.5), with Equations 2.37 and 2.38.

$$\mathbf{P} = \frac{\partial \Psi(\mathbf{F})}{\partial \mathbf{F}} = 2\mathbf{F}\frac{\partial \Psi(\mathbf{C})}{\partial \mathbf{C}} = \quad \text{or} \quad P_{aA} = \frac{\partial \Psi}{\partial F_{aA}} = 2F_{aB}\frac{\partial \Psi}{\partial C_{AB}} \tag{2.37}$$

$$\mathbf{S} = 2\frac{\partial \Psi(\mathbf{C})}{\partial \mathbf{C}} = \frac{\partial \Psi(\mathbf{E})}{\partial \mathbf{E}} \quad \text{or} \quad S_{AB} = 2\frac{\partial \Psi}{\partial C_{AB}} = \frac{\partial \Psi}{\partial E_{EA}} \tag{2.38}$$

Using the symmetry of the Cauchy-Green tensor (Equation 2.33), Equation 2.39 can be deduced.

$$\begin{gathered} \boldsymbol{\sigma} = J^{-1}\tfrac{\partial \Psi(\mathbf{F})}{\partial \mathbf{F}}\mathbf{F}^T = J^{-1}\mathbf{F}\left(\tfrac{\partial \Psi(\mathbf{F})}{\partial \mathbf{F}}\right)^T \\ \text{or} \quad \sigma_{ab} = J^{-1}F_{aA}\tfrac{\partial \Psi}{\partial F_{bA}} = 2J^{-1}F_{aA}F_{bB}\tfrac{\partial \Psi}{\partial C_{AB}} \end{gathered} \tag{2.39}$$

From these previous equations it is possible to retrieve that stress response of hyperelastic materials is derived from a given scalar-valued energy function, which implies that hyperelasticity has a conservative structure. These are the constitutive equations that allow to establish a constitutive model as the basis for approximating the behavior of a real material (Holzapfel, 2002).

As demonstrated in section 2.3.4, in the reference configuration $\mathbf{F}$=$\mathbf{I}$, therefore, the strain-energy function vanishes in this configuration, being possible to establish the normalization condition, Equation 2.40.

$$\Psi = \Psi(\mathbf{I}) = 0 \tag{2.40}$$

Therefore, the strain-energy function Ψ increases with deformation $\Psi = \Psi(\mathbf{F}) \geq 0$. It reaches its gobal minimum for $\mathbf{F}$=$\mathbf{I}$, where $\Psi(\mathbf{I})$ is zero. The relations stated ensure that, in theory, there is no residual stress in the reference configuration (Holzapfel, 2002).

On the other hand, it is required the scalar-valued function Ψ to satisfy the growth conditions in which Ψ tends to $+\infty$ if either J approaches $+\infty$ or 0^+.

$$\begin{cases} \Psi(\mathbf{F}) \to +\infty & \text{as} \quad J \to +\infty \\ \Psi(\mathbf{F}) \to +\infty & \text{as} \quad J \to 0^+ \end{cases} \tag{2.41}$$

Physically, Equation 2.41 means that it is necessary an infinite amount of strain energy in order to expand a continuum body to the infinite range or to compress it to a point with vanishing volume (Holzapfel, 2002).

A hyperelastic material depends only on the stretching part of $\mathbf{F}$, i.e., the deformation energy is not influenced by the rotation or translation of the material. Hence, the strain-energy function can be defined by the right Cauchy-Green tensor $\mathbf{C}$ and the Green-Lagrange strain tensor $\mathbf{E}$ (recall section 2.3.5) , Equation 2.42.

$$\Psi(\mathbf{F}) = \Psi(\mathbf{C}) = \Psi(\mathbf{E}) \tag{2.42}$$

2.5.2.2 Isotropic hyperelastic materials

In isotropic materials, the strain-energy function Ψ depends upon the principal invariants of the Cauchy-Green tensor, I_i (Equation 2.17) (Holzapfel, 2002) and, therefore, the principal stretches λ_i.

$$\Psi_{isotropic} = \Psi(I_1, I_2, I_3) = \Psi(\lambda_1, \lambda_2, \lambda_3) \tag{2.43}$$

with

$$I_1 = \sum_{i=1}^{3} \lambda_i^2 \qquad I_2 = \sum_{i=1}^{3} \lambda_i^2 \lambda_j^2, i \neq j \qquad I_3 = \prod_{i=1}^{3} \lambda_i^2 \tag{2.44}$$

Using Equation 2.38 and deriving in order of the invariants, the second-order Piola-Kirchhoff stress tensor turns into

$$\mathbf{S} = 2\left[\left(\frac{\partial\Psi}{\partial I_1} + I_1\frac{\partial\Psi}{\partial I_2}\right)\mathbf{I} - \frac{\partial\Psi}{\partial I_1}\mathbf{C} + I_3\frac{\partial\Psi}{\partial I_3}\mathbf{C}^{-1}\right] \tag{2.45}$$

The constitutive equation for isotropic materials can be written as in Equation 2.46, with $\mathbf{b}$ the left Cauchy-Green tensor, defined in Equation 2.19 (section 2.3.5).

$$\begin{aligned}\boldsymbol{\sigma}_{isotropic} = 2J^{-1}\mathbf{b}\frac{\partial\Psi(\mathbf{b})}{\partial\mathbf{b}} &= 2J^{-1}\left[I_3\frac{\partial\Psi}{\partial I_3}\mathbf{I} + \left(\frac{\partial\Psi}{\partial I_1} + I_1\frac{\partial\Psi}{\partial I_2}\right)\mathbf{b} - \frac{\partial\Psi}{\partial I_2}\mathbf{b}^2\right] \\ &= 2J^{-1}\left[\left(I_2\frac{\partial\Psi}{\partial I_2} + I_3\frac{\partial\Psi}{\partial I_3}\right)\mathbf{b} + \frac{\partial\Psi}{\partial I_1} + I_3\frac{\partial\Psi}{\partial I_2}\mathbf{b}^{-1}\right]\end{aligned} \tag{2.46}$$

2.5.2.3 Incompressible hyperelastic materials

In the incompressible case, the volume is constant during deformation ($J = 1$). Therefore, $I_3 = 1$ and $J{=}\lambda_1\lambda_2\lambda_3$, so Equation 2.43 takes the following aspect:

$$\Psi_{incompressible} = \Psi(I_1, I_2) \tag{2.47}$$

Also, the strain-energy function can be described as, Equation 2.48, where p is a Lagrange multiplier, which can be identified as the hydrostatic pressure. It represents a workless reaction to the kinematic constraint on the deformation field and can only be determined from the equilibrium equations and the boundary conditions (Holzapfel, 2002).

$$\Psi_{incompressible} = \Psi(\mathbf{F}) + p(J-1) \tag{2.48}$$

From Equation 2.37 and the relation between the first and second-order Piola-Kirchhoff stress tensors Equations 2.49 and 2.50 can be deduced.

$$\mathbf{P} = \frac{\partial\Psi(\mathbf{F})}{\partial\mathbf{F}} - p\frac{\partial J}{\partial\mathbf{F}} = -p\mathbf{F}^{-T} + \frac{\partial\Psi(\mathbf{F})}{\partial\mathbf{F}} \tag{2.49}$$

$$\mathbf{S} = -p\mathbf{F}^{-1}\mathbf{F}^{-T} + \mathbf{F}^{-1}\frac{\partial\Psi(\mathbf{F})}{\partial\mathbf{F}} = p\mathbf{C}^{-1} + 2\frac{\partial\Psi(\mathbf{C})}{\partial\mathbf{C}} \tag{2.50}$$

The Cauchy stress tensor may now be expressed as

$$\boldsymbol{\sigma}_{incompressible} = -p\mathbf{I} + \mathbf{F}\left(\frac{\partial\Psi(\mathbf{F})}{\partial(\mathbf{F})}\right)^T \tag{2.51}$$

2.5.2.4 Incompressible isotropic hyperelastic materials

If the material combines simultaneously incompressible, isotropic and hyperelastic properties, there is a new suitable strain-energy function, given by Equation 2.52, obtained from Equations 2.43 and 2.48. It respects both the incompressibility ($I_3 = 1$) and isotropy ($\Psi(\mathbf{C}) = \Psi[I_1, I_2, I_3]$) conditions.

$$\Psi = \Psi(I_1, I_2) - \frac{p}{2}(I_3 - 1) = \Psi(\lambda_1, \lambda_2, \lambda_3) - \frac{p}{2}(J - 1) \tag{2.52}$$

At this point, from Equations 2.46 and 2.51, the constitutive equation for incompressible isotropic hyperelastic materials can be deduced.

$$\boldsymbol{\sigma} = -p\mathbf{I} + 2\mathbf{b}\frac{\partial\Psi(\mathbf{b})}{\partial\mathbf{b}} = -p\mathbf{I} + 2\frac{\partial\Psi}{\partial I_1}\mathbf{b} - 2\frac{\partial\Psi}{\partial I_2}\mathbf{b}^{-1}. \tag{2.53}$$

The following relation can also be obtained.

$$\mathbf{S} = -p\mathbf{C}^{-1} + 2\left(\frac{\partial\Psi}{\partial I_1} + I_1\frac{\partial\Psi}{\partial I_2}\right)\mathbf{I} - 2\frac{\partial\Psi}{\partial I_2}\mathbf{C} \tag{2.54}$$

Several researchers developed suitable models for strain-energy functions of hyperelastic, incompressible and isotropic materials, adequate to model uniaxial, equi-biaxial or biaxial loading conditions. As aforementioned, the major loads on ligaments are uniaxial.

Holzapfel (2002) defined the Cauchy stress σ as a function of the strain invariants, Equation 2.55, and as a function of stretches, Equation 2.56, for hyperelastic, incompressible and isotropic materials under uniaxial loads.

$$\sigma = 2\left(\lambda^2 - \frac{1}{\lambda}\right)\left(\frac{\partial\Psi}{\partial I_1} + \frac{1}{\lambda}\frac{\partial\Psi}{\partial I_2}\right) \tag{2.55}$$

$$\sigma = \lambda_1\frac{\partial\Psi}{\partial\lambda_1} - \lambda_3\frac{\partial\Psi}{\partial\lambda_3} \tag{2.56}$$

2.5.2.5 Uniaxial and biaxial deformation

An hyperelastic material can suffer different types of loading tests, represented in Figure 2.12. For the purpose of this study only uniaxial (Figure 2.12a) and biaxial (Figure 2.12b) tests will be considered.

Recalling section 2.3, the extensions and deformations along the three directions of the Euclidean space $\mathbb{E}^3$ defined for a certain point $\mathbf{X}$ in the reference configuration Ω_0 as it moves to point $\mathbf{x}$ of the deformed configuration Ω are given by

$$x_1 = \lambda_1 X_1 \quad , \qquad x_2 = \lambda_2 X_2 \quad , \qquad x_3 = \lambda_3 X_3 \tag{2.57}$$

Taking the incompressibility ($\lambda_1\lambda_2\lambda_3 = 1$) and isotropy ($\lambda_2 = \lambda_3$) conditions into account, the conditions to consider and the resultant deformation gradient $\mathbf{F}$, as well as the right $\mathbf{C}$ and left $\mathbf{b}$ Cauchy-Green tensors and respective principal invariants (I_i) for both uniaxial and biaxial tests can be consulted in Table 2.2. For the uniaxial test it was considered that the load was applied in the x_1-axis and for the equi-biaxial test an equivalent load was applied in the x_1 and x_2-axis (see Figure 2.12).

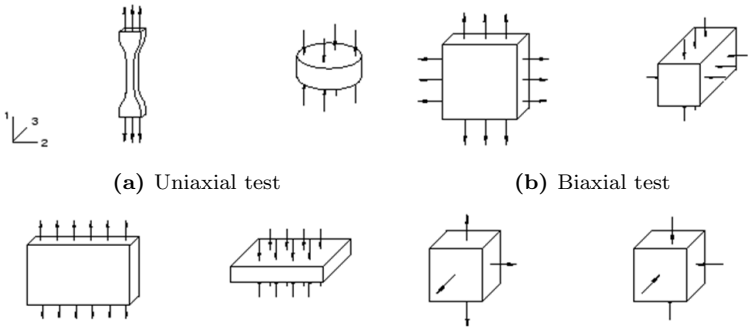

(a) Uniaxial test **(b)** Biaxial test

(c) Planar test **(d)** Volumetric test

Figure 2.12: Deformation modes under tension (left) and compression (right). Adapted from Martins (2013b).

Table 2.2: Conditions of the deformation gradient, right and left Cauchy Green tensors and respective invariants of uniaxial and equi-biaxial loads.

	Uniaxial	Equi-biaxial
Conditions	$\begin{cases} \lambda = \lambda_1 \\ \lambda_2 = \lambda_3 = 1/\sqrt{\lambda} \end{cases}$	$\begin{cases} \lambda_1 = \lambda_2 = \lambda \\ \lambda_3 = 1/\lambda^2 \end{cases}$
$\mathbf{F}$	$\begin{bmatrix} \lambda & 0 & 0 \\ 0 & \frac{1}{\sqrt{\lambda}} & 0 \\ 0 & 0 & \frac{1}{\sqrt{\lambda}} \end{bmatrix}$	$\begin{bmatrix} \lambda & 0 & 0 \\ 0 & \lambda & 0 \\ 0 & 0 & \lambda^{-2} \end{bmatrix}$
$\mathbf{C} = \mathbf{F}^T\mathbf{F} = \mathbf{F}\mathbf{F}^T = \mathbf{b}$	$\begin{bmatrix} \lambda^2 & 0 & 0 \\ 0 & \lambda^{-1} & 0 \\ 0 & 0 & \lambda^{-1} \end{bmatrix}$	$\begin{bmatrix} \lambda^2 & 0 & 0 \\ 0 & \lambda^2 & 0 \\ 0 & 0 & \lambda^{-4} \end{bmatrix}$
Invariants	$I_1 = \frac{2}{\lambda} + \lambda^2$ $I_2 = 2\lambda + \lambda^{-2}$ $I_3 = 1$	$I_1 = 2\lambda^2 + \lambda^{-4}$ $I_2 = \lambda^4 + 2\lambda^{-2}$ $I_3 = 1$

2.5.2.6 Hyperelastic material models

Each of the following constitutive models describe the mechanical behavior of incompressible, isotropic and hyperelastic materials. They constitute a starting point to understand the mechanical behavior of biological soft tissues.

Ogden material model

An example of materials undergoing finite strains relative to an equilibrium state are biomaterials such as biological soft tissues and solid polymers such as rubber-like materials (Holzapfel, 2002; Martins et al., 2006).

Ogden and Chadwick (1972) defined the strain-energy as a function of the principal stretches λ_i. He described the changes of the principal streches in the current configuration in comparison to the reference configuration. Ogden's model (Equation 2.58) is computationally simple and plays and important role in the theory of finite elasticity (Holzapfel, 2002).

$$\Psi^{Ogden} = \Psi(\lambda_1, \lambda_2, \lambda_3) = \sum_{i=1}^{N} \frac{\mu_i}{\alpha_i}(\lambda_1^{\alpha_i} + \lambda_2^{\alpha_i} + \lambda_3^{\alpha_i} - 3) \tag{2.58}$$

$$2\mu = \sum_{p=1}^{N} \mu_p \alpha_p \tag{2.59}$$

with N a positive integer (tipically 3), α_p dimensionless constants of the strain-energy function and μ the constant shear modulus in the reference configuration. This model is valid when $\mu_p \alpha_p < 0$, $i = 1, 2, ..., n$ and Equation 2.59 represents a correlation of the shear modulus.

If $\mu_i = c_{2i-1}$ and $\alpha_i = c_{2i}$, Equation 2.58 can now be written as in Equation 2.60, and for a material subjected to a simple tension be simplified into Equation 2.61.

$$\Psi^{Ogden} = \sum_{i=1}^{N} \frac{c_{(2i-1)}}{c_{2i}}(\lambda_1^{c_{2i}} + \lambda_2^{c_{2i}} + \lambda_3^{c_{2i}} - 3) \tag{2.60}$$

$$\Psi^{Ogden} = \sum_{i=1}^{N} \frac{c_{(2i-1)}}{c_{2i}} \left[\lambda^{c_{2i}} + 2\left(\frac{1}{\sqrt{\lambda}}\right)^{c_{2i}} - 3 \right] \tag{2.61}$$

From Equation 2.56 the constitutive equation of the Ogden material model is generally represented in Equation 2.62.

$$\sigma^{Ogden} = \sum_{i=1}^{N} c_{2i-1}(\lambda^{c_{2i}} - \lambda^{-c_{2i}/2}) \tag{2.62}$$

Both Mooney-Rivlin and neo-Hookean material models covered below are specific cases of the Odgen material model for incompressible materials, proposed by R. Rivlin (Holzapfel, 2002).

Mooney-Rivlin material model

The Mooney-Rivlin material model was proposed by Mooney (1940) and expressed in terms of invariants by Rivlin (1948). It sets that $N = 2$, $\alpha_1 = 2$ and $\alpha_2 = -2$. With the constraint condition of $I_3 = \lambda_1^2\lambda_2^2\lambda_3^2 = 1$ and defining $c_1 = \mu_1/2$ and $c_2 = -\mu_2/2$, the strain-energy function takes the form of Equation 2.63. This model is considered suitable for non-linear isotropic material behavior representation (Holzapfel, 2002).

$$\begin{aligned} \Psi^{Mooney-Rivlin} &= c_1(\lambda_1^2 + \lambda_2^2 + \lambda_3^2 - 3) + c_2(\lambda_1^{-2} + \lambda_2^{-2} + \lambda_3^{-2} - 3) \\ &= c_1(I_1 - 3) + c_2(I_2 - 3) \end{aligned} \tag{2.63}$$

As this model depends only upon I_1 and I_2, the Cauchy stress tensor of Mooney-Rivlin material model is derived from Equations 2.55 and 2.63.

$$\sigma^{Mooney-Rivlin} = 2\left(\lambda^2 - \frac{1}{\lambda}\right)\left(c_1 + c_2\frac{1}{\lambda}\right) \tag{2.64}$$

Neo-Hookean material model

The present model (Rivlin, 1948) adopts the strain-energy function configuration described in Equation 2.65. It sets $N = 1$, $\alpha_1 = 2$ with constant $c_1 = \mu_1/2$ and the shear modulus $\mu = \mu_1$.

$$\Psi^{neo-Hookean} = c_1(\lambda_1^2 + \lambda_2^2 + \lambda_3^2 - 3) = c_1(I_1 - 3) \tag{2.65}$$

The strain-energy function in Equation 2.65 was motivated by a statistical theory in which a vulcanized rubber is approached as a three dimensional network of long-chain molecules, connected at a few points (Holzapfel, 2002).

From Equation 2.55 and 2.65, the Cauchy stress can be defined as:

$$\sigma^{neo-Hookean} = 2\left(\lambda^2 - \frac{1}{\lambda}\right)c_1. \tag{2.66}$$

Yeoh material model

The material model proposed by Yeoh (1997) considers the strain-energy function depending only upon the first strain invariant I_1.

$$\Psi^{Yeoh} = c_1(I_1 - 3) + c_2(I_1 - 3)^2 + c_3(I_1 - 3)^3 \tag{2.67}$$

For this model, the relation between the shear modulus Ψ and the material constants c_1, c_2, c_3 is given by Equation 2.68.

$$\mu = 2c_1 + 4c_2(I_1 - 3) + 6c_3(I_1 - 3)^2 \tag{2.68}$$

Therefore, Equation 2.67 is valid for $\Psi > 0$ and $c_1 > 0, c_2 < 0, c_3 > 0$.

The Cauchy stress can be obtained from Equations 2.55 and 2.67, previously written, in the form of:

$$\sigma^{Yeoh} = 2\left(\lambda^2 - \frac{1}{\lambda}\right)(c_1 + 2c_2(I_1 - 3) + 3c_3(I_1 - 3)^2). \tag{2.69}$$

2.5.2.7 Incompressible transversely isotropic materials

When a fibered material is considered transversely isotropic, the fibers stretch λ depends on the fiber direction of the undeformed configuration, $\mathbf{m}_0$, and the modified right Cauchy-Green tensor $\mathbf{C}$.

$$\lambda^2 = \mathbf{m}_0 \cdot \bar{\mathbf{C}}\mathbf{m}_0 \tag{2.70}$$

Considering an incompressible, transversely isotropic and fibered hyperelastic material, the strain-energy function can be defined in terms of a dilatational (variable volume) and a distortional (constant volume) elastic contributions.

$$\Psi = \Psi_{Vol}(J) + \bar{\Psi}(\bar{\mathbf{I}}_1, \bar{\mathbf{I}}_2, \bar{\mathbf{I}}_4) \tag{2.71}$$

Transverse isotropy requires two other invariants I_4 and I_5, called pseudo-invariants of C:

$$\bar{\mathbf{I}}_4 = \mathbf{m}_0 \cdot \bar{\mathbf{C}}\mathbf{m}_0 = \lambda^2 \quad , \qquad \bar{\mathbf{I}}_5 = \mathbf{m}_0 \cdot \bar{\mathbf{C}}^2\mathbf{m}_0 \quad \text{with} \quad \bar{\mathbf{C}} = J^{\frac{2}{3}}\mathbf{C} \tag{2.72}$$

The rest of the invariants are similarly obtained.

$$\bar{\mathbf{I}}_1 = tr(\bar{\mathbf{C}}) \quad , \quad \bar{\mathbf{I}}_2 = \frac{1}{2}\left((tr(\bar{\mathbf{C}})^2 - tr(\bar{\mathbf{C}}^2)\right) \quad , \quad \bar{\mathbf{I}}_3 = J^2 = det(\bar{\mathbf{C}}) = 1 \tag{2.73}$$

Finally, an incompressible transversely isotropic material strain-energy function is defined by Equation 2.74 and its constitutive equation takes the form of Equation 2.75.

$$\Psi = \Psi[I_1(\mathbf{C}), I_2(\mathbf{C}), I_4(\mathbf{C}, \mathbf{m}_0), I_5(\mathbf{C}, \mathbf{m}_0)] - \frac{1}{2}p(I_3 - 1) \tag{2.74}$$

$$\boldsymbol{\sigma} = -p\mathbf{I} - q\mathbf{m}\otimes\mathbf{m} + 2\frac{\partial\Psi}{\partial I_1}\mathbf{b} - 2\frac{\partial\Psi}{\partial I_2}\mathbf{b}^{-1} + 2\frac{\partial\Psi}{\partial I_5}(\mathbf{m}\otimes\mathbf{bm} + \mathbf{mb}\otimes\mathbf{m}) \tag{2.75}$$

with q and additional Lagrange multiplier (Holzapfel, 2002).

2.5.2.8 Soft tissues' material models

Veronda and Westmann (1970); Humphrey (2002) and Weiss et al. (1996) also proposed constitutive models proper for soft biological tissues with the present mechanical behavior.

Veronda-Westmann's material model

One of the first studies cited by Fung (1993) was the work of Veronda and Westmann (1970), which developed an hyperelastic strain-energy function for large deformations under uniaxial loads (Equation 2.76), to model the mechanical behavior of cat skin.

$$\Psi^{Veronda-Westmann} = c_1[e^{\alpha(I_1-3)} - 1] - c_1\frac{\alpha}{2}(I_2 - 3) \tag{2.76}$$

The Cauchy stress tensor of this model results in Equation 2.77.

$$\sigma^{Veronda-Westmann} = 2\left(\lambda^2 - \frac{1}{\lambda}\right)c_1c_2\left(e^{c_2(I_1-3)} - \frac{1}{2\lambda}\right) \tag{2.77}$$

Humphrey material model

Humphrey (2002) studied the passive myocardium behavior and deduced the strain-energy function of Equation 2.78.

$$\Psi^{Humphrey} = c(e^Q - 1) \tag{2.78}$$

Q is a function of the components of the right Cauchy-Green tensor and depends on the isotropicity of the material. Particularly, Equation 2.78 can be written as

$$\Psi^{Humphrey} = c_1\left(e^{c_2(I_1-3)} - 1\right) \tag{2.79}$$

The Cauchy stress tensor of Humprey's model is presented in Equation 2.80

$$\sigma^{Humphrey} = 2\left(\lambda^2 - \frac{1}{\lambda}\right)c_1c_2e^{c_2(I_1-3)} \tag{2.80}$$

Weiss material model

A constitutive model for soft tissues and a finite element implementation that allows to fully describe incompressible material behavior was presented by Weiss et al. (1996). The objective of their work was to develop an efficient implementation of incompressible hyperelasticity that would accommodate transversely isotropic material symmetry. The authors proposed a strain-energy function which would be the result of the matrix $\bar{\Psi}_m$ and the fibers' $\bar{\Psi}_f$ strain energy.

$$\bar{\Psi}^{Weiss} = \bar{\Psi}_m + \bar{\Psi}_f \tag{2.81}$$

The first term, $\bar{\Psi}_m$, models the ground substance matrix and is made specific by assuming it is a Mooney-Rivlin material (see section 2.5.2.6, Equation 2.63). The second term, $\bar{\Psi}_f$ models the fibers as

$$\bar{\Psi}_f = \bar{\Psi}(\bar{\mathbf{I}}_4) = c_3(e^{(\bar{\mathbf{I}}_4-1)} - \bar{\mathbf{I}}_4) \tag{2.82}$$

The Cauchy-Green tensor of Weiss model is given by Equation 2.83.

$$\sigma^{Weiss} = p + \frac{2}{J}dev\left[\mathbf{F}\frac{\partial\Psi(\mathbf{C})}{\partial\mathbf{C}}\mathbf{F}^T\right] \tag{2.83}$$

where the operator $dev[\cdot]$ is the deviatoric projection operator for stress-like quantities in the reference configuration.

$$dev[\cdot] \equiv [\cdot] - \frac{1}{3} tr[\cdot][\mathbf{I}] \tag{2.84}$$

$$tr[\cdot] = 2\frac{\partial \Psi_m}{\partial I_1}\left(\lambda^2 + \frac{2}{\lambda}\right) + \frac{\partial \Psi_f}{\partial \lambda}\lambda \tag{2.85}$$

Weiss modified material model

A Weiss modified model was proposed by Calvo et al. (2009) to characterize the elastic behavior of vaginal tissue.

The strain energy function for this formulation can be subdivided into three regions described below and illustrated in Figure 2.13.

1. initial phase of an uniaxial tensile test where only the matrix supports the tension applied ($\bar{\mathbf{I}}_4 < \bar{\mathbf{I}}_{4_0}$ in Figure 2.13a), corresponds to the toe region (Figure 2.13b);
2. the phase when fibers start to stretch and both matrix and fibers work contributing to the mechanical response of tissues ($\bar{\mathbf{I}}_4 > \bar{\mathbf{I}}_{4_0}$ and $\bar{\mathbf{I}}_4 < \bar{\mathbf{I}}_{4_{ref}}$ in Figure 2.13a), corresponds to the heel region (Figure 2.13b), and
3. the linear region (Figure 2.13b) where only fibers can support the tension applied ($\bar{\mathbf{I}}_4 > \bar{\mathbf{I}}_{4_{ref}}$ in Figure 2.13a).

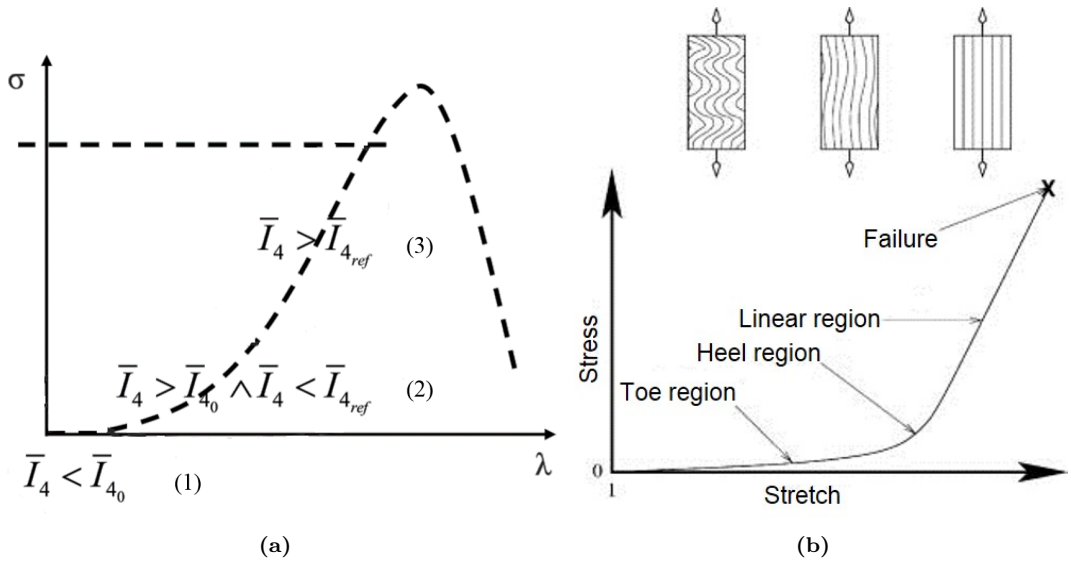

Figure 2.13: Regions considered for Weiss modified model proposed. In a stress vs. stretch graphic a) Weiss modified model division: (1) matrix mechanical work, (2) matrix + fibers work, (3) only fibers contribute to the mechanical response of tissues. Adapted from Martins (2013a). b) Collagen tissues characteristic graphic regions. Adapted from Freed and Doehring (2005).

The authors characterized the isotropic component (matrix work, $\bar{\Psi}_m$) by the Neo-Hookean material model (section 2.5.2.6, Equation 2.65) instead of the Mooney-Rivlin model, as proposed by Weiss et al. (1996), so that $\bar{\Psi} = \bar{\Psi}_m + \bar{\Psi}_f$.

The anisotropic component (fibers work, $\bar{\Psi}_f$) is further established in terms of the different regions:

$$\bar{\Psi}_f = \begin{cases} 0 & if \quad \bar{\mathbf{I}}_4 < \bar{\mathbf{I}}_{4_0} \\ \frac{c_3}{c_4}(e^{c_4(\bar{\mathbf{I}}_4 - \bar{\mathbf{I}}_{4_0})} - c_4(\bar{\mathbf{I}}_4 - \bar{\mathbf{I}}_{4_0}) - 1) & if \quad \bar{\mathbf{I}}_4 > \bar{\mathbf{I}}_{4_0} \wedge \bar{\mathbf{I}}_4 < \bar{\mathbf{I}}_{4_{ref}} \\ c_5\sqrt{\bar{\mathbf{I}}_4} + \frac{c_6}{2} ln(\bar{\mathbf{I}}_4) + c_7 & if \quad \bar{\mathbf{I}}_4 > \bar{\mathbf{I}}_{4_{ref}} \end{cases} \tag{2.86}$$

with $\bar{\mathbf{I}}_{4_0}$ the stretch where fibers start to work and $\bar{\mathbf{I}}_{4_{ref}}$ the strech at which collagen fibers start to be straightened. $c_1 > 0, c_3 > 0, c_5 > 0$ and $c_6 < 0$ are stress-like parameters, $c_4 > 0$ is dimensionless and $c_7 < 0$ a strain parameter. Moreover, c_5, c_6 and c_7 are not independent parameters that enforce strain, stress and stress derivative's continuity.

A damage model was proposed to understand the ligaments failure - the region where the tissues' behavior switches from elastic to plastic (Calvo et al., 2009):

$$\bar{g_k} = (1 - D_k) = \begin{cases} 1 & , \quad \Xi_{k_t} < \Xi^0_{min_k} \\ 1 - \zeta^2[1 - \beta_k(\zeta^2 - 1)] & , \quad \Xi^0_{min_k} \leq \Xi_{k_t} \leq \Xi^0_{max_k} \\ 0 & , \quad \Xi_{k_t} > \Xi^0_{max_k} \end{cases} \tag{2.87}$$

with k corresponding to either f fibers and m matrix, $\zeta = (\Xi_{k_t} - \Xi^0_{min_k})/(\Xi^0_{max_k} - \Xi^0_{min_k})$ a dimensionless variable and $\Xi^0_{min_k}$ the variables associated to the strain energies at the initial damage for matrix and fibers, respectively, $\Xi^0_{max_k}$ the variables associated to the strain energy at total damage for matrix and fibers, and β_k model exponential parameters. $(1 - D_k)$ is a reduction factor where D_k are normalized scalars reffered to as the damage variables.

Chapter 3

Methodology

3.1 Introduction

To understand the mechanical changes that the pelvic ligaments undergo through the aging process, two types of ligaments were extracted from female tissue samples from 15 cadavers with age ranging from 18 to 65 years old: the round and the uterosacral ligaments. Their function in the pelvic support was reviewed in sections 2.1 and 2.2.

The data used was provided by the uniaxial tensile tests performed by Martins et al. (2013) and processed using MATLAB® scripts. The material parameters were determined using an optimization process (Martins et al., 2010) and an adapted manual process. A comparison between the two methods was also performed.

In Figure 3.1 is a scheme of the work-flow. Although the first three stages were recovered from a previous study, its knowledge is important to a better integration in the project.

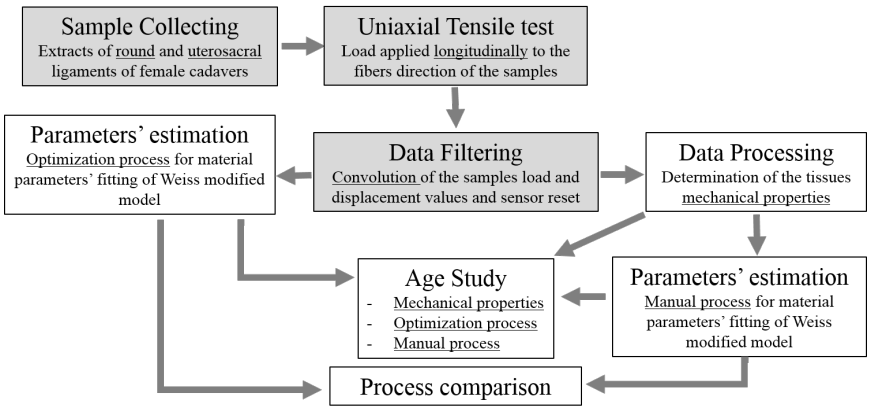

Figure 3.1: Scheme of the work-flow of this study. The gray steps represent the work previously performed by Martins et al. (2013).

3.2 Experimental Data

3.2.1 Round and uterosacral ligament samples

The ligament samples were collected from 15 female cadavers without clinically recognized pelvic floor dysfunctions or prolapse and the information provided can be consulted in Table 3.1. The cadavers were unformalized and preserved with refrigeration. The samples had been collected in accordance with a procedure approved by the direction board of the Forensic Pathology Service of the North Branch of National Institute of Legal Medicine (INML, I.P.).

The specimens used had approximate dimensions of 2 x 1 cm (along the fibers direction), extracted from the intermediate part of the ligaments at the end of the normal forensic autopsy procedures. To preserve their mechanical properties, the tissues were stocked in a salline solution bath at 5°C until 15 minutes prior to the mechanical tests. The time since the extraction to the moment of the mechanical tests did not exceed 6 hours, and most of the samples were stored less than 4 hours.

Table 3.1: Information of the individuals used for the experimental tests. R - round ligament. US - uterosacral ligament. (-) non-available information.

Individual	Samples		Age (years)	Height (cm)	Weight (Kg)	Parity	Menopausal
	R	US					
IML01	2	2	51	158	62.4	1	-
IML02	1	2	51	156	55	1	-
IML03	1	1	51	163	78	0	-
IML04	2	2	47	168	91	1	yes
IML05	2	1	43	159	80	2	yes
IML06	1	1	40	150	57.8	1	-
IML07	2	1	33	167	66	0	no
IML08	1	1	36	154	58	0	no
IML09	1	1	18	179	104.2	0	no
IML10	1	2	38	163	89	1	no
IML11	2	1	59	165	67.5	-	yes
IML12	1	1	40	158	53	1	-
IML13	2	1	51	160	66	2	-
IML15	1	1	54	151	-	-	no
IML17	2	2	65	159	65	-	yes

3.2.2 Mechanical protocol

All mechanical testes were developed at the Institute of Mechanical Engineering, University of Porto in the biomechanics laboratory (LBM-IDMEC). Geometrical properties were acquired through digital analysis. The measurements of the samples' dimensions was achieved using ImageJ software and the images were captured by two USB webcams (frontal and side views) connected to the data acquisition PC.

An uniaxial tensile test was performed in the longitudinal direction of the fibers, as demonstrated in Figure 3.2b, in a costume-made uniaxial tension machine designed to work with soft tissues, as in Figure 3.2a. The support assembly is made from high-density polymer. The mechanical test had been previously validated form different hyperelastic material.

The test was performed with a constant displacement rate of 5mm/min (the same to all samples). A load cell (F_{max} =200N) and a displacement sensor were used to aquire the load (N) and displacement (mm) of the test until complete rupture of the sample. The tests were also recorded on video by one of the previously mentioned webcams. The frequency of acquisition was 100Hz.

From this phase it is possible to collect both load (N) and consequent displacement (mm) of the samples for future analysis, as well as geometry information (length, width and thickness). The mean and standard deviation error of the mean of the geometry characteristics of both ligaments' samples can be accessed in Table 3.2. These informations are crucial for the subsequent data processing.

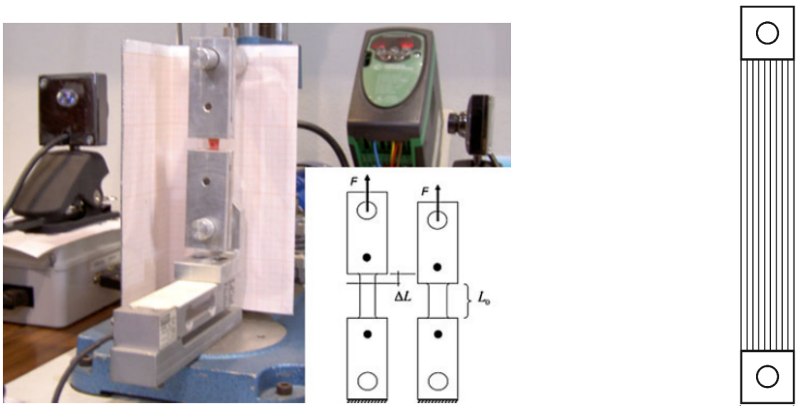

(a) Overall assembly **(b)** Fibers direction in the support frame

Figure 3.2: Uniaxial tensile test in the direction of the fibers for assessment of biomechanical properties of round and uterosacral ligaments. From Martins et al. (2013).

Table 3.2: Round and uterosacral ligaments' samples geometry. Mean±SEM (standard error of the mean).

Ligament	N	Length (mm)	Width (mm)	Thickness (mm)
Round	22	16.940±0.820	9.060±0.350	1.630±0.088
Uterosacral	20	16.140±1.084	7.408±0.518	1.347±0.101

3.2.3 Mechanical properties determination

For mechanical properties determination, MATLAB® scripts were used for data filtering and data processing.

3.2.3.1 Experimental data filtering

First of all, it was necessary to filter the data acquired during the tests (load (N) and correspondent displacement (mm)). For this step, *Data Filter.m* script was used. It allows to reset both load and displacement sensors and define the last point to consider. Its graphical appearance is shown in Figure 3.3. Therefore, as aforementioned, this point had been previously performed for the studies of Martins et al. (2013), it is represented an example of an uniaxial tensile test performed with polydimethylsiloxane (PDMS) commonly referred to as silicone rubber.

The frequency of acquisition was 100Hz the points obtained form small steps in the graphic (blue dots in Figure 3.3). Therefore, those points are convoluted via *conv.m* function (Equation 3.1) with the aperture of the sliding window able to be defined by the user. This allows to obtain a correlated curve that better mimics the Load (N) vs. Displacement (mm) behavior of the sample concerned.

$$w(k) = \frac{\sum_j u(j)v(k-j+1)}{n} \tag{3.1}$$

being u and v the vectors with the data (load or displacement). n is the size of the aperture (vector v) and m the length of the data vector u. So, $k = m + n - 1$.

The resulting points (black points of Figure 3.3) can be saved in a new *.dat* file that allows the introduction of the sample geometry (length, width, thickness and cross-sectional area).

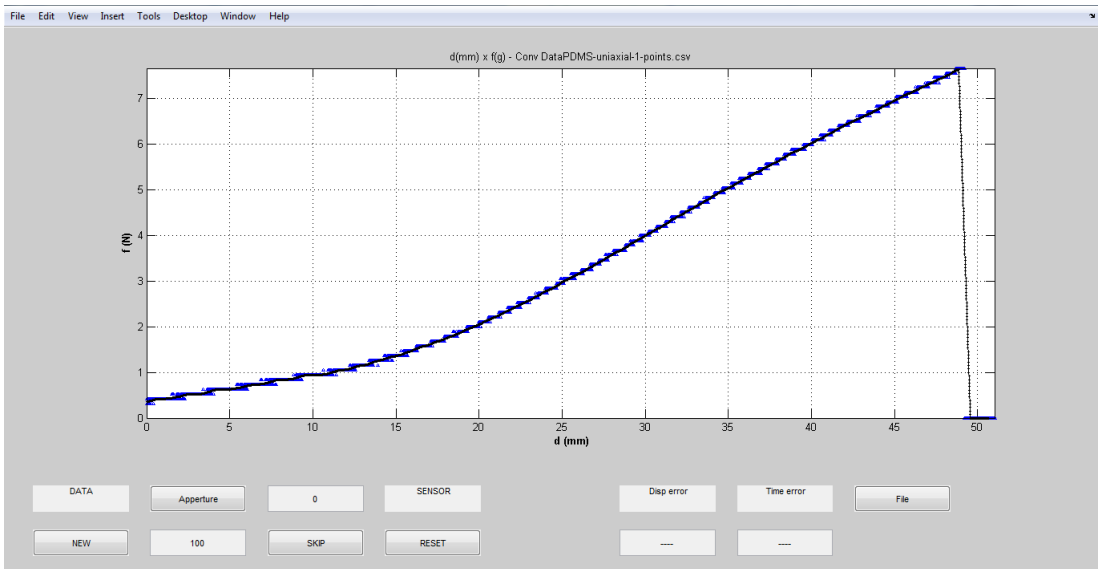

Figure 3.3: *Data Filter* MATLAB® script example used to filter the data from the uniaxial tensile test performed. For this example a PDMS sample was used.

3.2.3.2 Experimental data analysis

The data processing was executed with help of $dPrev - dProc.m$ MATLAB® script and an example is demonstrated in Figure 3.4. During this phase, some samples were eliminated due to visible discrepancy when comparing to other samples graphic visualization and values obtained.

As well as the display of the geometric measurements of each sample, it allows the plot of three different types of graphics and the calculus of its mechanical properties:

- Force (N) vs Displacement (mm):
  - Load max (N) - maximum load applied (F^{max});
  - Displacement max (mm) - maximum displacement obtained (d^{max});
  - Work of the force (mJ) - area behind the correspondent graphic curve (W_{force}).
- Stress (σ MPa) vs Stretch (λ):
  - Tensile strength (MPa) - maximum stress applied (σ^{max});
  - Ultimate stretch - maximum stretch obtained ($\lambda^{ultimate}$);
  - Energy density (nJ/m^3) - area behind the correspondent graphic curve (U_{stress}).
- Stress (σ MPa) vs Strain (ε):
  - Tensile strength (MPa) - maximum stress measured (σ^{max});
  - Ultimate strain - maximum strain obtained ($\varepsilon^{ultimate}$);
  - Strain energy density (SED) - area behind the correspondent graphic curve (Ψ).

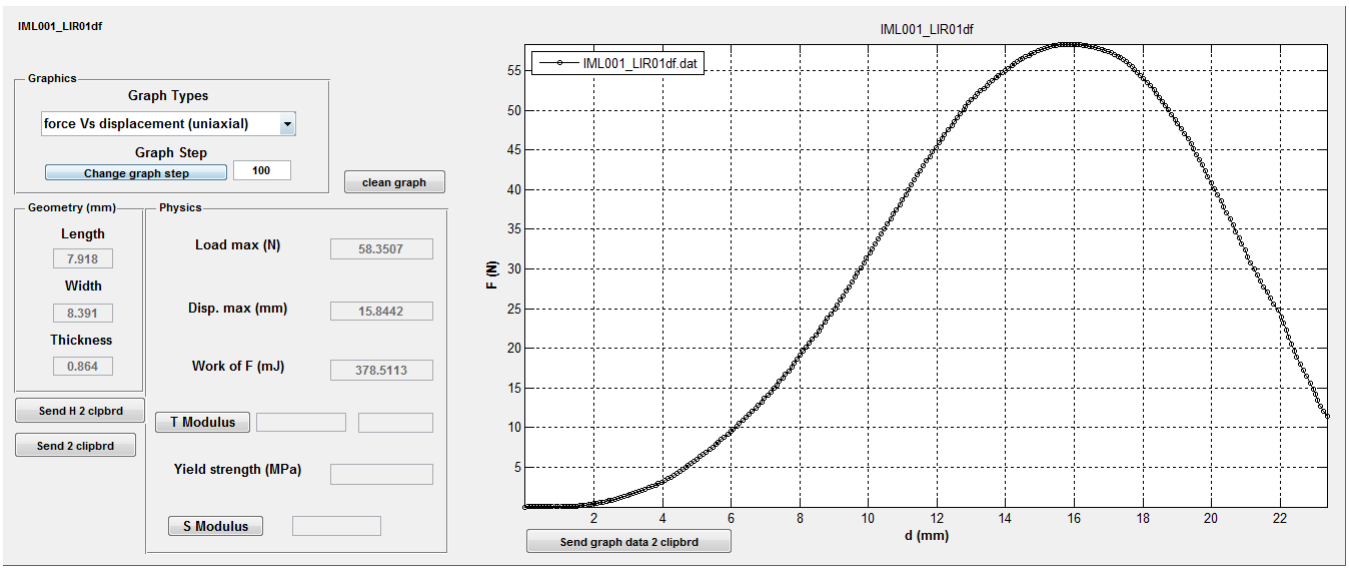

Figure 3.4: $dPrev - dProc$ MATLAB® script used to process the data previously filtered.

The stress (σ_i) can be computed by Equation 3.2, using Equation 3.3 to obtain the cross-sectional area (A_i), admitting that the overall volume is constant, as demonstrated in Figure 3.5.

The cross-sectional area is related to the correspondent stretch, λ_i (Equation 3.4).

$$\sigma_i = \frac{F_i}{A_i} \tag{3.2}$$

$$A_i = \frac{A_0}{\lambda_i} \qquad \text{with} \qquad A_0 = width \quad \text{x} \quad thickness \tag{3.3}$$

$$\lambda_i = \frac{l_i + l_0}{l_0} \tag{3.4}$$

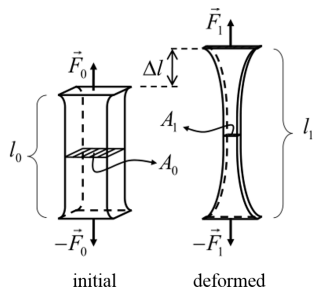

Figure 3.5: Volume maintenance of the samples through the uniaxial tensile test. Adapted from Martins (2013a).

with l_i the length of the sample at i point and l_0 the initial length. l_i is obtained by summing the displacement of that moment with the initial length ($l_i = d_i + l_0$).

Regarding the strain (ε_i) measurements, those are calculated by the Equation 3.5, which is similar to Equation 2.21, already explained in section 2.3.5.

$$\varepsilon_i = \frac{l_i}{l_0} = \lambda_i - 1 \tag{3.5}$$

Apart from these calculations, the secant (E_S) and the tangent (E_T) modulus can also be determined when the graphic types "Stress vs Stretch" and "Stress vs Strain" are selected (often called S modulus and T modulus). These modulus are obtained as schematically demonstrated in Figure 3.6 and with Equations 3.6 and 3.7. The interpolation is meant to distinguish the mechanical behavior of these regions correlated with the regions (1) and (2) of Figure 2.13. The yield strength (σ^{yield}) corresponds to the stress value of the damage point, the limit of the elastic region (see Figure 2.13). This point is related to the last point considered to plot the T modulus (E_T).

$$E_S = \frac{\Delta\sigma_1}{\Delta\lambda_1} \tag{3.6}$$

$$E_T = \frac{\Delta\sigma_2}{\Delta\lambda_2} \tag{3.7}$$

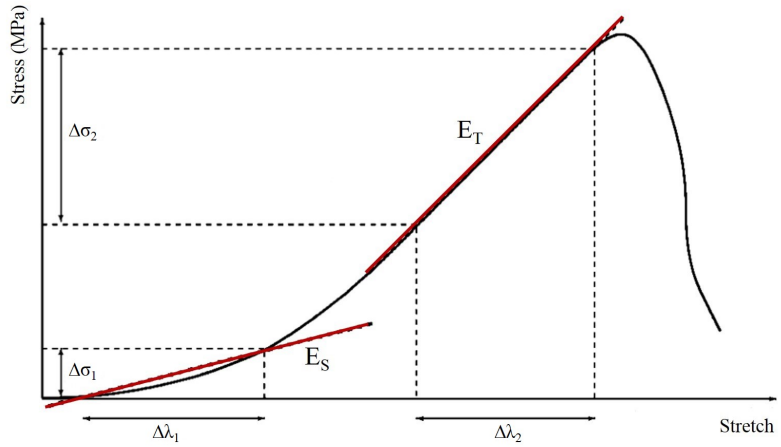

Figure 3.6: Scheme of the secant and tangent modulus determination in a stress vs stretch graphic. Adapted from Afonso et al. (2007).

3.3 Material Parameters' Estimation

As the linear mechanical properties were already analyzed, it becomes necessary to find curves that can mimic those behaviors. The model chosen to study these ligaments' load bearing capability was Weiss modified model proposed by Martins et al. (2010), previously described in section 2.5.2.8, without the damage component. This model revealed to be adequate for these tissues, accordingly to the studies of Martins et al. (2010). The parameters' estimation was achieved with two processes: automatic optimization process and manual process. These methods were applied to all the experimental data of the previous section samples.

3.3.1 Optimization process

The automatic optimization process (OP) was defined by Martins et al. (2010) and estimates the material model parameters values by fitting the experimental data using the Levenberg-Marquardt optimization algorithm. This algorithm is based upon the minimization of an objective function written in terms of the uniaxial tensile test experimental values (Martins et al., 2005).

$$O(\vec{C}) = \sum_{i=1}^{n} w_i^2 [\sigma_i^{an}(\vec{C}) - \sigma_i^{exp}]^2 \tag{3.8}$$

where w_i is the weight coefficient (equal to 1, since all n experimental points are considered to have the same weight in the overall function), σ_i^{an} the model approximation and σ_i^{exp} the experimental measurements.

The Weiss modified material model approximation stress values can be obtained using Equation 3.9, that is defined for the three regions (toe, heel and linear) considered in a ligaments'

deformation process. This Cauchy stress was determined by means of Equation 3.10.

$$\sigma^{Weiss-modified} = \begin{cases} \frac{2c_1(-1+\lambda^3)}{\lambda} & , \quad \bar{\mathbf{I}}_4 < \bar{\mathbf{I}}_{4_0} \\ \frac{2\left(c_1\left(\lambda^3-1\right)+c_3\bar{\mathbf{I}}_4\lambda\left(e^{c_4(\bar{\mathbf{I}}_4-\bar{\mathbf{I}}_{4_0})}-1\right)\right)}{\lambda} & , \quad \bar{\mathbf{I}}_4 > \bar{\mathbf{I}}_{4_0} \wedge \bar{\mathbf{I}}_4 < \bar{\mathbf{I}}_{4_{ref}} \\ \frac{2c_1\left(\lambda^3-1\right)}{\lambda} + c_5\sqrt{\bar{\mathbf{I}}_4} + c_6 & , \quad \bar{\mathbf{I}}_4 > \bar{\mathbf{I}}_{4_{ref}} \end{cases} \tag{3.9}$$

$$\begin{aligned} \sigma = p\mathbf{I} + \frac{2}{J}\Bigg[&\left(\frac{\partial\bar{\Psi}}{\partial\bar{\mathbf{I}}_1} + \bar{\mathbf{I}}_1\frac{\partial\bar{\Psi}}{\partial\bar{\mathbf{I}}_2}\right)\bar{\mathbf{b}} - \frac{\partial\bar{\Psi}}{\partial\bar{\mathbf{I}}_2}\bar{\mathbf{b}}^2 + \bar{\mathbf{I}}_4\frac{\partial\bar{\Psi}}{\partial\bar{\mathbf{I}}_4}\mathbf{m}\otimes\mathbf{m} \\ &-\frac{1}{3}\left(\frac{\partial\bar{\Psi}}{\partial\bar{\mathbf{I}}_1}\bar{\mathbf{I}}_1 + 2\frac{\partial\bar{\Psi}}{\partial\bar{\mathbf{I}}_2}\bar{\mathbf{I}}_2 + \frac{\partial\bar{\Psi}}{\partial\bar{\mathbf{I}}_4}\bar{\mathbf{I}}_4\right)\mathbf{I}\Bigg] \end{aligned} \tag{3.10}$$

The parameters to fit are c_1, c_3 and c_4, since these are the only independent parameters as already mentioned in section 2.5.2.8. Therefore, c_5, c_6 and c_7 are calculated considering the previous values' estimation and Equations 3.11, 3.12 and 3.13, respectively.

$$c_5 = 4c_3\lambda_{ref}\left(-1 + e^{c_4\left(I_{4_{ref}}-I_{4_0}\right)} + I_{4_{ref}}c_4e^{c_4\left(I_{4_{ref}}-I_{4_0}\right)}\right) \tag{3.11}$$

$$c_6 = -2c_3I_{4_{ref}}\left(-1 + e^{c_4\left(I_{4_{ref}}-I_{4_0}\right)} + 2c_4I_{4_{ref}}e^{c_4\left(I_{4_{ref}}-I_{4_0}\right)}\right) \tag{3.12}$$

$$\begin{aligned} c_7 = \frac{1}{c_4}c_3\Big(&c_4I_{4_0} + 3c_4I_{4_{ref}} - 1 + e^{c_4\left(I_{4_{ref}}-I4_0\right)}\left(1 - 4c_4I_{4_{ref}} - 4c_4^2I_{4_{ref}}^2\right) \\ &+c_4I_{4_{ref}}log\left(I_{4_{ref}}\right)\left(e^{c_4\left(I_{4_{ref}}-I_{4_0}\right)}\left(1 + 2c_4I_{4_{ref}}\right) - 1\right)\Big) \end{aligned} \tag{3.13}$$

with λ_{ref} the stretch related to $I_{4_{ref}}$ value (recall Equation 2.72, section 2.5.2.7).

The quality of the fitting process is evaluated by computing the correlation coefficient R^2 (Equation 3.14) and the normalized mean square root error ϵ (Equation 3.15).

$$R^2 = 1 - \frac{\sum_{i=1}^{n}\left[\sigma_i^{an} - \sigma_i^{exp}\right]^2}{\sum_{i=1}^{n}\left[\sigma_i^{an} - \mu_i\right]^2} \tag{3.14}$$

$$\epsilon = \frac{\sqrt{O(\vec{C})/(n-q)}}{\mu} \tag{3.15}$$

with q the number of parameters of the strain energy function, $n - q$ the number of degrees of freedom and μ the mean shear stress defined as

$$\mu = \frac{1}{n}\sum_{i=1}^{n}\sigma_i^{exp} \tag{3.16}$$

This method was also coded in a MATLAB® script represented in Figure 3.7. *Optim02.m* was also build to enable the parameters' fitting of other material models as Ogden's, Mooney-Rivlin's, Neo-Hookean's, Yeoh's and Veronda-Westmann's. For the optimization process it is necessary to define the seed from which the parameters will be estimated. The seeds used for Weiss modified model were the default ones, Figure 3.7b.

The division of the graphic concerning the different deformation behaviors was defined. Initially, it is observed a relative linearity, followed by an exponential behavior (the heel region) until the linearity is reached again. After the damage (where the fibers start to break) the points are discarded - elastic limit. With use of "End Point" button it was defined the limit of the curve fitting.

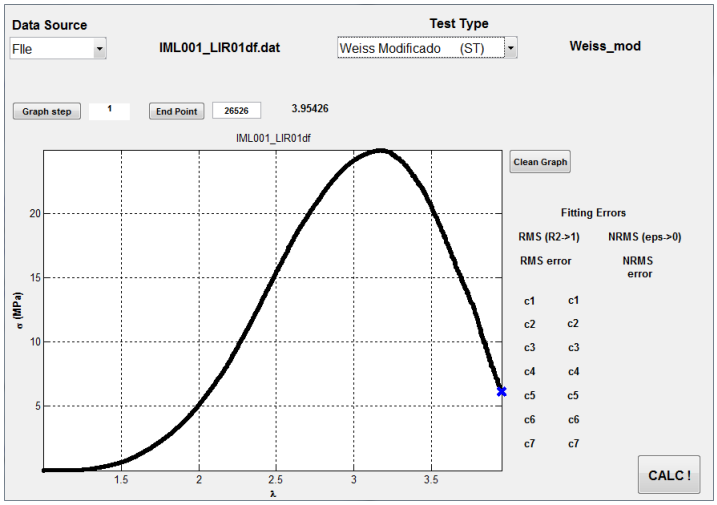

(a) Optimization process main graphic user interface

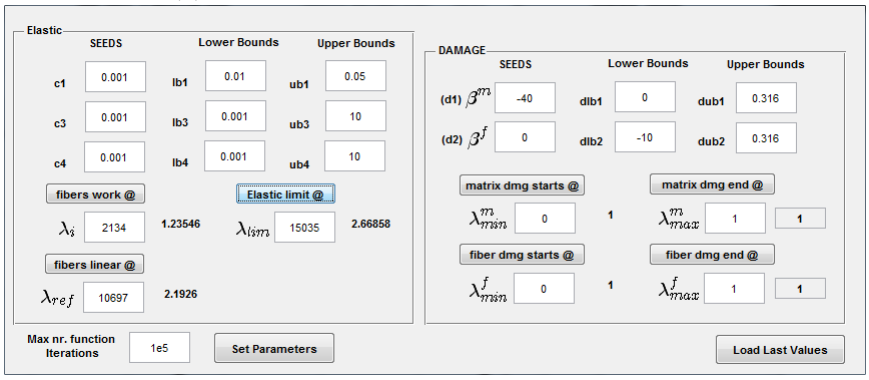

(b) Seeds definition for the optimization process

Figure 3.7: Optimization process MATLAB® graphical user interface.

3.3.2 Manual process

The manual process (MP) was also built in MATLAB® graphic user interface and allows the determination of the material parameters by graphical visualization. Figure 3.8 is a representation of this method's implementation which was designed to be an alternative to the previous process. Together with the plot of the uniaxial tension test experimental values (Data - black curve), an analytical curve of the Weiss modified model is also shown, using Equation 3.9.

Initially, there is a need to select the graphic visualization preferred (stress vs stretch or stress vs strain) and the last point of the graphic to consider (damage point) so that the curve fitting can be more accurate (Figure 3.9). From this point forward, the plot will be restricted to the elastic deformation of the sample, as in Figure 3.8.

The manual process guides the user to select the stretch points to separate the graphic in its different deformation regions (I_{4_0} and $I_{4_{ref}}$) in a similar manner of Figure 2.13. As aforementioned (section 2.5.2.8), c_5, c_6 and c_7 are not independent parameters, as c_1, c_3 and c_4 are. Therefore, the former can be obtained from the values defined for the latter, as already described in Equations 3.11, 3.12 and 3.13, respectively (section 3.3.1).

As Figure 3.8 shows, the definition of the independent parameters c_1, c_3 and c_4 is determined by three independently controlled sliders. All the sliders respect the model constraints ($c_1 > 0$, $c_3 > 0$ and $c_4 > 0$).

The similarity between the two curves was computed by a correlation coefficient R^2 function of MATLAB® (*corr2.m*) which implements the following algorithm:

$$R^2 = \frac{\sum_{i=1}^{n} \left(\sigma_i^{an} - \bar{\sigma}^{an}\right)\left(\sigma_i^{exp} - \bar{\sigma}^{exp}\right)}{\sqrt{\left(\sum_{i=1}^{n} \left(\sigma_i^{an} - \bar{\sigma}^{an}\right)^2\right)\left(\sum_{i=1}^{n} \left(\sigma_i^{exp} - \bar{\sigma}^{exp}\right)^2\right)}} \tag{3.17}$$

with $\bar{\sigma}^{an}$ and $\bar{\sigma}^{exp}$ the mean of the analytical and experimental stresses, respectively, and n the number of samples.

At any moment it was possible to adjust the I_{4_0} and $I_{4_{ref}}$ values so that the fitting could be precise.

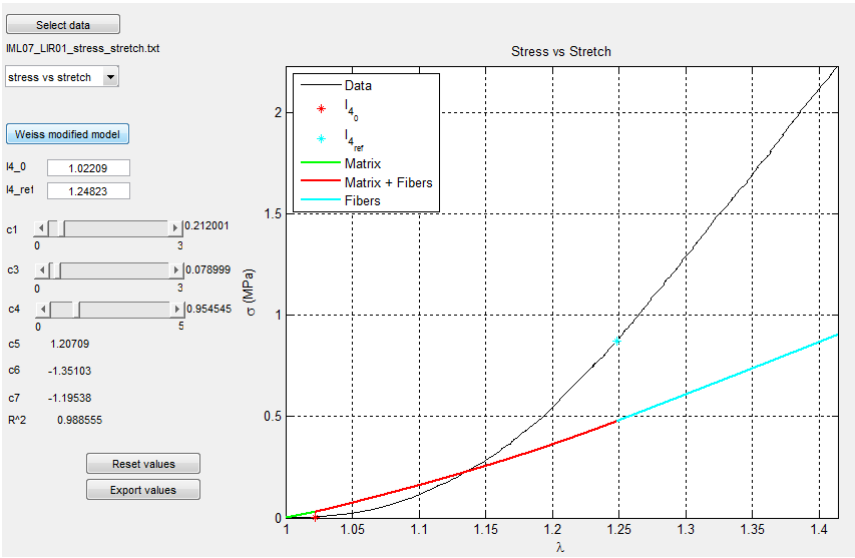

Figure 3.8: Manual process graphic user interface built in MATLAB® environment for material parameters' determination.

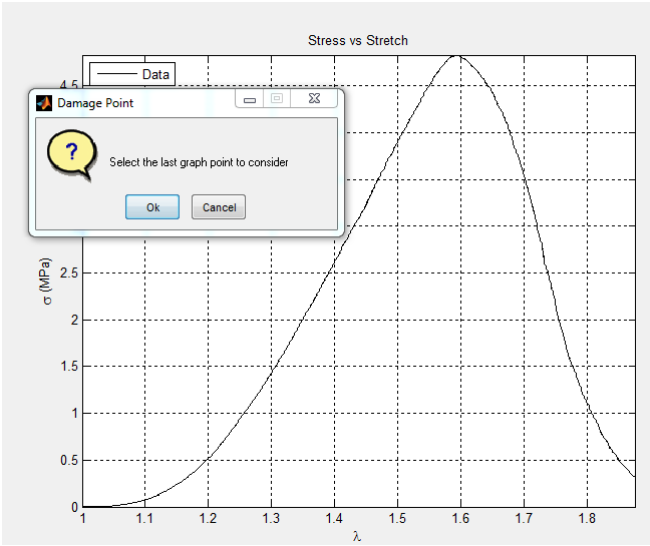

Figure 3.9: Example of the manual process guidance for better parameters' estimation.

3.4 Process Comparison

The parameters' estimation processes were compared relating each analytical curve to a correlation coefficient, R^2, defined by Equation 3.18. This comparison was performed in a MATLAB® code, using the parameters values obtained from both processes and the I_{4_0} and $I_{4_{ref}}$ values of each. To a better understanding of the differences, both analytical curves were plotted in the same graphic for all the samples measured.

$$R^2 = \frac{\sum_{i=1}^{n} \left(\sigma_i^{opt} - \bar{\sigma}^{opt}\right)\left(\sigma_i^{man} - \bar{\sigma}^{man}\right)}{\sqrt{\left(\sum_{i=1}^{n} \left(\sigma_i^{opt} - \bar{\sigma}^{opt}\right)^2\right)\left(\sum_{i=1}^{n} \left(\sigma_i^{man} - \bar{\sigma}^{man}\right)^2\right)}} \tag{3.18}$$

3.5 Statistical Analysis

The statistical analysis was performed using the GraphPad Prism software program version 6.01 (GraphPad Software, Inc).

To understand the age-induced changes of the round and uterosacral ligaments' mechanical properties and material parameters of the Weiss modified model, computed with both processes, a two-way ANOVA test and a Student's t-test were executed.

The uneven results were eliminated and two extractions from the same ligament type of one individual were treated as a single collection and, for data analysis, the mean value was used. All the results are presented by their means and standard errors of the means (SEM).

3.5.1 Two-way ANOVA test

The two-way ANOVA test was performed in order to verify if age could be considered an influence factor on the mechanical properties and material parameters of both ligaments, independently

of the type. Therefore, for this analysis, the samples were divided accordingly to the following criteria:

- less than 50 years (N=15):
  - round ligament (N=8);
  - uterosacral ligament (N=7);
- greater than or equal to 50 years (N=13):
  - round ligament (N=6);
  - uterosacral ligament (N=7).

To compute the confidence intervals and significances, the Sidak's test was chosen. The family-wise significance and level of confidence considered were $\alpha < 0.05$ and 95%.

3.5.2 Student's t-test

As it was necessary to understand the age-effect on each ligament, for the Student's unpaired-samples t-test, all data was divided by the following criteria:

- round ligament (N=14):
  - less than 50 years (N=8);
  - greater than or equal to 50 years (N=6);
- uterosacral ligament (N=14):
  - less than 50 years (N=7);
  - greater than or equal to 50 years (N=7).

The significance level was established as $p<0.05$, assuming a Gaussian distribution of the samples. The calculations were performed for a two-tailed p value.

Chapter 4

Results and Discussion

4.1 Mechanical Properties

4.1.1 Ligaments' aging phenomena

From data processing it was possible to measure several mechanical properties of the round and uterosacral ligaments. For each ligament, their properties were divided in two different age-groups: less and more than 50 years old (-50 and +50, respectively) and statistically analyzed.

In Figure 4.1, a graphic visualization of relevant mechanical properties measured for both the round and uterosacral ligaments can be found. It was also tested if age was considered an influence factor in these properties, independently of the ligament type (two-way ANOVA test). From this analysis it was not observed an overall age-related change. Although, it can be noticed that the round ligament samples are more susceptible to age and a difference between the mechanical properties of the ligaments. Therefore, in Table 4.1 are summarized all the mechanical properties of the round and uterosacral ligaments for the different age-groups considered, as well as the statistical difference calculated between them (Student's t-test). The statistical differences are indicated with boldface numbers. In Appendix (section A.1), the graphic representation of all measurements performed during data processing for the round and uterosacral ligaments can be found in Figures A.1 and A.2, respectively.

The round ligament's tensile strength, revealed to be higher for older individuals even though the ultimate stretch is relatively similar. This fact indicates that, as age progresses, for the same stretch, the tensile strength increases. The higher yield strength and strain energy density can also support this statement, since the amount of energy stored in the samples due to deformations is higher. With age, the T modulus, which is many times associated with the elastic modulus, is significantly higher. As this modulus is almost completely defined by the fibers mechanical work, the increase found may be proof of the fibers age-related increased stiffness (Martins et al., 2013; Rivaux et al., 2013). As these findings are in contrast with the literature review for other ligament types (Iida et al., 2002; Weiss et al., 2005; Tinelli et al., 2010; Petros, 2010), one can propose a different behavior of each tissues with aging. Nonetheless, age may still induce the collagen cellular content to change in quantity and in quality (Woo et al., 1999; Natali et al., 2008). A better understanding of what happens over the years should be complemented with an histological study. The secant modulus (S modulus) also increases. Since this ligament contributes to the maintenance of the uterus' anteversion position in the pelvic cavity, a weaker ligament can contribute to this organs instability or intra-abdominal pain. During pregnancy, the growth of the uterus may cause the stretch of the round ligament, which, in older women, may be compromised.

Concerning the uterosacral ligament, it was not found any age-induced significant difference suggesting that there is no mobility of the pelvic viscera during senescence (Martins, 2013a). As already mentioned in previous studies (Martins, 2013a; Rivaux et al., 2013), normally the uterosacral ligament is stiffer and bears a higher maximum stress than the round ligament, which was also observed during this study. Nevertheless, as the uterosacral ligament has the function to support the uterus in the pelvic cavity, a significant difference in its mechanical properties could end up in this organ's prolapse. This hypothesis could only be verified if a positive control (women with POP) was assessed. Though age is a contributing factor to this disorder, apparently none of the studied individuals (even the older) did suffer from it.

Table 4.1: Analysis of round and uterosacral ligaments' mechanical characteristics as a function of age using Student's unpaired-samples t-test ($p<0.05$). SED - Strain Energy Density. The values displayed are the mean±SEM. Boldface numbers indicate statistical differences.

Mechanical Properties	Round Ligament			Uterosacral Ligament		
	Age N(14)			Age N(14)		
	-50 N(8)	+50 N(6)	p	-50 N(7)	+50 N(7)	p
Tensile strength (MPa)	2.741±0.459	4.475±0.693	0.051	6.893±0.718	5.687±1.485	0.479
Ultimate stretch	1.780±0.066	1.763±0.028	0.833	1.767±0.082	1.660±0.072	0.348
SED	0.920±0.193	1.303±0.170	0.179	2.427±0.457	1.676±0.613	0.345
T modulus	**5.837±0.942**	**11.02±2.279**	**0.039**	13.80±0.817	13.78±2.730	0.994
Yield strength (MPa)	2.187±0.383	3.475±0.514	0.062	5.465±0.549	4.657±1.232	0.561
S modulus	1.670±0.240	2.681±0.548	0.089	4.029±0.501	3.688±0.747	0.712

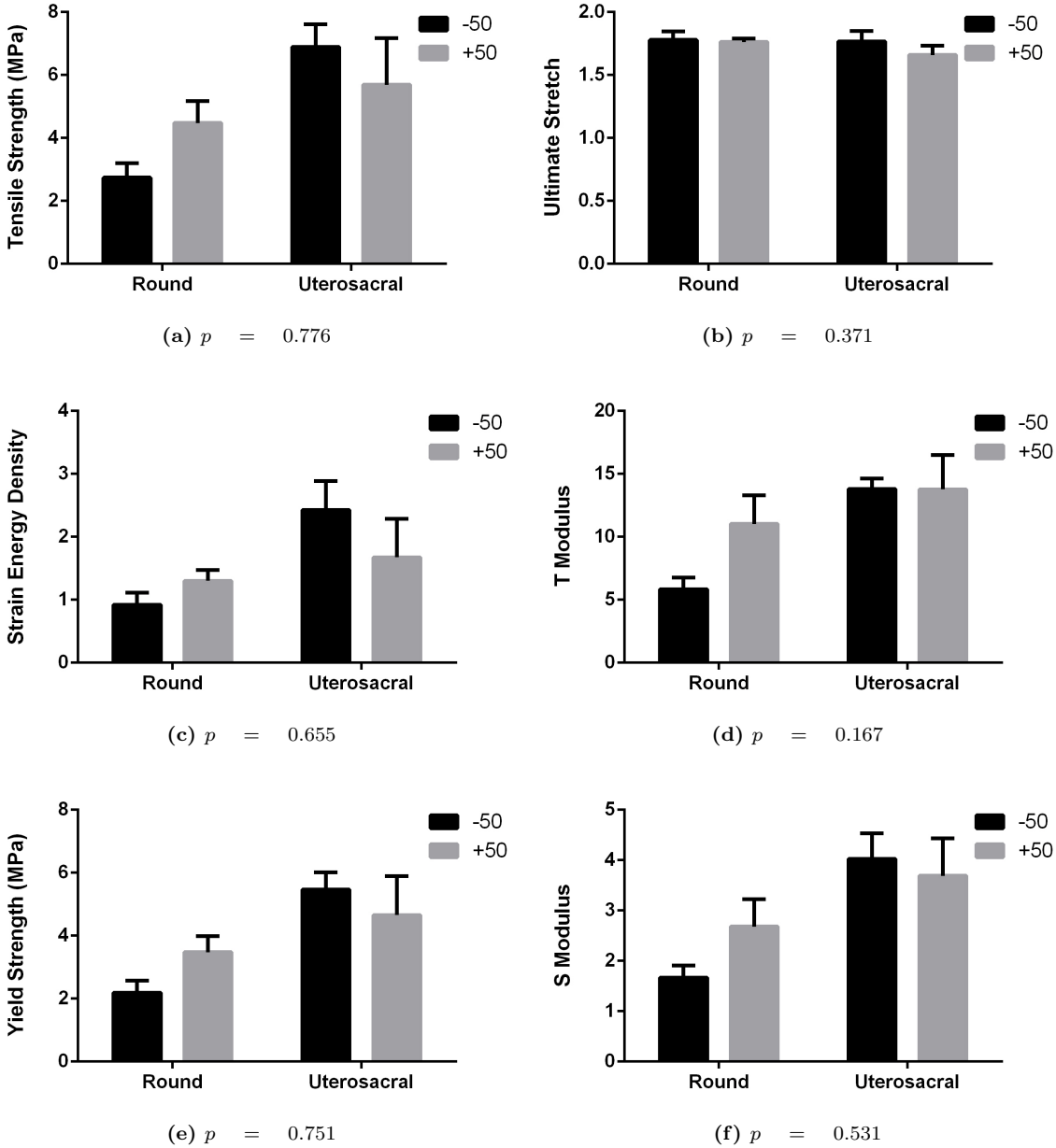

(a) $p = 0.776$ **(b)** $p = 0.371$

(c) $p = 0.655$ **(d)** $p = 0.167$

(e) $p = 0.751$ **(f)** $p = 0.531$

Figure 4.1: Round and uterosacral ligaments' (a) tensile strength, (b) ultimate stretch, (c) strain energy density, (d) T modulus (e) yield strength and (f) S modulus in different age intervals (-50 years and+50). Statistical analysis was performed using a two-way ANOVA test, with $\alpha<0.05$, to test the significant differences of each mechanical property between the age-groups considered, independently of the ligament type.

4.2 Material Parameters' Estimation

After gathering the mechanical properties of the round and uterosacral ligaments, their behavior under uniaxial tension was modeled with Weiss modified material model. Its parameters' estimation was achieved using Martins et al. (2010) optimization process and a developed manual process.

4.2.1 Optimization process

The parameters of all round and uterosacral ligaments' samples were estimated using this process and the values obtained can be consulted in Table B.1 in Appendix (section B.1). Their I_{4_0} and $I_{4_{ref}}$ values are also resumed in the same table.

As the correlation coefficient R^2 off all the samples (both from the round and the uterosacral ligaments) revealed to be close to 1, the Weiss modified material model was confirmed to be suitable for these kinds of tissues and this method a fast process to estimate its parameters. Also, the normalized mean square root error ϵ was, in all cases, was close to 0, as expected.

In Figure 4.2 is an example of this method's result that almost perfectly mimics the incompressible transversely isotropic hyperelastic behavior of the round (Figure 4.2a) and uterosacral (Figure 4.2b) ligaments under uniaxial longitudinal tension. For these two cases the R^2 found were 0.99987 and 0.99977, respectively, and the ϵ results were 0.01112 and 0.01313 for the round and uterosacral samples.

As previously explained, this parameters' fitting was performed for all of the samples collected and from each of them, a small graphic was displayed that demonstrates only the area of elastic deformation considered (until damage point selected) and the correspondent parameters obtained (Figure 4.3).

However, there are some exceptions in which the mechanical behavior of the tissues is not the expected, for example, the one of Figure 4.4. In these cases this model was able to calculate the model parameters, although its R^2 (0.998935) and ϵ (0.0411497) values were not so good.

All the graphic results are available in Appendix (section B.1) in Figures B.1 and B.3, for the round and uterosacral ligaments' samples, respectively. The analytical curves obtained for each ligament can be consulted in Figures B.2 and B.4.

4.2.2 Manual process

All the collected stress-stretch curves from data processing were also modeled with Weiss modified material model, adjusting manually their parameters.

In Table B.2 (Appendix, section B.2) are all the parameters obtained with the manual method and correspondent correlation coefficients. Each of the I_{4_0} and $I_{4_{ref}}$ considered points are also written.

From the R^2 values it was possible to classify this material model and implementation method, reliable for both ligaments' behavior under uniaxial tension in the fiber direction. The best fitting obtained with the round ligament samples was the 11th individual, sample 2 ($R^2 = 0.99994$), whereas with the uterosacral samples was the individual number 17 ($R^2 = 0.99990$). Both results can be seen in Figures 4.5a and 4.5b, respectively. It can be observed an almost perfect overlap of the two analytical curves with the correspondent experimental data.

Exceptional cases, as the one explained in the Optimization process section, were also not possible to model so perfectly as others, as can be seen in Figure 4.6. However, in these situations, it can be set a compromise between the regions that the user desires to overlap. If the ligament will only be subjected to a smaller stretch, the first and second regions of the graphic can be almost

perfectly modeled, jeopardizing the rest of the graphic. In other scenario, it could be important to analyze the fibers work, being necessary to achieve a perfectly linear behavior in the last third of the graphic. These different situations are exemplified in Figures 4.7a and 4.7b, respectively.

The manual fitting of the analytical function allowed a better understanding of its parameters relationship and influence in the overall result. c_1 was thought to be strictly responsible for the first part of the graphic (matrix mechanical response, $\bar{\mathbf{I}}_4 < \bar{\mathbf{I}}_{4_0}$) but it also influences the rest of it by establishing an initial slope for the rest of the graphic. c_3 and c_4 only take part in the heel region function (matrix and fibers response) defining the slope and exponential behavior of the graphic, respectively. A smaller c_3 value characterizes a larger stretch for a certain stress and a larger c_4 allows a higher stretch dependency. These three parameters are the independent ones, manually controlled and their values have consequences on the rest of the graphic (fibers mechanical response under tension) by defining c_5, c_6 and c_7, the dependent parameters. These are the ones responsible for linear region, designing a linear continuity from $I_{4_{ref}}$ until the elastic limit - end of the graphic.

Moreover, the complete user-dependent fitting of the curve, despite being a time-consuming process, enables the constant adjustment of the different graphic limits (I_{4_0} and $I_{4_{ref}}$) which strongly influences a better modeling result. Therefore, the complete manipulation of the parameters and graphic regions allows a positive control of curve fitting, leading to good results.

The fitting results of this method, for the round and uterosacral ligaments, are available in Figures B.5 and B.7 of Appendix B.2, respectively. The analytical curves computed for each ligament can be verified in Figures B.6 and B.8.

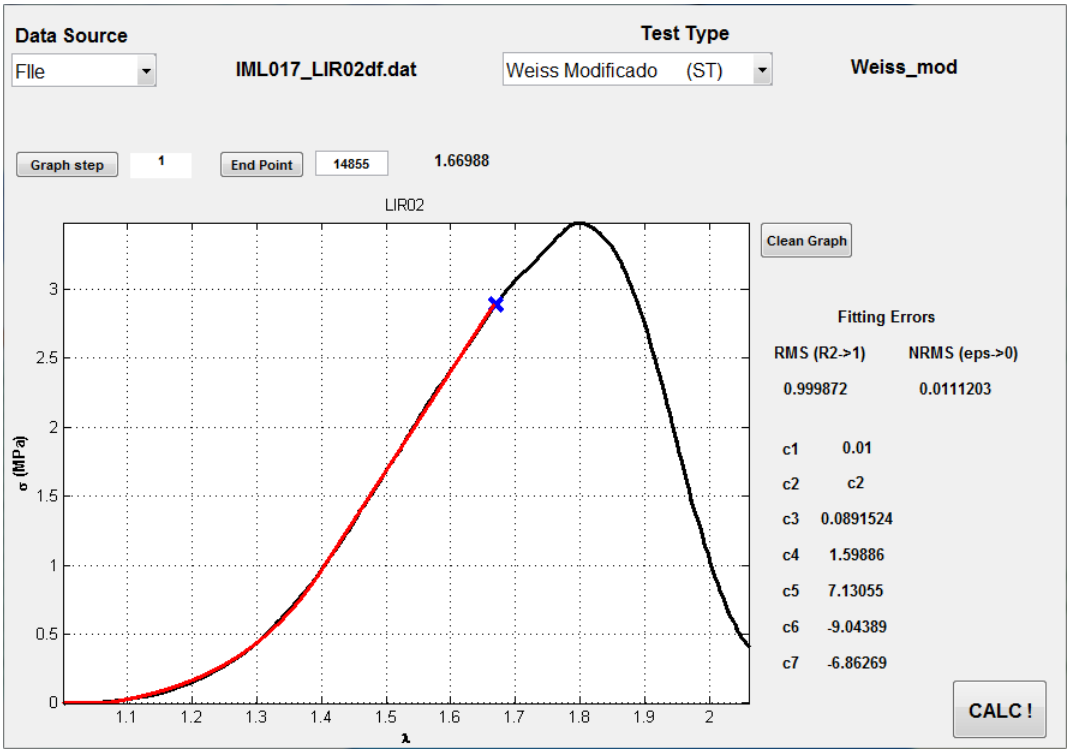

(a) Round ligament sample

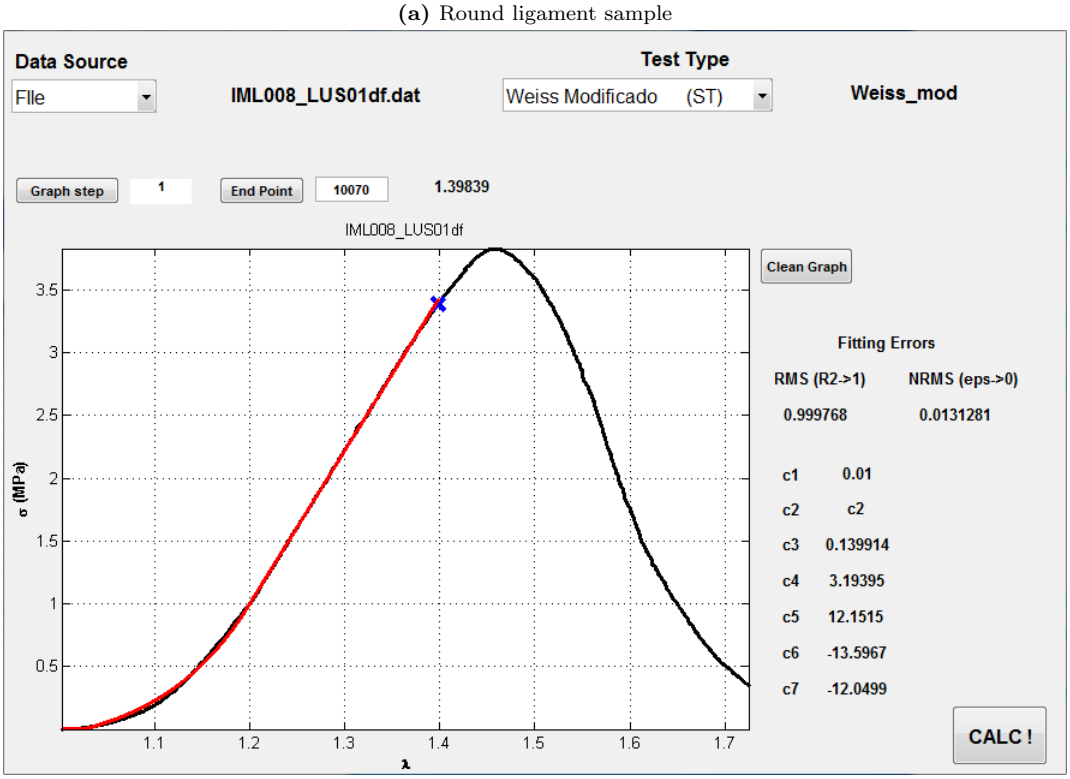

(b) Uterosacral ligament sample

Figure 4.2: Result obtained from the optimization process parameters' fitting, using Weiss modified model for the round and uterosacral ligaments' samples.

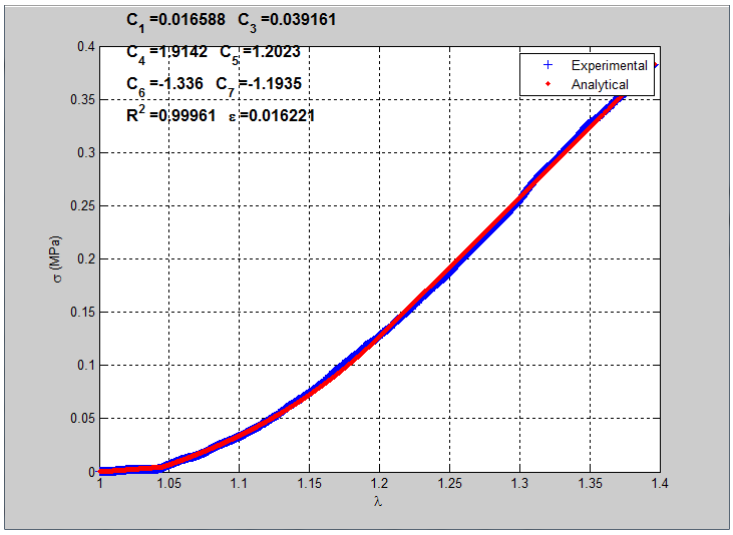

Figure 4.3: Curve fitting of the optimization process of the elastic region selected from the original stress-stretch graphic.

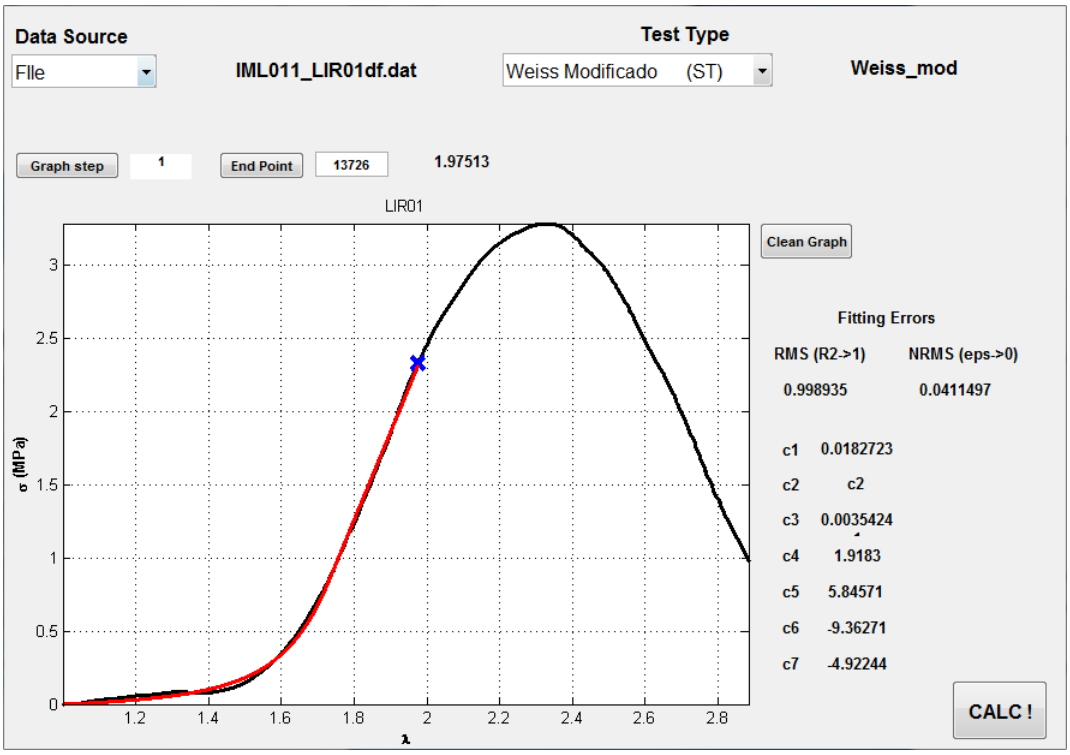

Figure 4.4: Abnormal behavior of a round ligament sample and respective parameters' estimation with the optimization process.

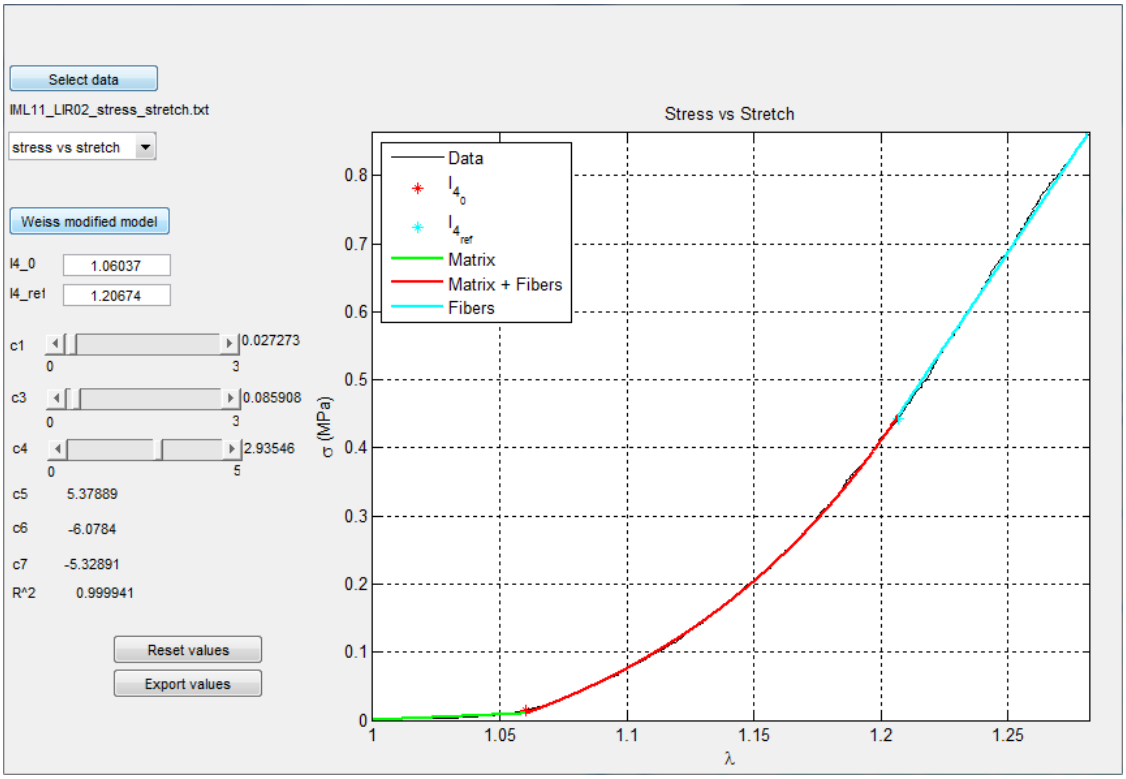

(a) Round ligament sample

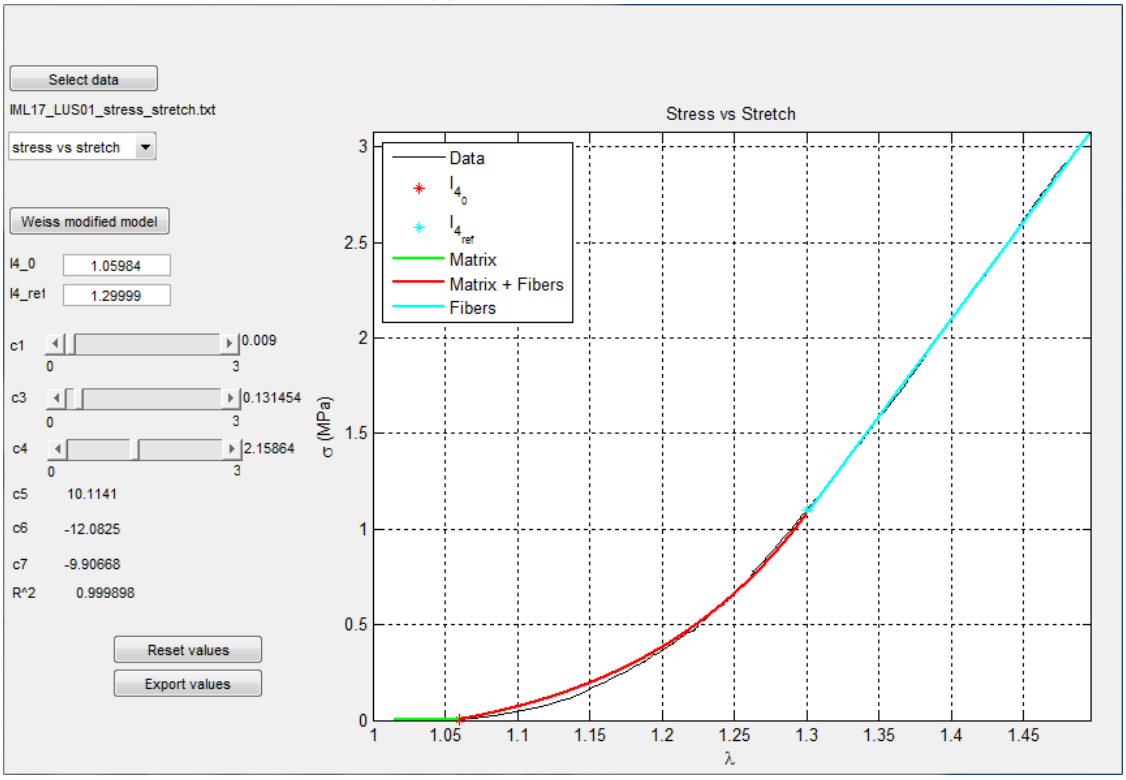

(b) Uterosacral ligament sample

Figure 4.5: Best results obtained with the manual parameters' estimation process.

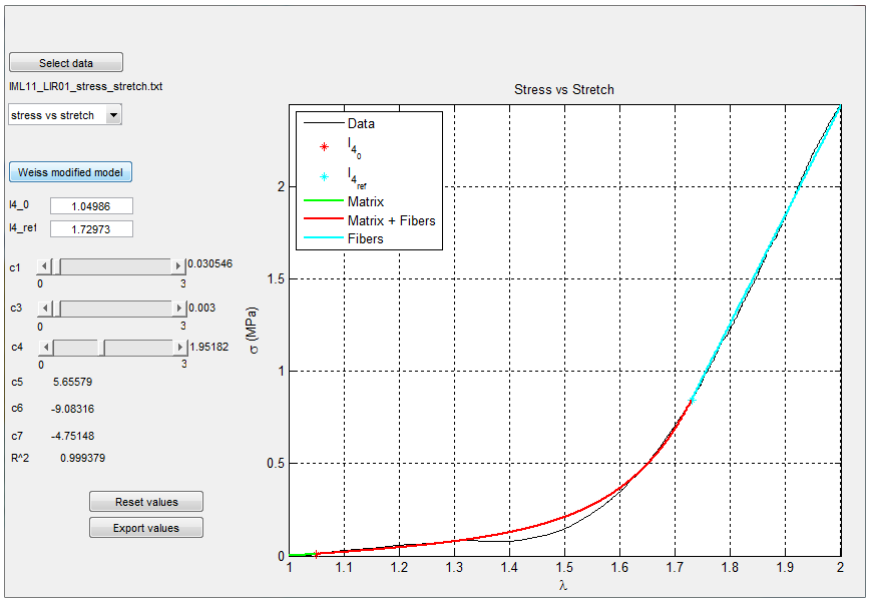

Figure 4.6: Abnormal behavior of a round ligament sample and respective parameters' estimation with the manual process.

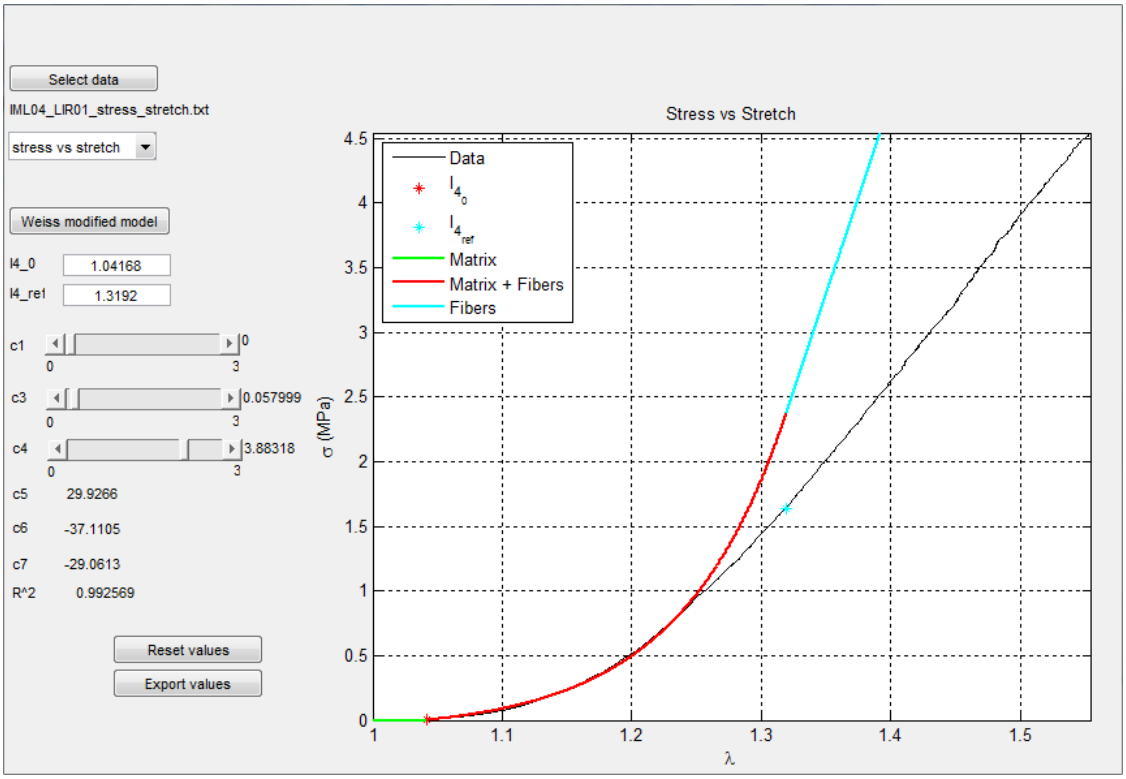

(a) Nearly perfect overlap of the matrix and matrix+fibers response

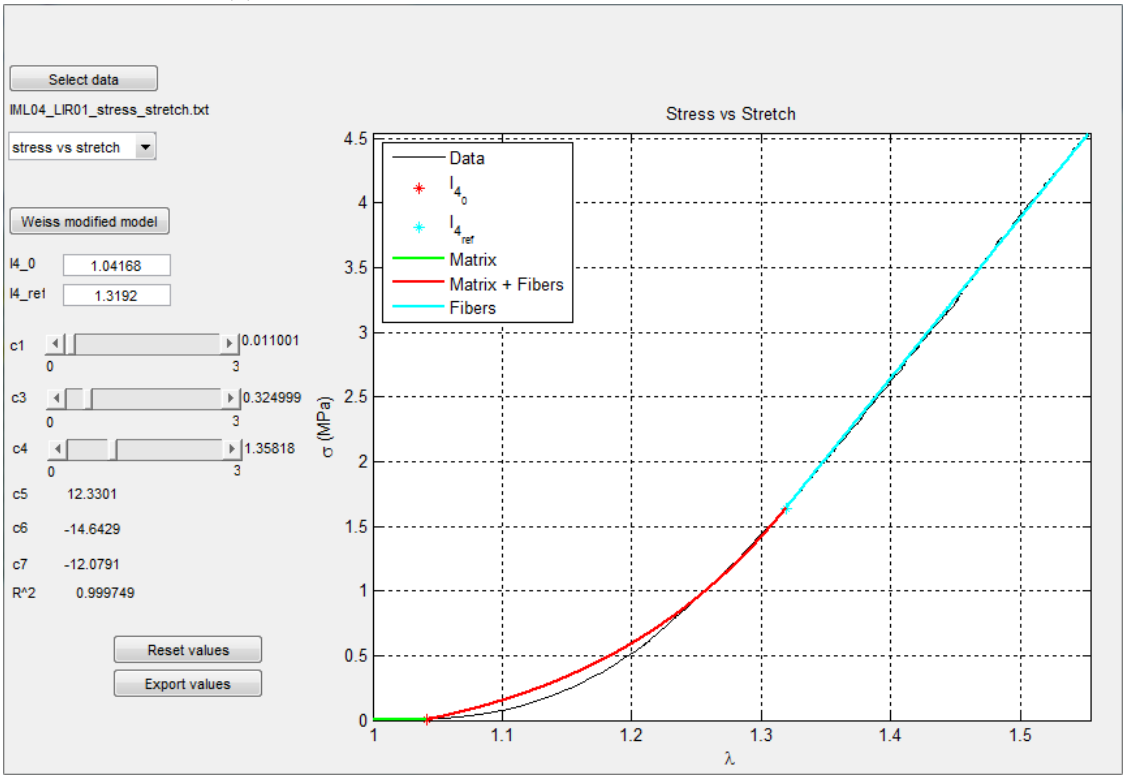

(b) Nearly perfect overlap of the fibers response

Figure 4.7: Two different perfect curve fitting regions that compromise the rest of the model, with manual process.

4.3 Age-related Changes of Material Parameters

The Weiss modified model parameters define an analytical curve that was designed to mimic the material's behavior under tension. This behavior, as analyzed in previous sections, may change with age progression. Therefore, comprehension of the different parameters values for different life spans is an important factor that would allow one to establish an age-dependent model that could more precisely be used in simulations of these tissues' behavior.

Therefore, the parameters obtained, for both round and uterosacral ligament samples, with the optimization and manual processes described above were divided in two different age-groups (-50 and +50) and statistical differences were analyzed.

4.3.1 Optimization process

As the optimization process enabled an accurate parameters' fitting, these were divided into separate age-groups (-50 and +50) and were analyzed using Student's unpaired samples t-test with $p < 0.05$ for the round and uterosacral ligament samples. The resultant means and standard errors of the means are written down in Table 4.2. The boldface numbers indicate that statistical differences were found between the different age groups considered. A graphical representation of these values is also showed in Figure 4.8. In these, it was evaluated the influence of aging in the tissues considered, regardless of the ligament type and, for each parameter, the p value obtained for this test is displayed.

It can be noticed in Figure 4.8 that age is not a relevant factor when considering both ligaments. However, there are visible differences between all the parameters values of round and uterosacral ligaments with exception of c_4, and in some, a difference among the age-groups. Likewise, I_{4_0} and $I_{4_{ref}}$ were not found to be different between both ligaments and with advancing age.

Consulting Table 4.2, statistical differences were observed for parameters c_5, c_6 and c_7 of the round ligament samples: their values increase in modulus as age evolves. As these parameters are associated with the fibers response to tension, these differences support the ones found for the T modulus in section 4.1.1. Thereby, an increase in these parameters modulus may be proof of the ligaments' higher stiffness.

In contrast, the uterosacral samples did not show a age-related significant difference in their parameters values. This fact does not allow the establishment of age-influenced parameters for the Weiss modified model, but it can set and approximation of the inherent uterosacral ligament parameters.

Thus, for future round ligament Weiss modified material modeling with the optimization process the parameters values should be close to

$c_1 = 0.016 \pm 0.003$	c_5 (-50) $= 5.854 \pm 0.940$	c_5 (+50) $= 11.200 \pm 2.347$
$c_3 = 0.520 \pm 0.350$	c_6 (-50) $= -7.104 \pm 1.179$	c_6 (+50) $= -14.20 \pm 3.080$
$c_4 = 1.757 \pm 0.208$	c_7 (-50) $= -5.693 \pm 0.911$	c_7 (+50) $= -10.70 \pm 2.248$

Regarding the uterosacral ligament's parameters, their values should be close to

$c_1 = 0.013 \pm 0.003$	$c_4 = 1.664 \pm 0.265$	$c_6 = -16.73 \pm 1.658$
$c_3 = 0.657 \pm 0.241$	$c_5 = 13.86 \pm 1.359$	$c_7 = -13.49 \pm 1.326$

When no significant differences where found among different ages, the parameters were calculated taking into account all measurements of the same ligament.

The average stretch values that define the graphic limits of ligamentous tissue for Weiss modified model were found to be approximately $I_{4_0} = 1.061 \pm 0.004$ and $I_{4_{ref}} = 1.350 \pm 0.012$. Since these features did not present any significant differences between the ligaments and their age groups, the calculations was made with all values measured.

In section C.1 of Appendix, the values of Table 4.2 are graphically represented in Figure C.1 for the round ligament samples parameters and Figure C.2 for the uterosacral samples.

Table 4.2: Analysis of round and uterosacral ligaments' material constants as a function of age, obtained with the optimization process. Statistical analysis was performed using Student's unpaired-samples t-test (p<0.05). Boldface numbers demonstrate significant differences found. The material constants are in MPa.

Parameters	Round Ligament			Uterosacral Ligament		
	Age N(14)			Age N(14)		
	-50 N(8)	+50 N(6)	p	-50 N(7)	+50 N(7)	p
c_1	0.017±0.005	0.014±0.003	0.670	0.016±0.006	0.010±1.02E-7	0.337
c_3	0.139±0.043	1.029±0.805	0.221	0.976±0.452	0.337±0.112	0.195
c_4	1.778±0.266	1.729±0.361	0.912	1.639±0.477	1.690±0.278	0.927
c_5	**5.854±0.940**	**11.200±2.347**	**0.037**	13.830±0.801	13.880±2.712	0.987
c_6	**-7.104±1.179**	**-14.200±3.080**	**0.034**	-16.540±0.969	-16.920±3.310	0.915
c_7	**-5.693±0.911**	**-10.730±2.248**	**0.040**	-13.500±0.800	-13.490±2.642	0.998
I_{4_0}	1.063±0.011	1.064±0.006	0.931	1.053±0.010	1.063±0.004	0.402
$I_{4_{ref}}$	1.328±0.042	1.416±0.024	0.125	1.327±0.045	1.342±0.038	0.805

4.3.2 Manual process

The manual process, in its turn, also accurately determined the material parameters of both the round and uterosacral ligaments. The age-related differences found in their values are summarized in Table 4.3 and Figure 4.9. In the same way as described before, the parameters obtained for each type of ligament samples were divided in two groups considering the age of the individual (-50 or +50).

From Figure 4.9, one can notice that no significant differences are associated to age when it comes to both tissues considered. For all parameters, the p value obtained from the two-way ANOVA test was always higher than the confidence interval established. However, the ligaments present a difference between them and, in some cases, in the same ligament type are observable differences associated with age.

A smaller c_1 value for the uterosacral ligament when comparing to the round ligament may suggest that, for the same stretch point (at a low deformation), the round ligament is under a higher tension, concerning the matrix response region. This relation can only be set since the I_{4_0} stretches are similar with age and for either ligaments.

Table 4.3 indicates the differences found between the -50 and +50 years for each pelvic ligaments by means of a Student's unpaired t-test, with $p < 0.05$. One can start by noticing that these

results are in conformity with the optimization process. In section C.2 are these values graphical representation for round (Figure C.3) and uterosacral (Figure C.4) ligament samples.

Table 4.3: Analysis of round and uterosacral ligaments' material constants as a function of age, obtained with the manual process. Statistical analysis was performed using Student's unpaired-samples t-test (p<0.05). Boldface numbers demonstrate significant differences found. Material constants are in MPa.

Parameters	Round Ligament			Uterosacral Ligament		
	Age N(14)			Age N(14)		
	-50 N(8)	+50 N(6)	p	-50 N(7)	+50 N(7)	p
c_1	0.017±0.004	0.021±0.007	0.623	**0.009±0.002**	**0.016±0.002**	**0.016**
c_3	0.114±0.022	0.131±0.030	0.660	0.443±0.134	0.276±0.091	0.320
c_4	1.877±0.318	2.042±0.247	0.706	1.811±0.403	2.026±0.380	0.704
c_5	5.972±0.978	11.200±2.557	0.055	13.950±0.832	13.610±2.815	0.912
c_6	-7.282±1.240	-14.240±3.436	0.055	-16.680±0.984	-16.560±3.454	0.974
c_7	-5.797±0.945	-10.730±2.424	0.057	-13.610±0.834	-13.240±2.773	0.901
I_{4_0}	1.048±0.075	1.060±0.004	0.243	1.049±0.010	1.061±0.005	0.323
$I_{4_{ref}}$	1.334±0.045	1.396±0.028	0.304	1.321±0.043	1.329±0.039	0.881

Significant differences were found for c_1 parameters for the lifespans considered in the uterosacral ligament samples. The increased value with age may suggest an increase role of the matrix in the supporting tissues. It may also suggest the improved accuracy obtained with the manual determination of parameters, since, with the optimization process, no significant differences were found even thought in the last the standard error of means are smaller.

The p values obtained when comparing c_5, c_6 and c_7 of the round ligament with different ages did not show significant differences, in contrary of what was observed with the optimization process. Nevertheless, these parameters can be considered significantly different for a confidence interval of 90% ($p < 0.10$). Again, it could be set a relationship between the significant age-related differences of the round ligament's T modulus calculated and the obtained c_5, c_6 and c_7 parameters of Weiss modified material model. As both property and parameters define the fibers mechanical response to tension, it could be established an age-dependent relationship.

Moreover, beyond the similarity of the all parameters obtained with both processes for different ligaments and their age-groups, c_5 values are nearly equal to the correspondent T modulus values. These findings can support both methods implementation and properties calculations once both are responsible for the same region of graphical slope.

The material parameters for the round ligaments behavior, modeled with Weiss modified material model, obtained with the manual process were close to

$c_1 = 0.018 \pm 0.004$ $\quad$ c_5 (-50) $= 5.972 \pm 0.978$ $\quad$ c_5 (+50) $= 11.200 \pm 2.557$

$c_3 = 0.121 \pm 0.018$ $\quad$ c_6 (-50) $= -7.282 \pm 1.240$ $\quad$ c_6 (+50) $= -14.24 \pm 3.436$

$c_4 = 1.948 \pm 0.204$ $\quad$ c_7 (-50) $= -5.797 \pm 0.945$ $\quad$ c_7 (+50) $= -10.73 \pm 2.424$

In other hand, the uterosacral ligament parameters were

c_1 (-50)=0.009 ± 0.003	c_3 =0.360 ± 0.081	c_5 =13.780 ± 1.411	c_7 =-13.420 ± 1.375
c_1 (+50)=0.016 ± 0.002	c_4 =1.918 ± 0.268	c_6 =-16.62 ± 1.725	

Because I_{4_0} and $I_{4_{ref}}$ were similar in all samples the correspondent averages are 1.054 ± 0.004 and 1.343 ± 0.020. These values were calculated in accordance with the optimization process.

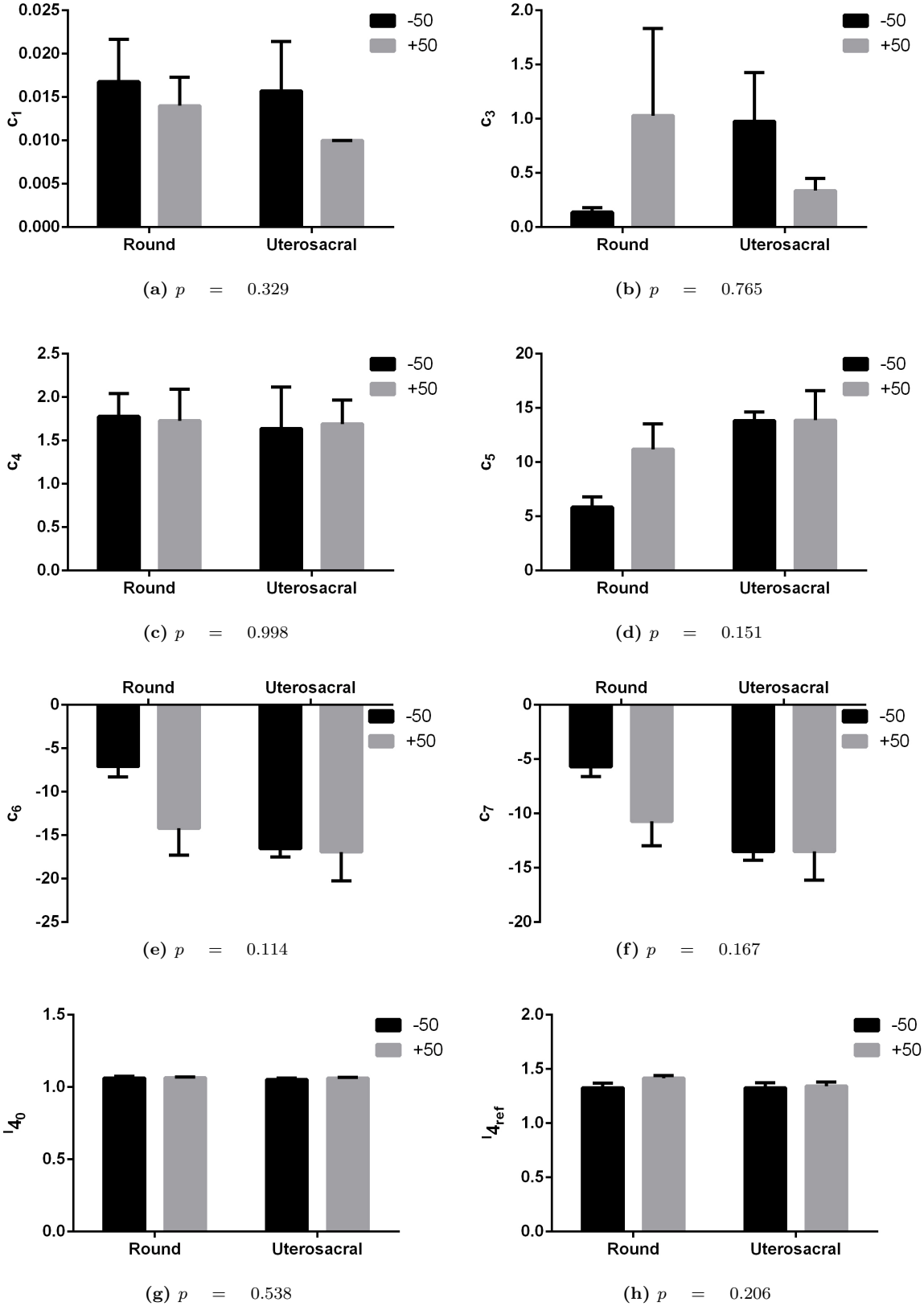

(a) $p = 0.329$ **(b)** $p = 0.765$

(c) $p = 0.998$ **(d)** $p = 0.151$

(e) $p = 0.114$ **(f)** $p = 0.167$

(g) $p = 0.538$ **(h)** $p = 0.206$

Figure 4.8: Round and uterosacral ligaments' material parameters, obtained with optimization process: (a) c_1, (b) c_3, (c) c_4, (d) c_5, (e) c_6, (f) c_7, (g) I_{4_0} and (h) $I_{4_{ref}}$ for different lifespans (with less and more than 50 years of age). Statistical analysis was performed using a two-way ANOVA test, with α<0.05, to test the influence of age in the parameters, independently of the ligament type. Material constants are in MPa.

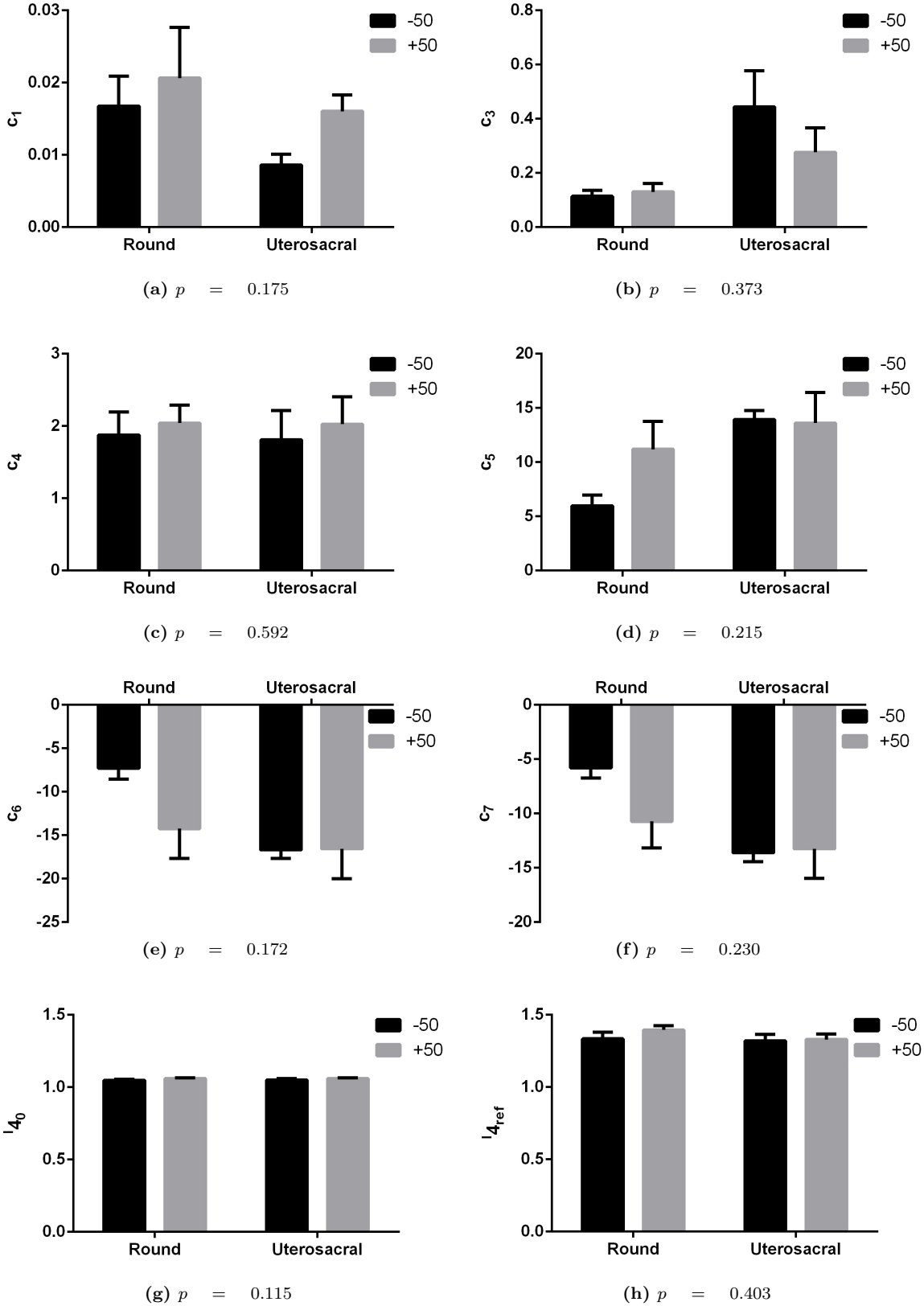

(a) $p = 0.175$ (b) $p = 0.373$

(c) $p = 0.592$ (d) $p = 0.215$

(e) $p = 0.172$ (f) $p = 0.230$

(g) $p = 0.115$ (h) $p = 0.403$

Figure 4.9: Round and uterosacral ligaments' material parameters, obtained with manual process: (a) c_1, (b) c_3, (c) c_4, (d) c_5, (e) c_6, (f) c_7, (g) I_{4_0} and (h) $I_{4_{ref}}$ for different lifespans (with less and more than 50 years of age). Statistical analysis was performed using a two-way ANOVA test, with α<0.05, to test the influence of age on the parameters, independently of the ligament type. Material constants are in MPa.

4.4 Process Comparison

Previous sections about parameters' estimation processes, demonstrated that both processes enabled to fulfill the proposed goal: to establish age-dependent parameters of Weiss modified material model of pelvic floor ligaments, in this particular case, the round and uterosacral ligaments. Now, it becomes important to compare the optimization and manual processes.

The similar results are proof of both methods good implementation, giving reliability to each other. Despite being a slower process to determinate the material parameters, the manual method allowed more flexibility, contributing to better correlation coefficients, as can be seen in Table 4.4. In this table are indicated the obtained correlation coefficients of each sample with both methods.

Table 4.4: Correlation coefficients obtained for all round and uterosacral ligaments' samples considered using the optimization and manual processes. OP - optimization process; MP - manual process.

Round Ligament			Uterosacral Ligament		
Sample	R^2_{OP}	R^2_{MP}	Sample	R^2_{OP}	R^2_{MP}
IML01	0.9991	0.9993	IML01	0.9997	0.9997
IML02	0.9987	0.9996	IML02-1	0.9996	0.9994
IML03	0.9995	0.9998	IML02-2	0.9996	0.9997
IML04-1	0.9997	0.9998	IML03	0.9992	0.9998
IML04-2	0.9997	0.9998	IML04-1	0.9996	0.9998
IML05-1	0.9995	0.9996	IML04-2	0.9997	0.9999
IML05-2	0.9997	0.9998	IML05	0.9995	0.9998
IML06	0.9995	0.9999	IML06	0.9989	0.9992
IML07	0.9998	0.9999	IML07	0.9997	0.9999
IML08	0.9995	0.9998	IML08	0.9998	0.9999
IML09	0.9994	0.9996	IML10-1	0.9993	0.99934
IML10	0.9996	0.9996	IML10-2	0.9997	0.9998
IML11-1	0.9989	0.9994	IML11	0.9997	0.9999
IML11-2	0.9991	0.9999	IML12	0.9998	0.9998
IML12	0.9996	0.9998	IML13	0.9986	0.9999
IML13-1	0.9998	0.9999	IML15	0.9995	0.9997
IML13-2	0.9965	0.9962	IML17-1	0.9997	0.9999
IML17-1	0.9995	0.9998	IML17-2	0.9990	0.9998
IML17-2	0.9999	0.9999			

In addition, as was demonstrated in previous examples (Figures 4.7a and 4.7b), with the manual process it was possible to mimic a certain region of the graphic, compromising the rest of it. This may be useful when the user only wants to model the behavior of the tissues until a certain stress or stretch. Or, in the other hand, if the user wishes to get a perfect modulation of the fibers work or after a certain stress/stretch.

By comparing each of the curves that modeled both ligaments behavior under longitudinal tension a correlation was also calculated and annotated in Table 4.5. This gave another evidence of the similarly between results for both processes, supporting the reliability of the implementation of Weiss modified material model. In Figure D.1 of the Appendix (section D) are the resultant graphics of the analytical curves obtained by parameters' fitting with manual and optimized processes of the round ligament and in Figure D.2 of the uterosacral ligament. As expected from the correlation results, the two curves almost overlap.

Thus, both processes revealed to be accurate for Weiss modified model parameters' fitting and no greater differences were found between them. The optimization process was the faster way to determinate the material constants, whereas the manual process enabled a higher manipulation of the analytical model, and a better understanding of the parameters influence on the general graphical outcome.

Table 4.5: Comparison of the parameters' estimation processes - correlation coefficient (R^2) - for the round and uterosacral ligaments' specimens.

Round Ligament		Uterosacral Ligament	
Sample	R^2	Sample	R^2
IML01	0.99980	IML01	0.99997
IML02	0.99989	IML02-1	0.99985
IML03	0.99975	IML02-2	0.99998
IML04-1	0.99998	IML03	0.99985
IML04-2	0.99999	IML04-1	0.99998
IML05-1	0.99993	IML04-2	0.99995
IML05-2	0.99999	IML05	0.99996
IML06	0.99991	IML06	0.99998
IML07	0.99999	IML07	0.99999
IML08	0.99997	IML08	0.99999
IML09	0.99992	IML10-1	0.99986
IML10	0.99988	IML10-2	0.99995
IML11-1	0.99986	IML11	0.99999
IML11-2	0.99999	IML12	0.99997
IML12	0.99999	IML13	0.99987
IML13-1	0.99999	IML15	0.99999
IML13-2	0.99949	IML17-1	0.99998
IML17-1	0.99995	IML17-2	0.99994
IML17-2	0.99999		

Chapter 5

Conclusions

5.1 Conclusions

From the results obtained, it can be concluded that age does not play a similar effect in the round and uterosacral ligaments. For instance, the round ligament's mechanical properties revealed to be more susceptible to age-related changes: the tensile and yield strength as well as the strain energy density and T modulus increase as age progresses. These may be due to the different collagen quantity and quality of this tissues during senescence. On the other hand, uterosacral ligaments did not show an age dependency. Their higher strength and stiffness is characteristic of their role in the support of pelvic viscera

Considering the model formulation, Weiss modified material model proved to be a suitable option. One can also conclude that both the optimization and manual processes were good methods for this model implementation. The automatic and manual parameters' fitting was adequate even when the samples behavior under tension was relatively different to the theoretical prediction. In these situations, the higher degree of curve manipulation of the manual process enables to accurately fit a desired graphic region, compromising the rest of the fitting.

Evaluating the parameters and graphical limits, age-induced changes demonstrated that although the I_{4_0} and $I_{4_{ref}}$ limits did not change significantly with age, the ligaments parameters had a different behavior. The parameters obtained for each ligament were different. As its mechanical properties, the round ligament material parameters c_5, c_6 and c_7 were significantly different for the lifespans considered. This result was supported by both estimation processes. However, the uterosacral ligament showed inherent parameters that are not age-influenced.

In conclusion, different tissues behave differently against the age factor, with varying mechanical responses under tension. These changes can be accurately modeled by Weiss modified material model, with its parameters estimated using both the optimization and manual processes.

5.2 Future Work

An improvement to this work would be the assessment of the performed tests in living tissues, instead of cadaveric and with a larger number of samples for each type of ligament. With this, the results would be more reliable and conclusive, rising less questions regarding the samples quality. It could also be possible to divide the samples into more specific age groups, allowing a more accurate study of the age-related changes.

Other types of ligaments, important for pelvic support, as the broad and the cardinal ligament would also be an interesting subject for this study.

Histological and immunohistochemical analysis of the tissues studied could support the hypothesis raised regarding the quantity and quality of collagen content of samples.

Pelvic organ prolapse cases could be used as positive control, establishing a relationship between the damaged and undamaged tissues. A interrelated study of the aging process and pairity would also be an interesting effect to study.

A future development could be the automatic determination of the I_{4_0} and $I_{4_{ref}}$ values, by derivative analysis of the experimental curve. With this, the automatic process could be more precise and user-independent.

Appendices

Appendix A

Mechanical Properties

A.1 Aging phenomena

A.1.1 Round ligament

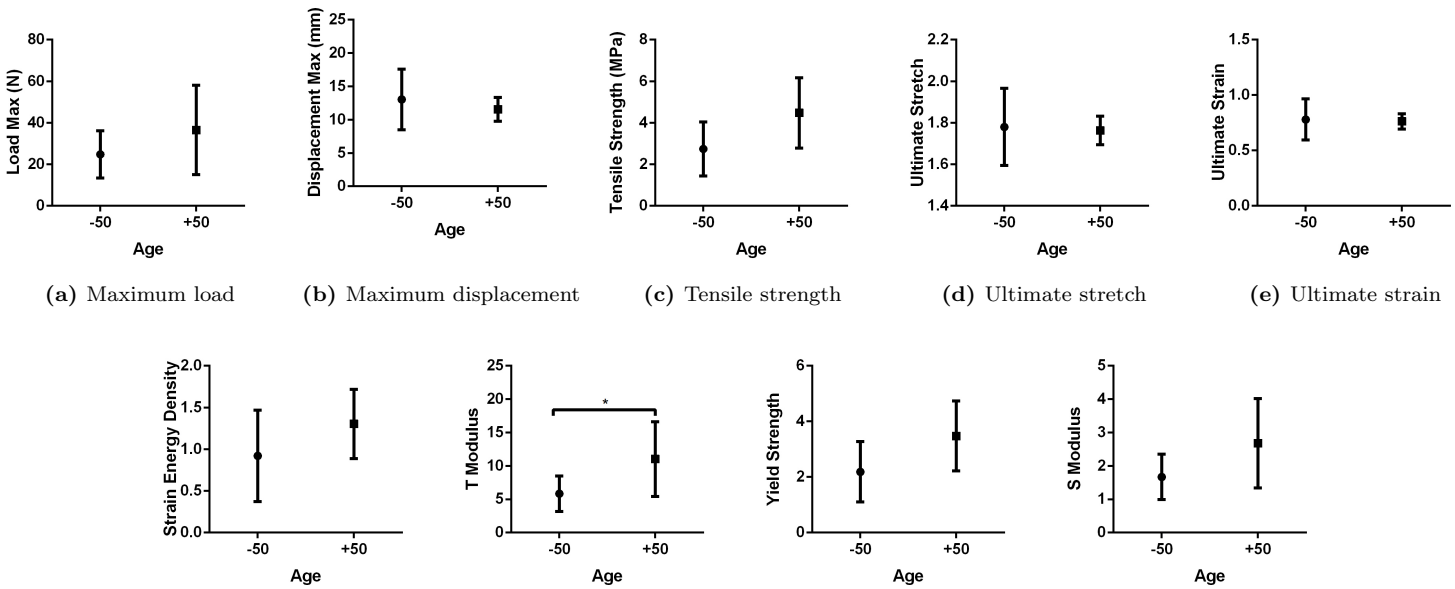

(a) Maximum load **(b)** Maximum displacement **(c)** Tensile strength **(d)** Ultimate stretch **(e)** Ultimate strain

(f) Strain energy density **(g)** T modulus **(h)** Yield strength **(i)** S modulus

Figure A.1: All measurements obtained from the experimental data processing of the round ligament, for the different age groups considered. Statistical analysis was performed using Student's unpaired-samples t-test, with $p<0.05$. (*) implies significant differences.

A.1.2 Uterosacral ligament

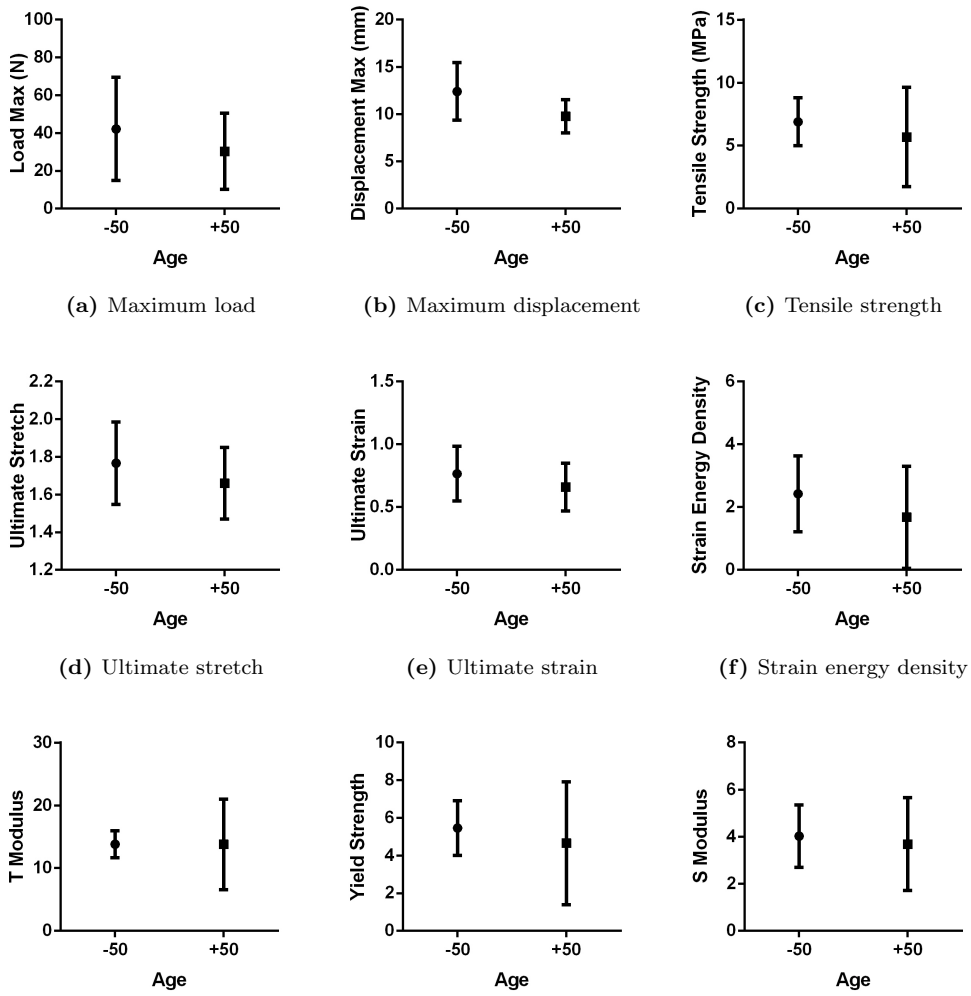

(a) Maximum load **(b)** Maximum displacement **(c)** Tensile strength

(d) Ultimate stretch **(e)** Ultimate strain **(f)** Strain energy density

(g) T modulus **(h)** Yield strength **(i)** S modulus

Figure A.2: All measurements obtained from the experimental data processing of the uterosacral ligament, for the different age groups considered. Statistical analysis was performed using Student's unpaired-samples t-test, with $p<0.05$. (*) implies significant differences.

Appendix B

Material Parameters' Estimation

B.1 Optimization process

Table B.1: Material constants for the round and uterosacral ligaments obtained with Weiss modified model optimization process. Constant values are in MPa.

Round Ligament											
Age	Sample	c_1	c_3	c_4	c_5	c_6	c_7	I_{4_0}	$I_{4_{ref}}$	R^2	ϵ
51	IML01	0.0100	0.1119	1.9166	20.6780	-27.3650	-19.6003	1.0586	1.4494	0.9991	0.0349
51	IML02	0.0100	0.2534	0.6783	5.7008	-7.3341	-5.4482	1.0828	1.4703	0.9987	0.0345
51	IML03	0.0100	0.5600	0.8171	13.7891	-17.2758	-13.3053	1.0750	1.4193	0.9995	0.0219
47	IML04-1	0.0100	0.1655	2.1435	12.2131	-14.4713	-11.9829	1.0501	1.2910	0.9997	0.0169
	IML04-2	0.0118	0.0207	3.3997	3.4654	-4.1193	-3.4009	1.0618	1.2703	0.9997	0.0184
43	IML05-1	0.0100	0.1039	2.8313	10.8548	-12.6689	-10.6884	1.0455	1.2572	0.9995	0.0212
	IML05-2	0.0100	0.0567	1.1216	3.8006	-5.1844	-3.5516	1.1207	1.5252	0.9997	0.0179
40	IML06	0.0500	0.0815	1.4953	7.7754	-10.4135	-7.3344	1.1191	1.4775	0.9995	0.0235
33	IML07	0.0100	0.1172	2.4926	8.0153	-9.1384	-7.9236	1.0334	1.2336	0.9998	0.0122
36	IML08	0.0100	0.1778	1.3658	3.5136	-3.8535	-3.4912	1.0236	1.2019	0.9995	0.0185
18	IML09	0.0168	0.4207	0.3181	3.6125	-4.6244	-3.4521	1.0717	1.4991	0.9994	0.0212
38	IML10	0.0100	0.0990	1.894	7.5429	-9.2441	-7.3395	1.0701	1.3412	0,9996	0.0209
59	IML11-1	0.0183	0.0035	1.9183	5.8457	-9.3627	-4.9224	1.0579	1.7270	0.9989	0.0411
	IML11-2	0.0100	0.0338	4.2621	5.4860	-6.1823	-5.4363	1.0279	1.1960	0.9991	0.0294
40	IML12	0.0166	0.0392	1.9142	1.2023	-1.3360	-1.1935	1.0449	1.2017	0.9996	0.0162
51	IML13-1	0.0100	0.0773	3.7448	9.2362	-10.5095	-9.1400	1.0477	1.2104	0.9998	0.0122
	IML13-2	0.0500	9.9999	0.0363	8.2863	-10.6787	-7.8924	1.0905	1.5420	0.9965	0.0520
65	IML17-1	0.0100	0.2954	2.3627	18.0671	-20.6564	-17.8534	1.0409	1.2380	0.9995	0.0197
	IML17-2	0.0100	0.0892	1.5989	7.1306	-9.0439	-6.8627	1.0696	1.4005	0.9999	0.0111
Uterosacral Ligament											
Age	Sample	c_1	c_3	c_4	c_5	c_6	c_7	I_{4_0}	$I_{4_{ref}}$	R^2	ϵ
51	IML01	0.0100	0.1490	2.5100	11.8648	-13.9497	-11.6673	1.0649	1.2601	0.9997	0.0181
51	IML02-1	0.0100	0.7610	0.9799	17.6009	-20.9088	-17.2352	1.0481	1.3334	0.9996	0.0172
	IML02-2	0.0100	0.4073	0.8657	20.1475	-27.6834	-18.7297	1.099 0	1.5586	0.9996	0.0187
51	IML03	0.0100	0.2550	0.7717	8.7374	-11.5810	-8.2500	1.0737	1.5135	0.9992	0.0281
47	IML04-1	0.0100	0.4300	1.2089	22.2298	-28.8383	-21.2259	1.1081	1.4445	0.9996	0.0200
	IML04-2	0.0100	0.0973	2.0951	6.0296	-7.0659	-5.9303	1.0521	1.2759	0.9997	0.0153
43	IML05	0.0100	0.1167	3.1141	16.1396	-18.6411	-15.9189	1.0160	1.2434	0.9995	0.0200
40	IML06	0.0500	3.0690	0.4282	16.3928	-18.3309	-16.2420	1.0431	1.2553	0.9989	0.0270
33	IML07	0.0100	0.1328	2.2675	13.5567	-16.3782	-13.2408	1.0494	1.3148	0.9997	0.0143
36	IML08	0.0100	0.1399	3.1940	12.1515	-13.5967	-12.0499	1.0260	1.1990	0.9998	0.0131
38	IML10-1	0.0100	2.5923	0.2468	15.4536	-19.5661	-14.8265	1.0747	1.4858	0.9993	0.0235
	IML10-2	0.0100	1.8359	0.2014	12.7320	-17.4708	-11.7939	1.1031	1.6342	0.9997	0.0155
59	IML11	0.0100	0.1875	2.3253	15.7491	-18.6536	-15.4561	1.0514	1.2859	0.9997	0.0165
40	IML12	0.0100	0.8960	0.5913	10.3711	-12.3921	-10.1424	1.0700	1.3547	0.9998	0.0130
51	IML13	0.0100	0.0751	2.3805	4.9164	-5.6547	-4.8533	1.0431	1.2456	0.9986	0.0366
54	IML15	0.0100	0.9010	1.1827	26.4729	-31.7427	-25.8880	1.0708	1.3322	0.9995	0.0218
65	IML17-1	0.0100	0.1759	1.8660	10.2934	-12.3363	-10.0744	1.0702	1.3097	0.9997	0.0158
	IML17-2	0.0100	0.2401	1.6089	10.7910	-12.8143	-10.5793	1.0588	1.3063	0.9990	0.0303

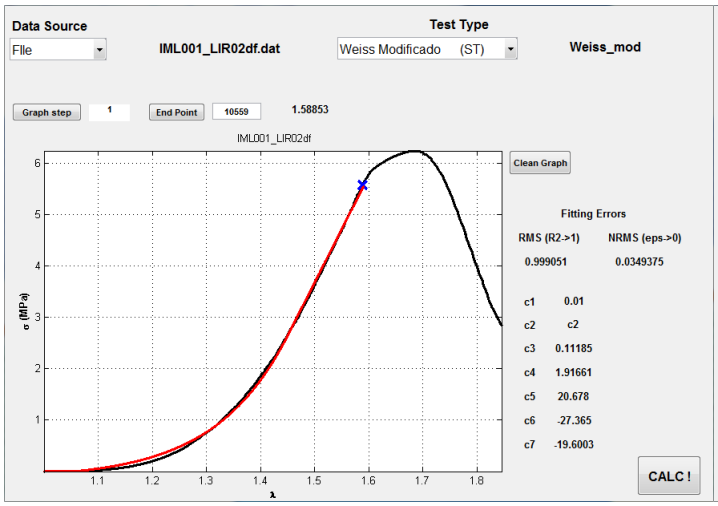

(a) IML01

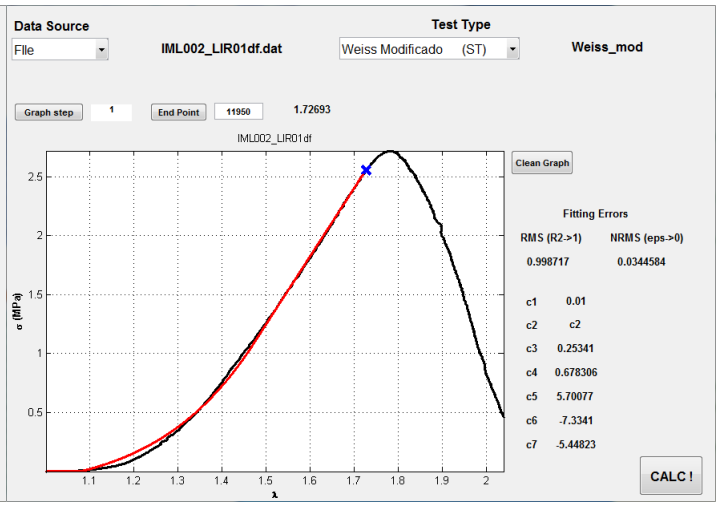

(b) IML02

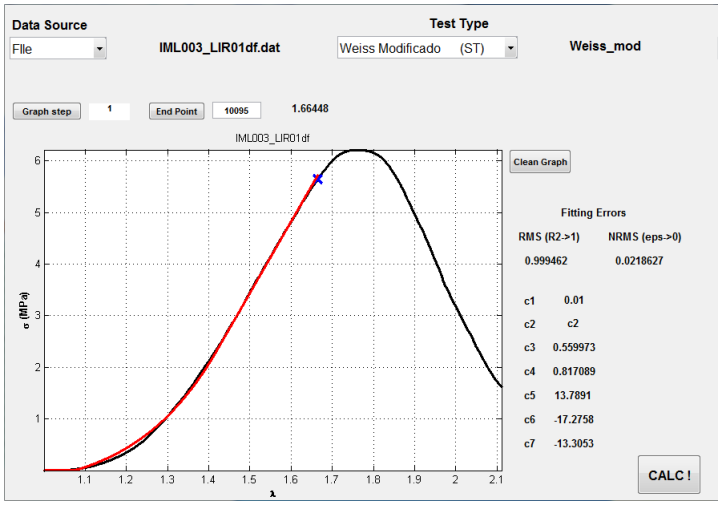

(c) IML03

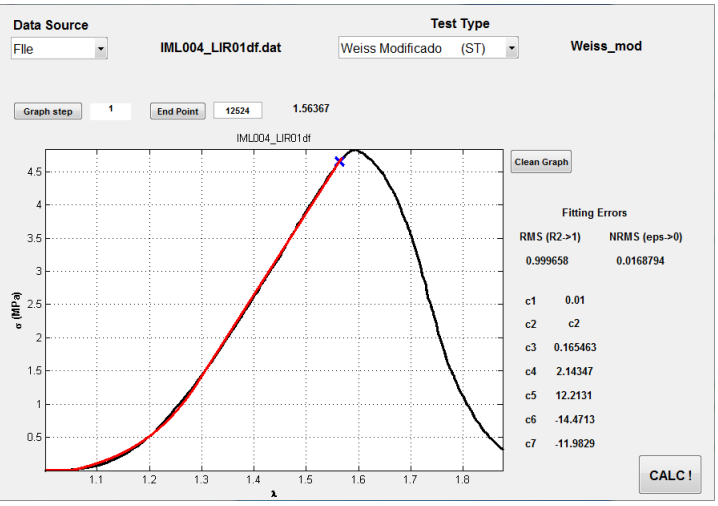

(d) IML04-1

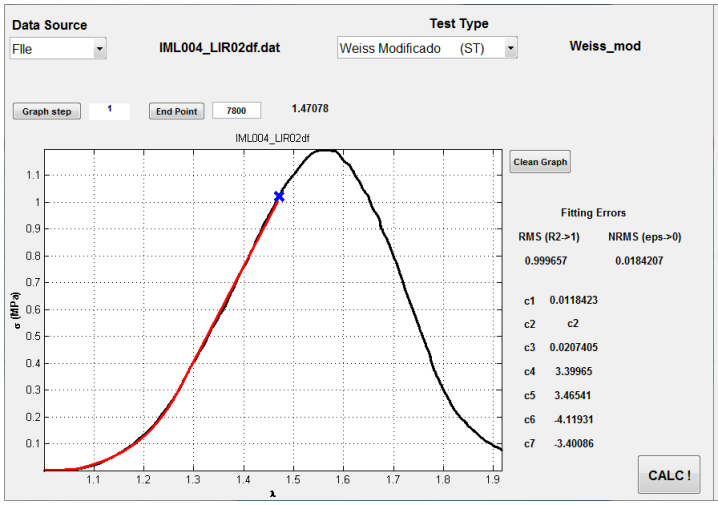

(e) IML04-2

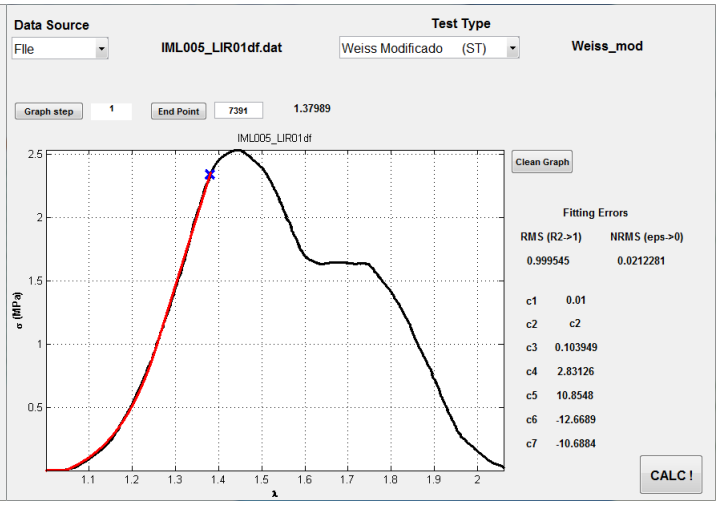

(f) IML05-1

Figure B.1: Round ligament samples' parameters computed with optimization process (1 of 4).

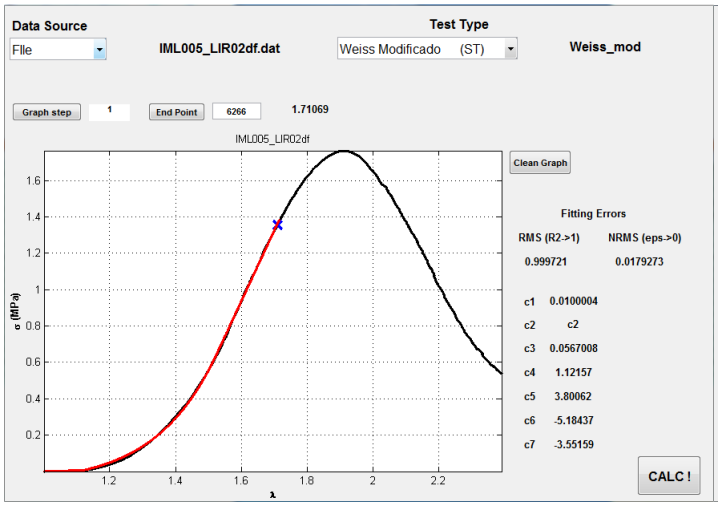

(g) IML05-2

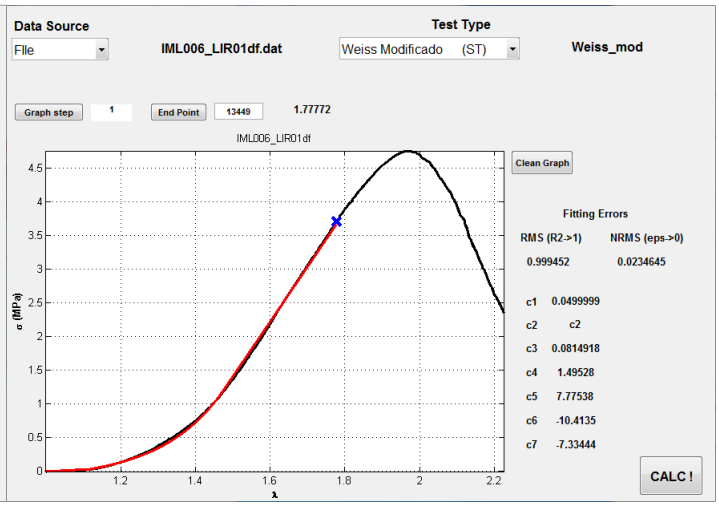

(h) IML06

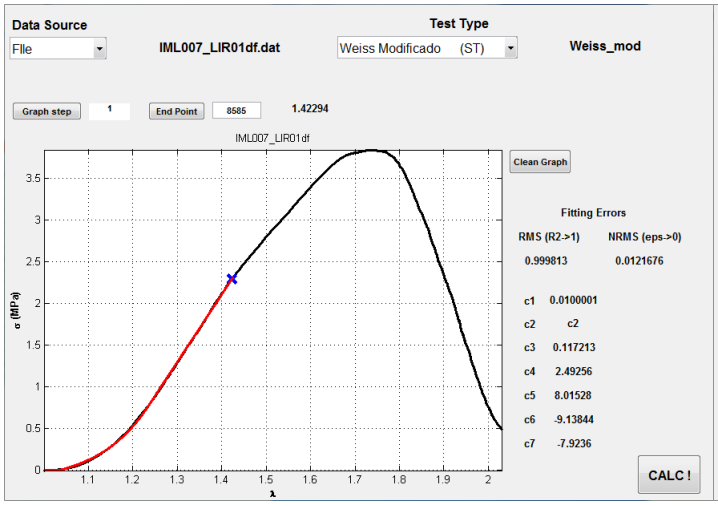

(i) IML07

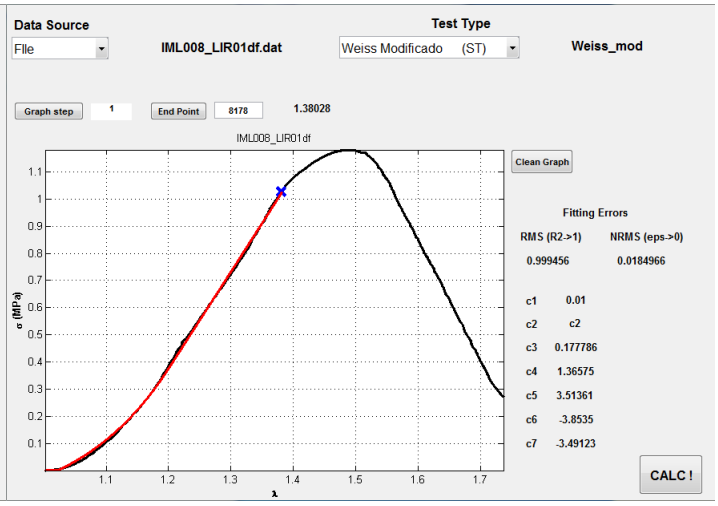

(j) IML08

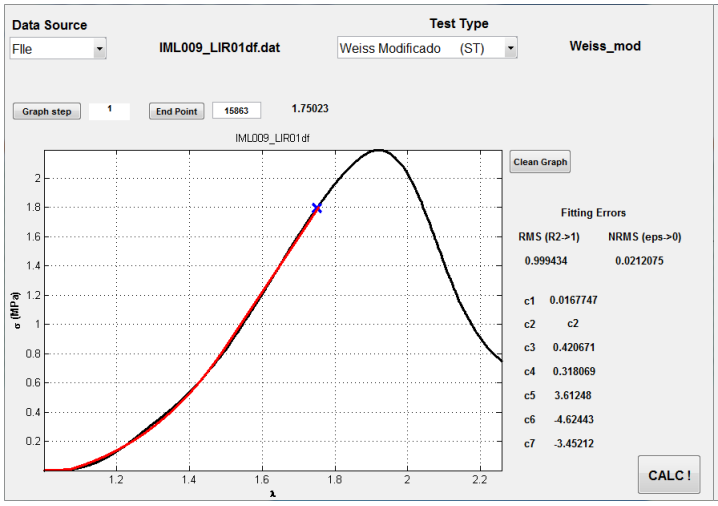

(k) IML09

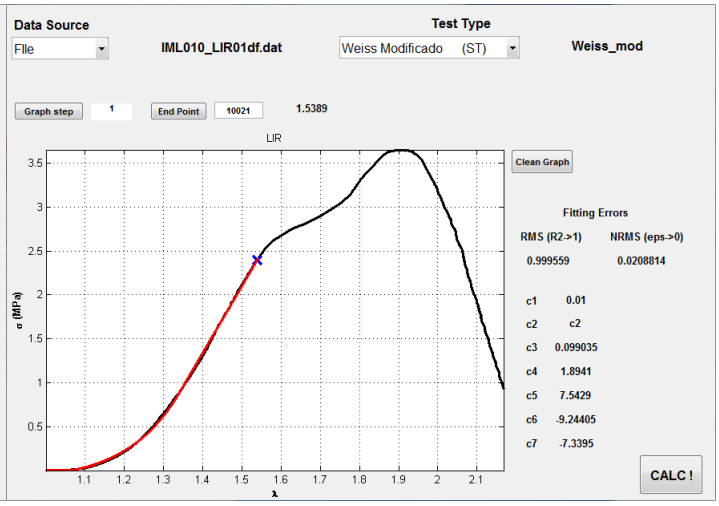

(l) IML10

Figure B.1: Round ligament samples' parameters computed with optimization process (2 of 4).

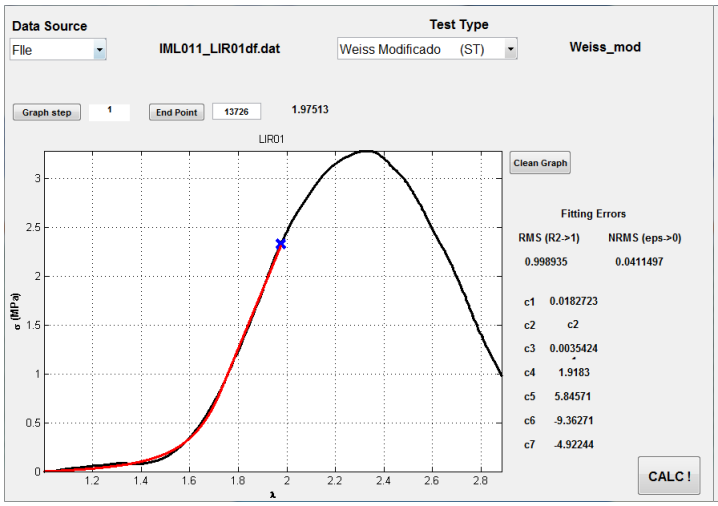

(m) IML11-1

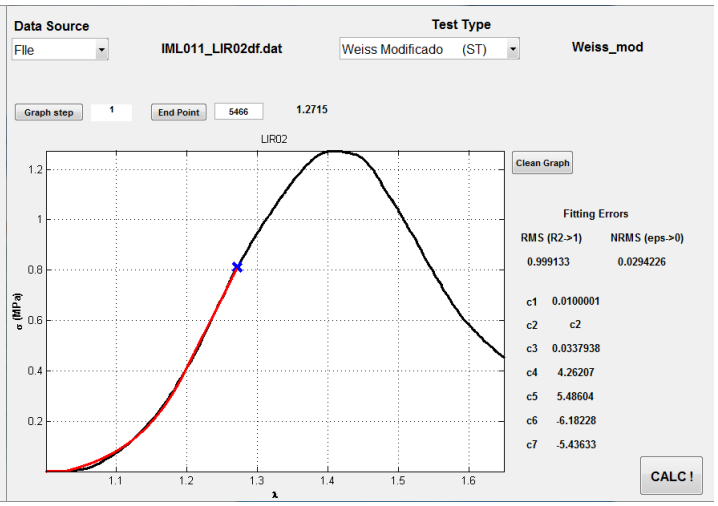

(n) IML11-2

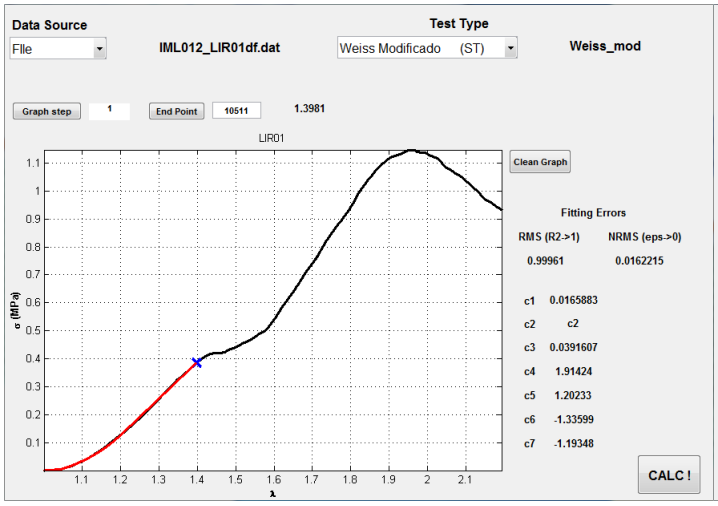

(o) IML12

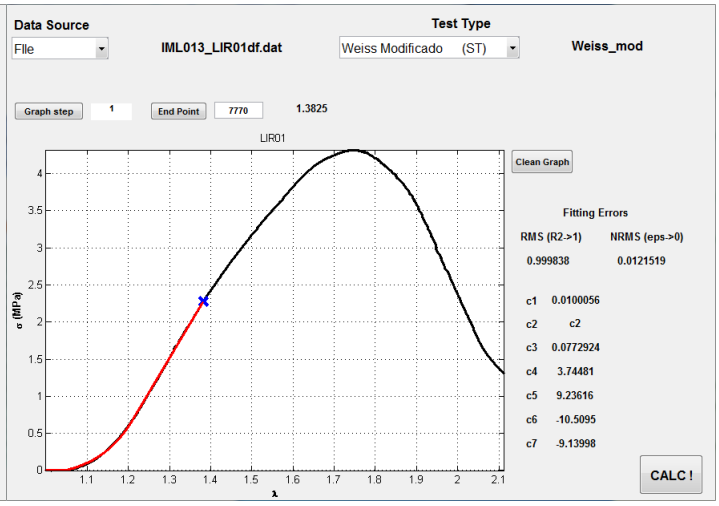

(p) IML13-1

Figure B.1: Round ligament samples' parameters computed with optimization process (3 of 4).

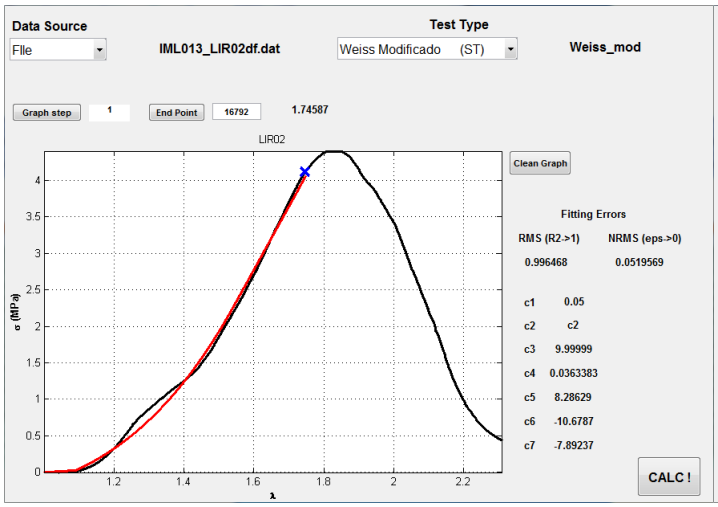

(q) IML13-2

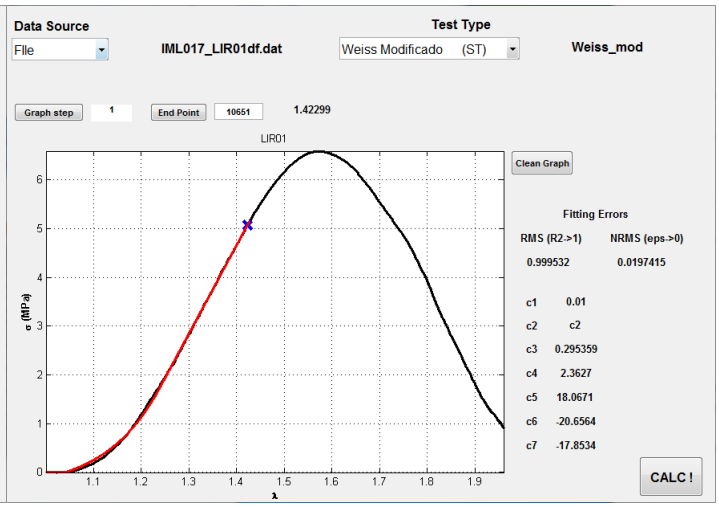

(r) IML17-1

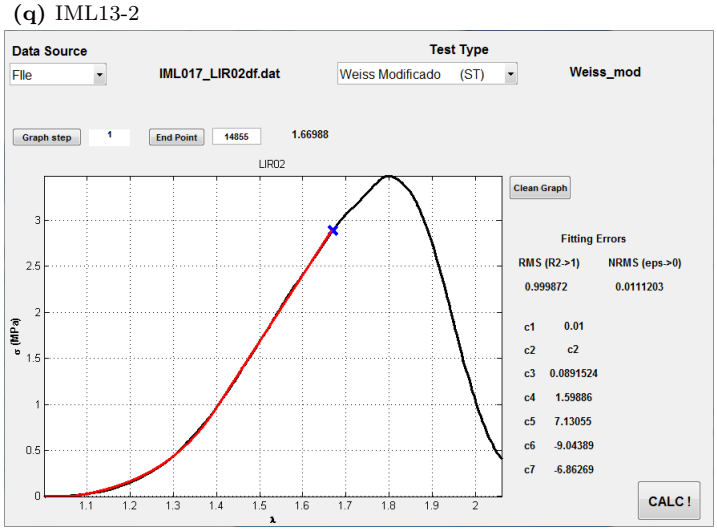

(s) IML17-2

Figure B.1: Round ligament samples' parameters computed with optimization process (4 of 4).

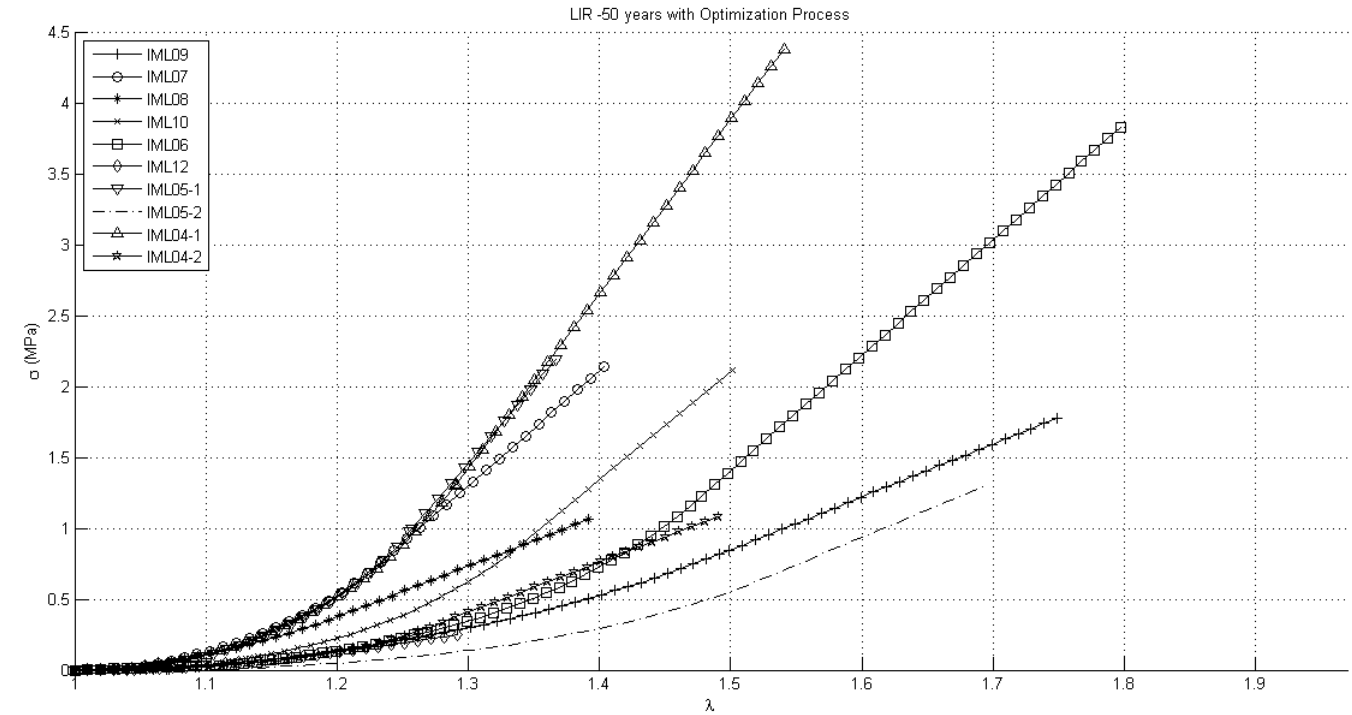

(a) Less than 50 years

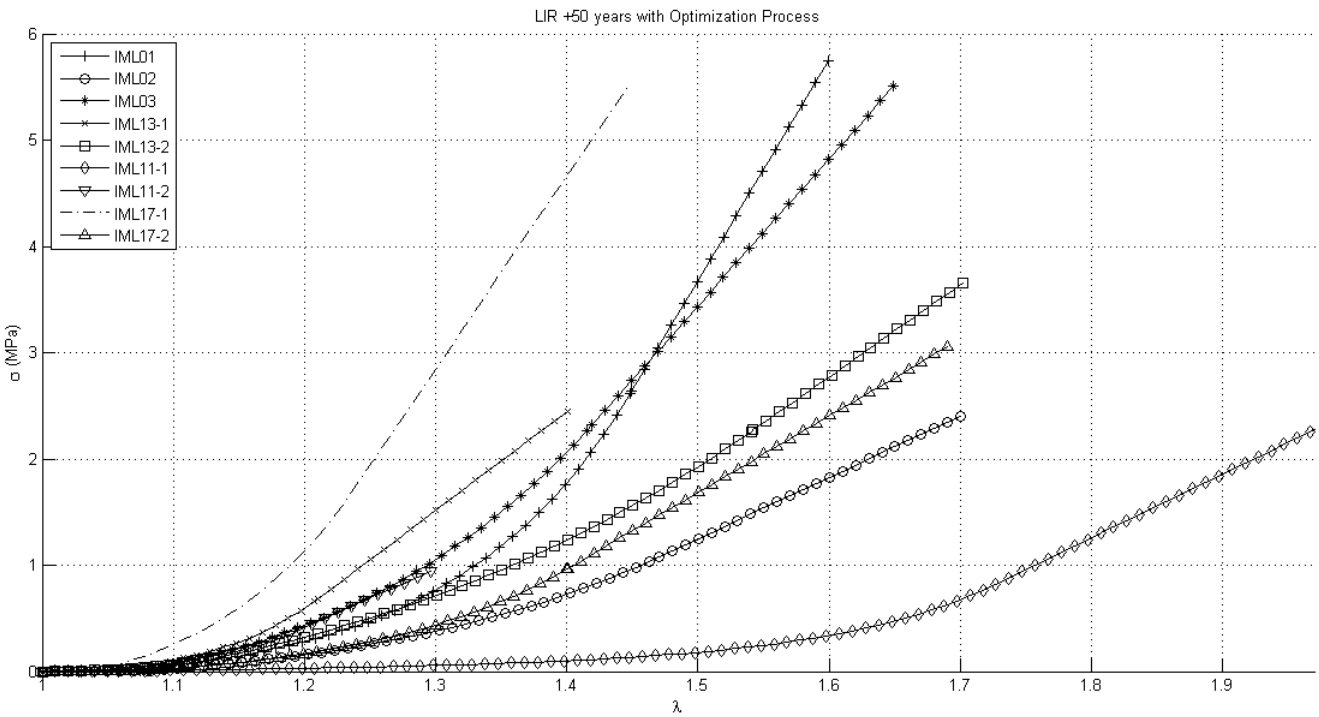

(b) Greater than or equal to 50 years

Figure B.2: Round ligament samples' analytical curves obtained with optimization process.

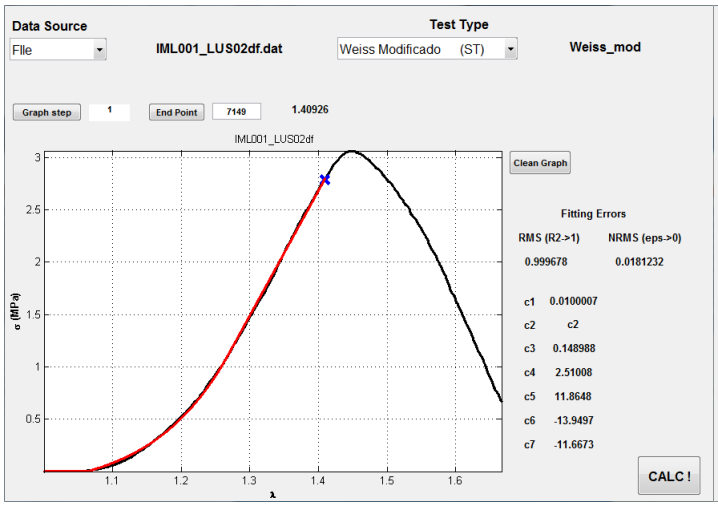

(a) IML01

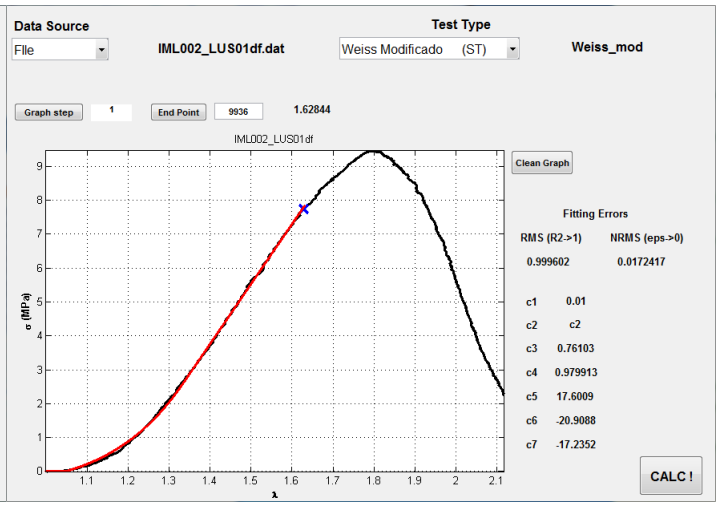

(b) IML02-1

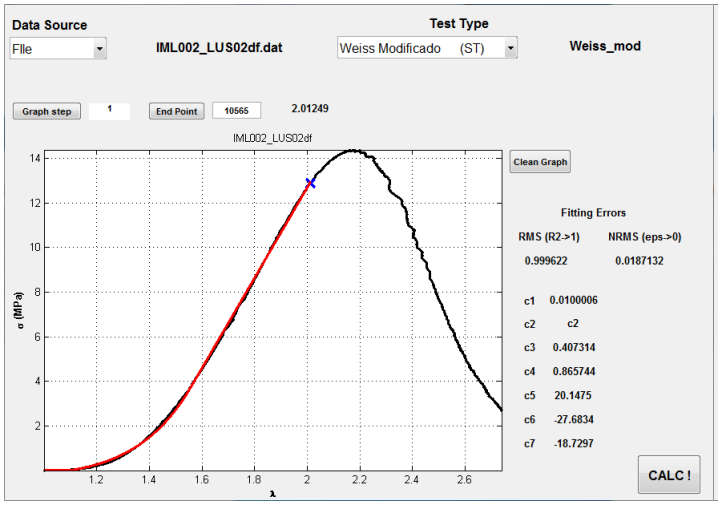

(c) IML02-2

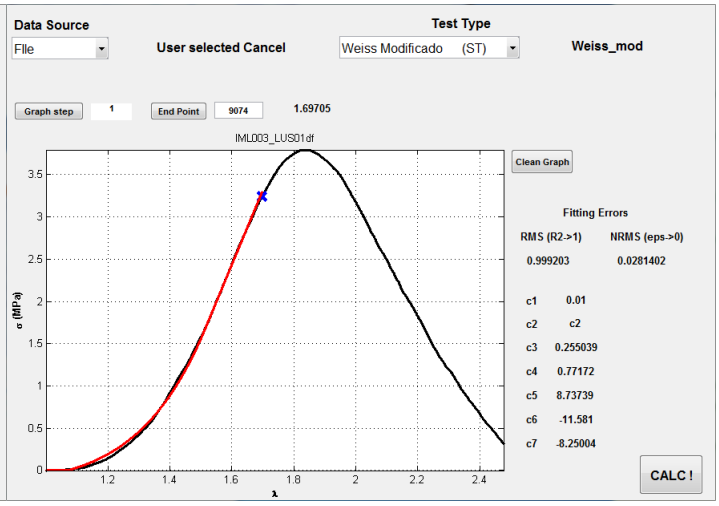

(d) IML03

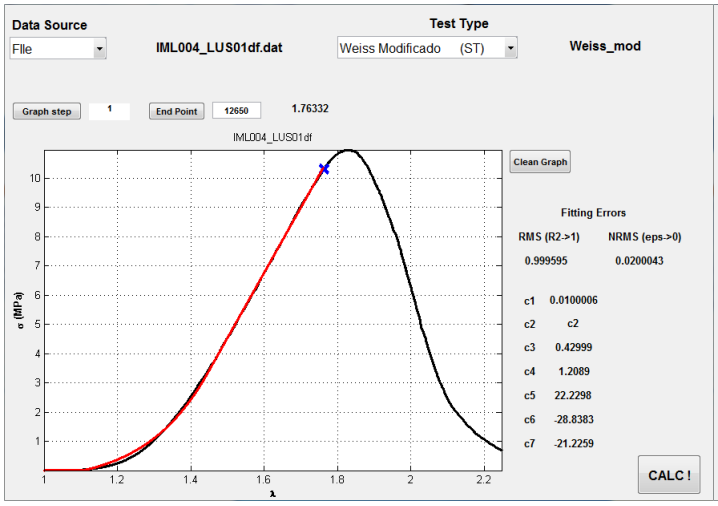

(e) IML04-1

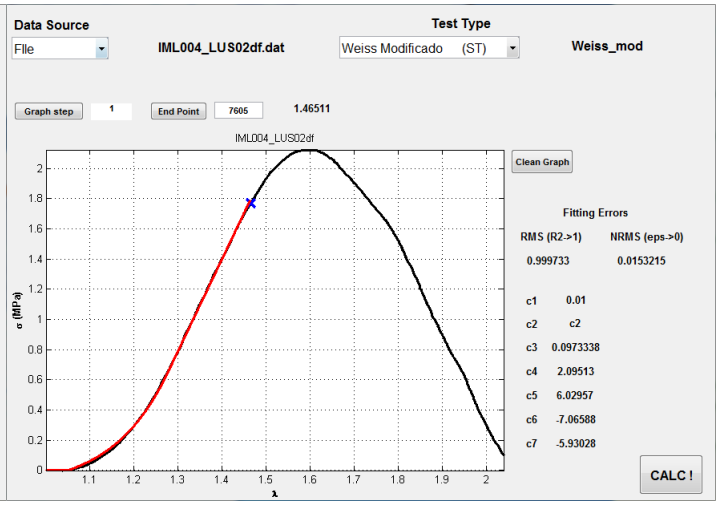

(f) IML04-2

Figure B.3: Uterosacral ligament samples' parameters computed with optimization process (1 of 3).

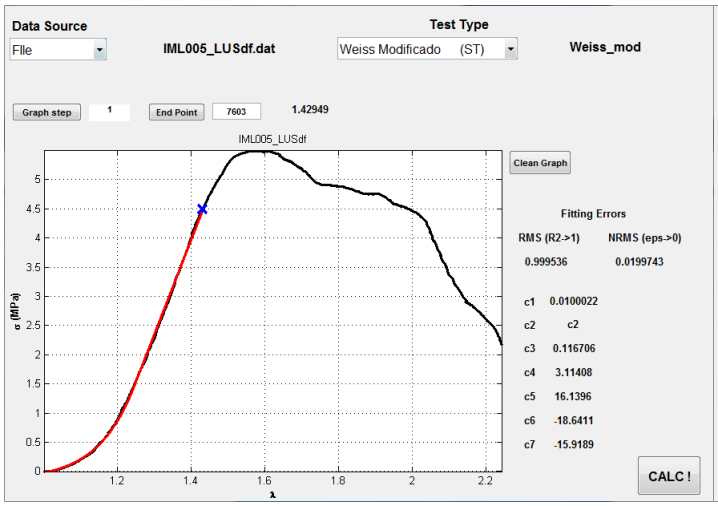

(g) IML05

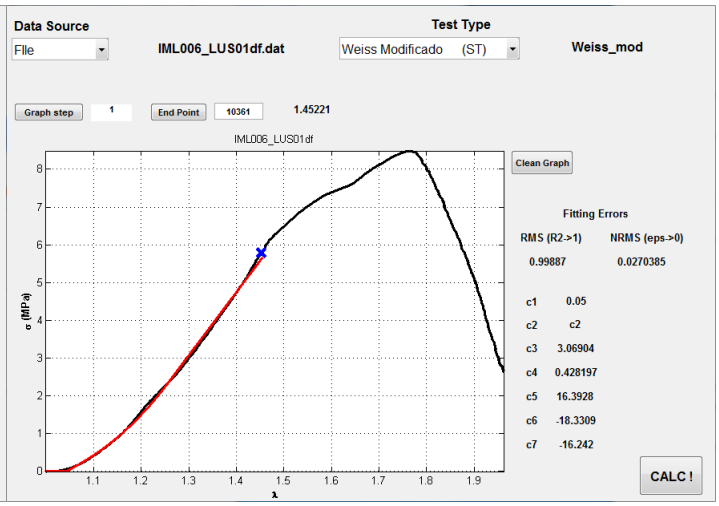

(h) IML06

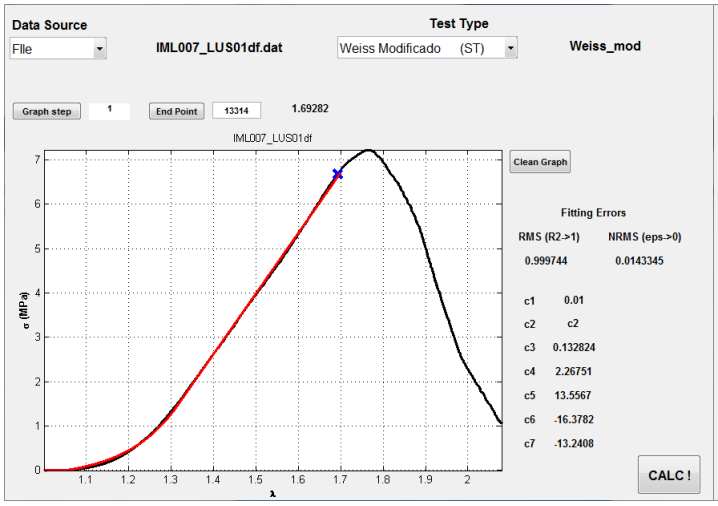

(i) IML07

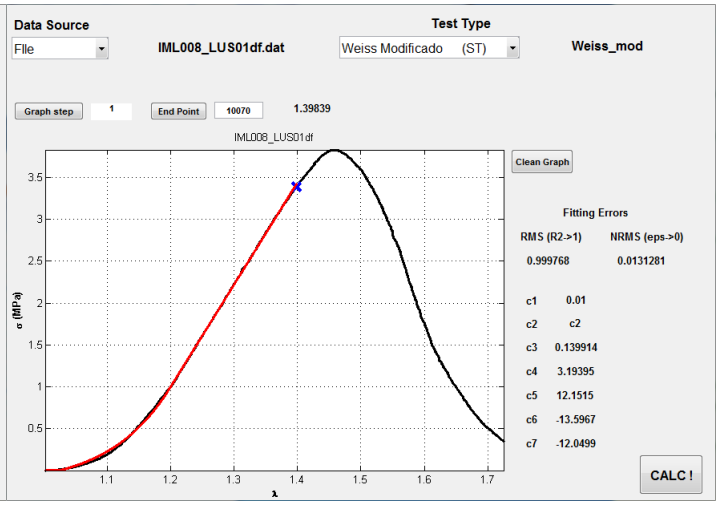

(j) IML08

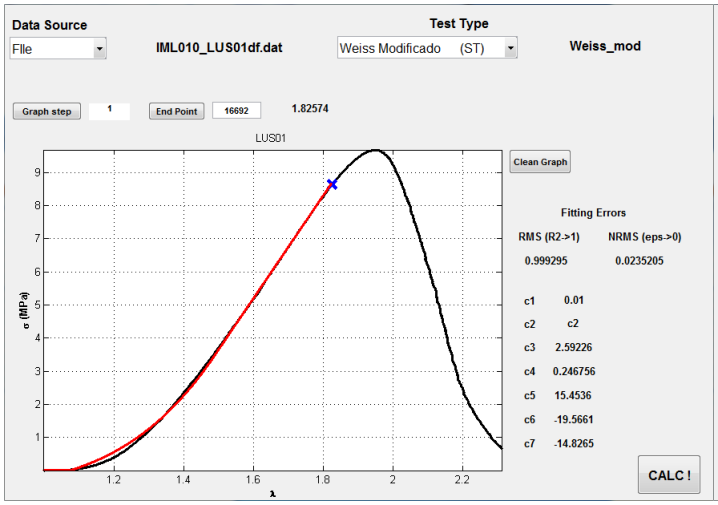

(k) IML10-1

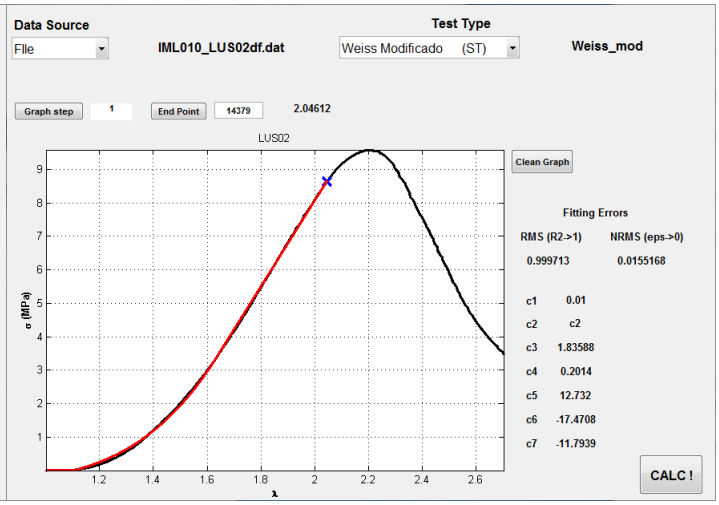

(l) IML10-2

Figure B.3: Uterosacral ligament samples' parameters computed with optimization process (2 of 3).

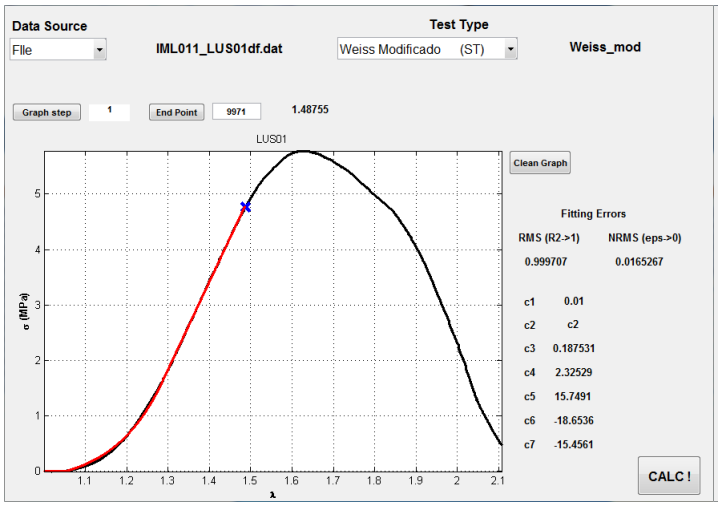

(m) IML11

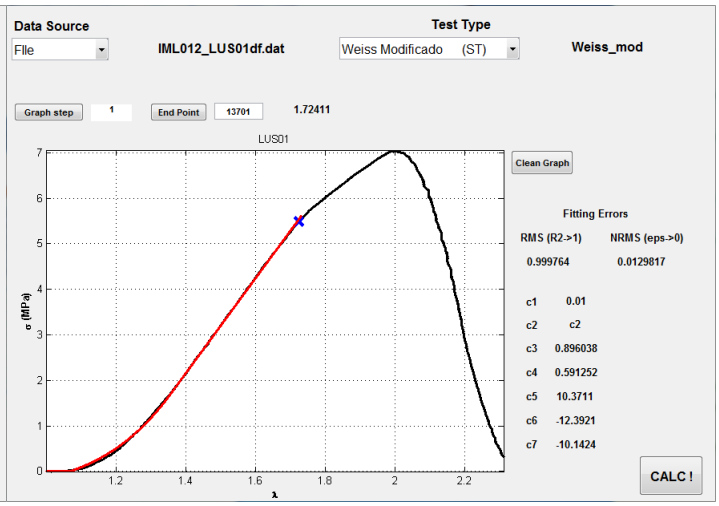

(n) IML12

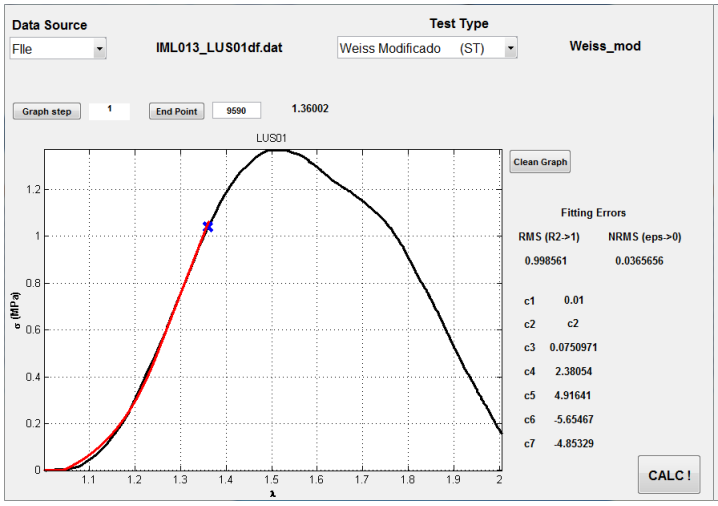

(o) IML13

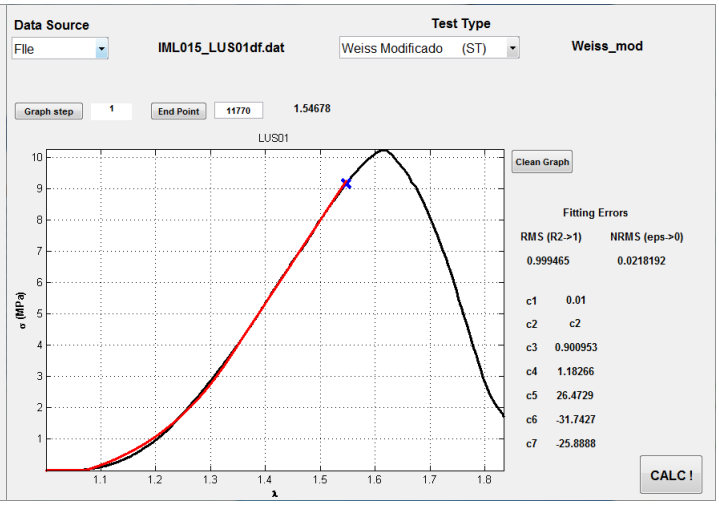

(p) IML15

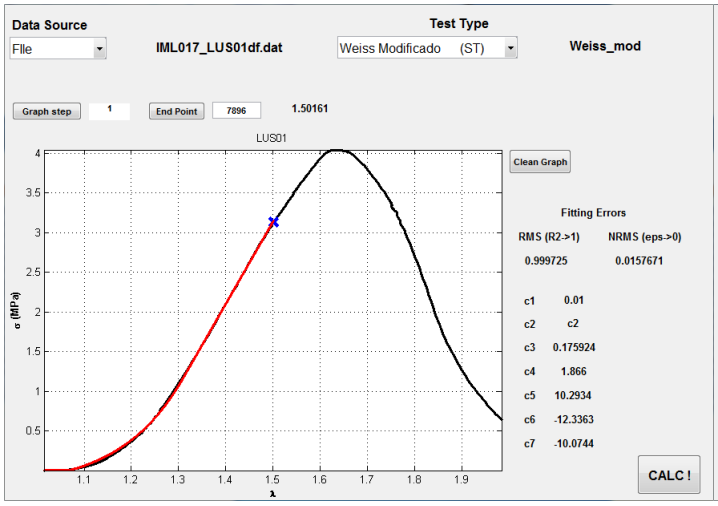

(q) IML17-1

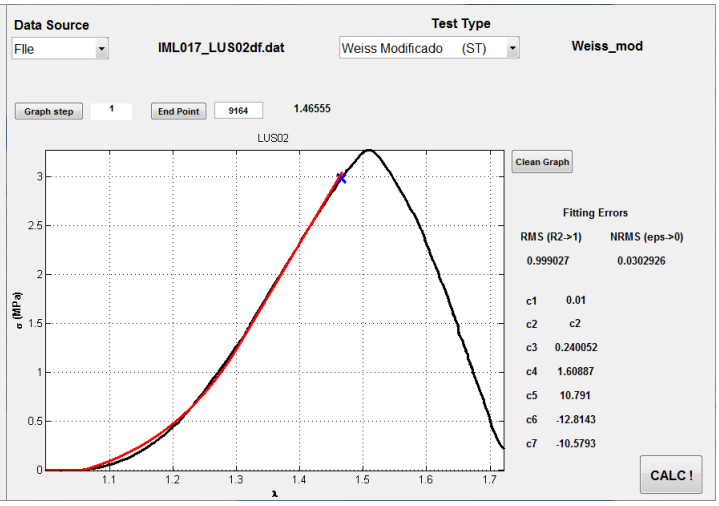

(r) IML17-2

Figure B.3: Uterosacral ligament samples' parameters computed with optimization process (3 of 3).

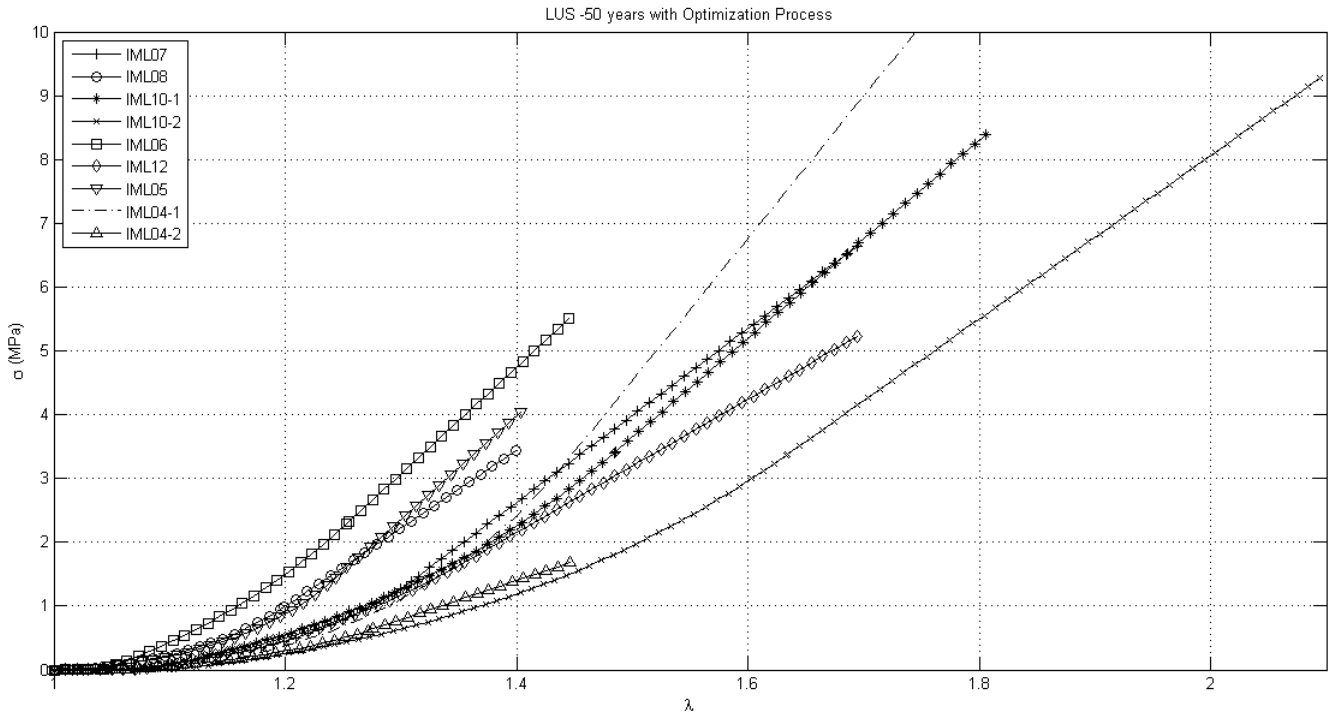

(a) Less than 50 years

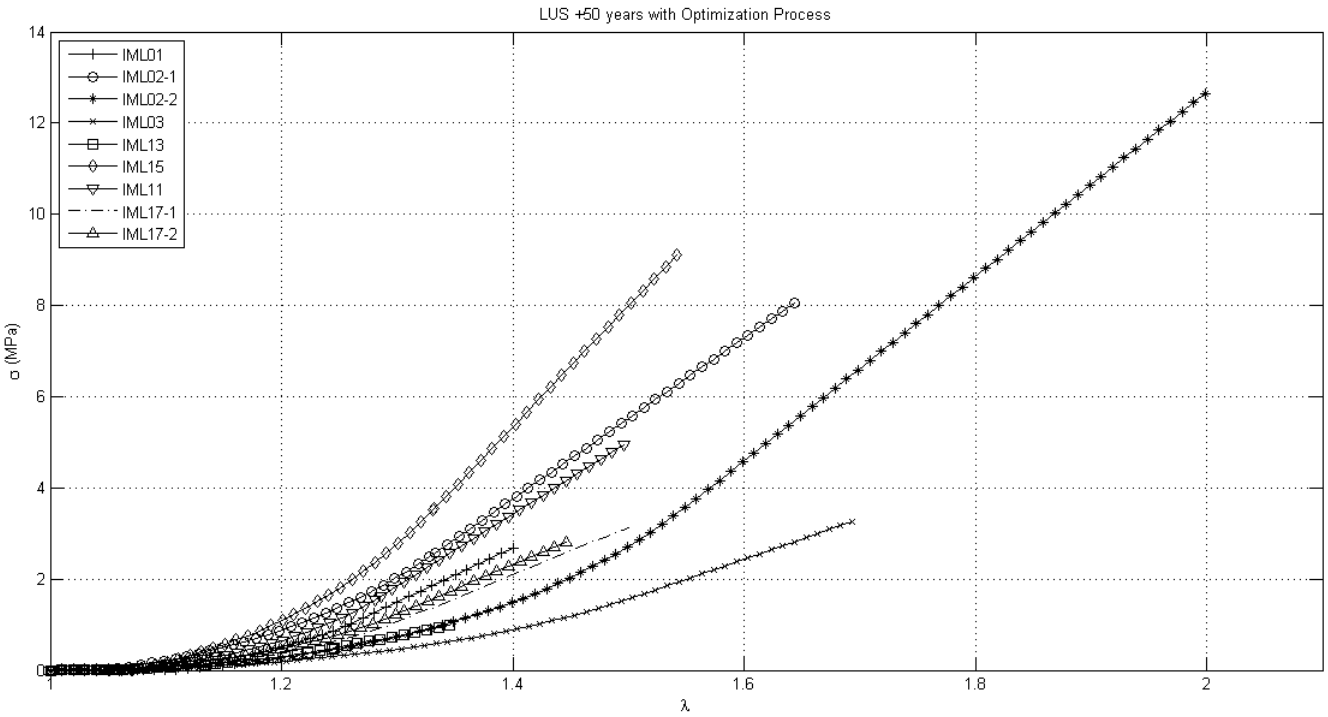

(b) Greater than or equal to 50 years

Figure B.4: Uterosacral ligament samples' analytical curves obtained with optimization process.

B.2 Manual process

Table B.2: Material constants for the round and uterosacral ligaments obtained with Weiss modified model manual process. Constant values are in MPa.

Round Ligament										
Age	Sample	c_1	c_3	c_4	c_5	c_6	c_7	I_{4_0}	$I_{4_{ref}}$	R^2
51	IML01	0.0030	0.1390	1.7550	22.3585	-29.9295	-21.0895	1.0726	1.4707	0.9993
51	IML02	0.0090	0.0930	1.3018	5.5195	-7.0457	-5.2973	1.0697	1.4228	0.9996
51	IML03	0.0290	0.1690	1.7241	12.7142	-15.7043	-12.3375	1.0567	1.3601	0.9998
47	IML04-1	0.0060	0.3153	1.4182	12.3198	-14.6108	-12.0754	1.0465	1.3138	0.9998
	IML04-2	0.0060	0.0185	3.4818	3.4708	-4.1194	-3.4070	1.0521	1.2684	0.9998
43	IML05-1	0.0030	0.1660	2.1223	11.6261	-13.6756	-11.4234	1.0430	1.2826	0.9996
	IML05-2	0.0030	0.0550	1.1191	3.7959	-5.1517	-3.5537	1.0994	1.5208	0.9998
40	IML06	0.0380	0.0940	1.2600	8.0899	-10.8837	-7.6038	1.0762	1.5020	0.9999
33	IML07	0.0200	0.0880	2.7646	7.9256	-9.0450	-7.8331	1.0224	1.2325	0.9999
36	IML08	0.0290	0.0458	3.2850	3.2678	-3.5704	-3.2500	1.0163	1.1679	0.9998
18	IML09	0.0128	0.2350	0.4932	3.7288	-4.8052	-3.5551	1.0587	1.4962	0.9996
38	IML10	0.0128	0.1240	1.5250	7.9173	-9.7983	-7.6749	1.0505	1.3712	0.9996
59	IML11-1	0.0305	0.0030	1.9518	5.6558	-9.0832	-4.7515	1.0499	1.7297	0.9994
	IML11-2	0.0273	0.0859	2.9355	5.3789	-6.0784	-5.3289	1.0604	1.2067	0.9999
40	IML12	0.0125	0.0488	1.6182	1.2372	-1.3741	-1.2278	1.0396	1.2092	0.9998
51	IML13-1	0.0110	0.0910	3.4336	9.3141	-10.6122	-9.2146	1.0495	1.2153	0.9999
	IML13-2	0.0030	0.4145	0.6050	8.9525	-11.6161	-8.5181	1.0620	1.4961	0.9962
65	IML17-1	0.0710	0.1126	4.1396	16.9403	-19.2926	-16.7626	1.0453	1.2080	0.9998
	IML17-2	0.0230	0.0580	1.8777	6.9848	-8.8683	-6.7207	1.0498	1.3942	0.9999

Uterosacral Ligament										
Age	Sample	c_1	c_3	c_4	c_5	c_6	c_7	I_{4_0}	$I_{4_{ref}}$	R^2
51	IML01	0.0060	0.1300	2.6809	11.3594	-13.2700	-11.1846	1.0571	1.2588	0.9997
51	IML02-1	0.0030	0.9205	0.8027	18.7385	-22.5495	-18.2749	1.0367	1.3667	0.9994
	IML02-2	0.0363	0.3550	0.9382	19.9335	-27.3374	-18.5531	1.0960	1.5503	0.9997
51	IML03	0.0245	0.1887	0.9577	8.0968	-10.6279	-7.6849	1.0849	1.4820	0.9998
47	IML04-1	0.0060	0.3760	1.3009	22.0249	-28.4799	-21.0557	1.1000	1.4367	0.9998
	IML04-2	0.0030	0.0545	2.9832	5.9097	-6.8839	-5.8221	1.0497	1.2514	0.9999
43	IML05	0.0090	0.2410	2.1123	16.4594	-19.0873	-16.2122	1.0210	1.2676	0.9998
40	IML06	0.0090	0.8643	1.2218	16.7256	-18.5846	-16.5874	1.0247	1.2265	0.9992
33	IML07	0.0060	0.1150	2.5405	13.5041	-16.2985	-13.1980	1.0590	1.3058	0.9999
36	IML08	0.0060	0.1150	3.4668	12.1509	-13.5989	-12.0490	1.0210	1.1969	0.9999
38	IML10-1	0.0060	0.9970	0.5300	15.9799	-20.4196	-15.2949	1.0703	1.4750	0.9993
	IML10-2	0.0272	0.8452	0.3736	12.5378	-17.2230	-11.6225	1.0998	1.6105	0.9998
59	IML11	0.0150	0.2105	2.1764	15.5001	-18.3265	-15.2158	1.0508	1.2869	0.9999
40	IML12	0.0090	0.6340	0.7386	10.5536	-12.6798	-10.3039	1.0586	1.3604	0.9998
51	IML13	0.0180	0.0376	3.7100	4.4165	-5.0250	-4.3705	1.0477	1.2107	0.9999
54	IML15	0.0120	0.5984	1.5386	26.4375	-31.6724	-25.8662	1.0653	1.3199	0.9997
65	IML17-1	0.0090	0.1315	2.1586	10.1141	-12.0825	-9.9067	1.0508	1.3000	0.9999
	IML17-2	0.0254	0.1295	2.3418	10.2008	-12.0304	-10.0214	1.0552	1.2788	0.9998

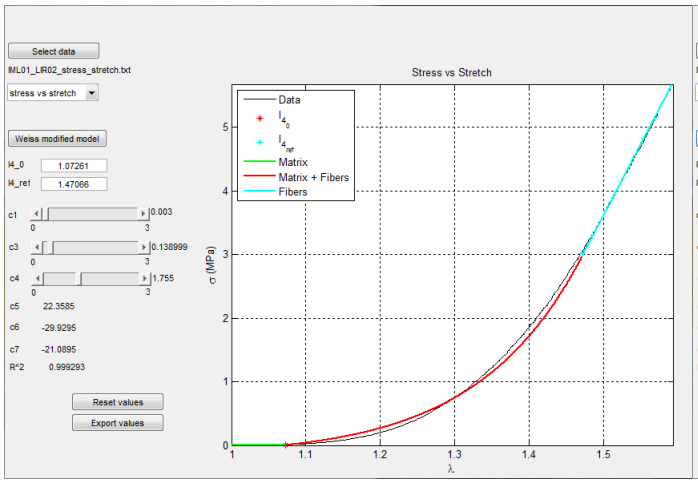

(a) IML01

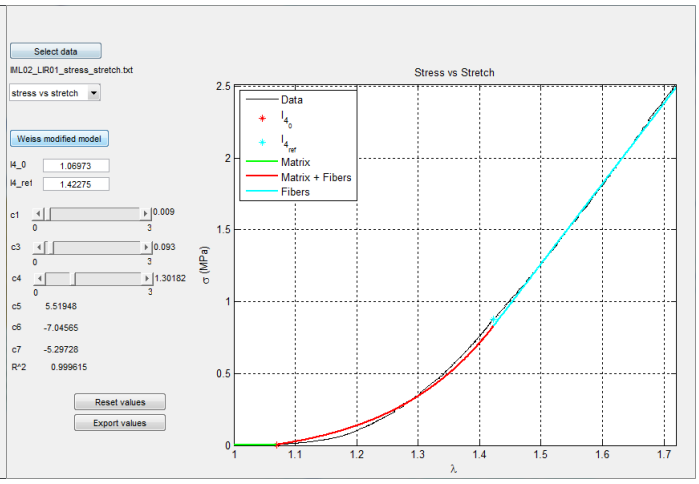

(b) IML02

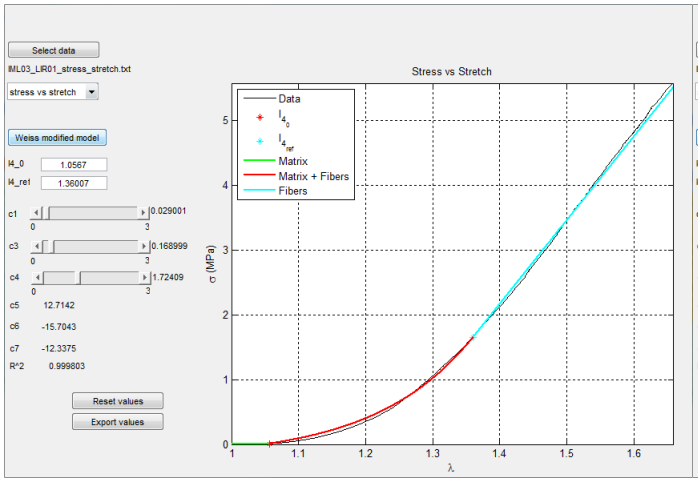

(c) IML03

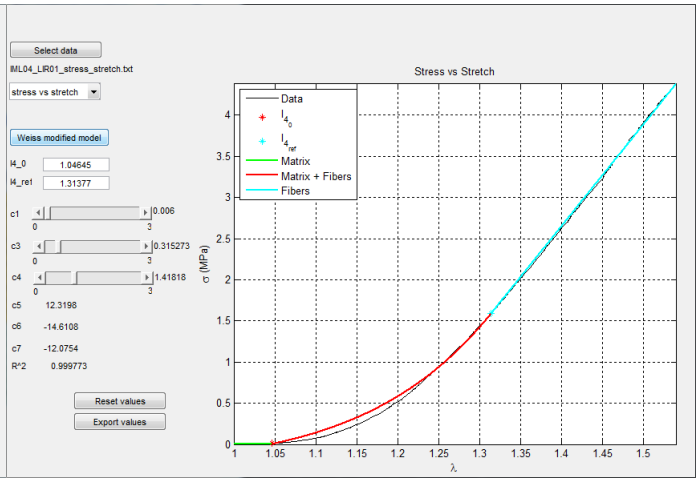

(d) IML04-1

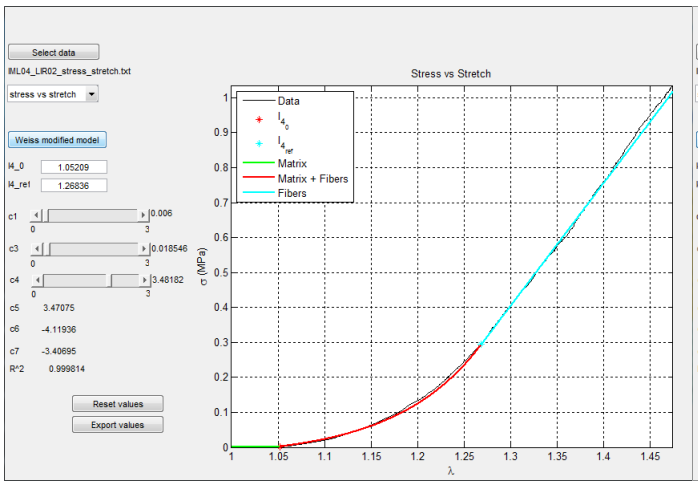

(e) IML04-2

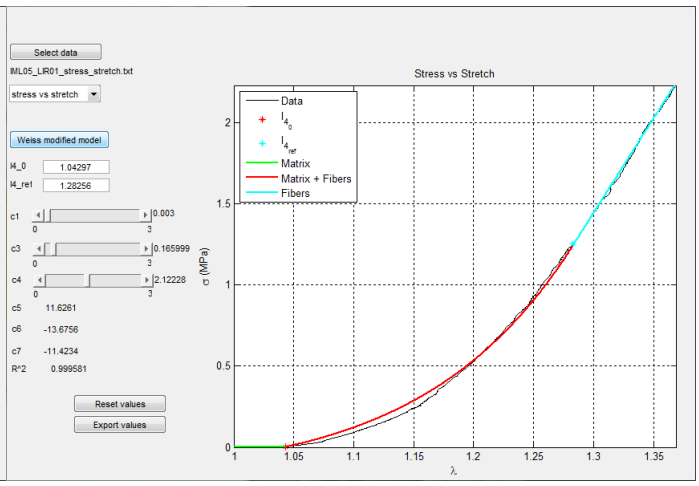

(f) IML05-1

Figure B.5: Round ligament samples' parameters computed with manual process (1 of 4).

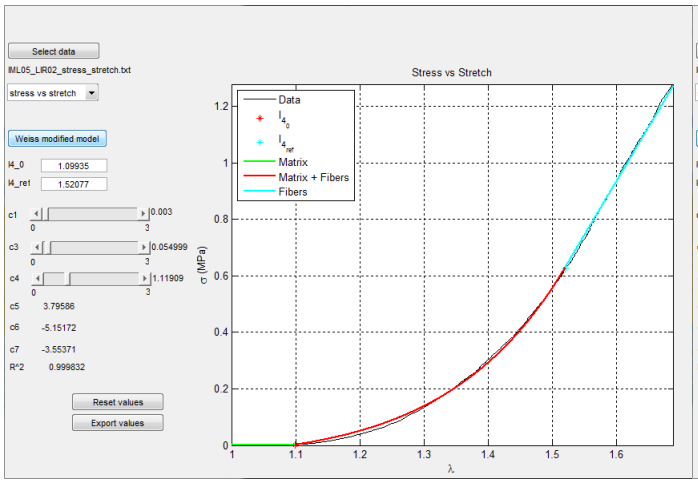

(g) IML05-2

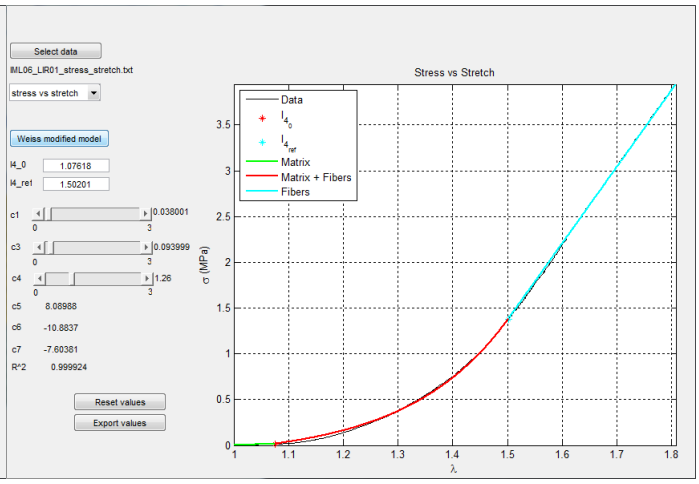

(h) IML06

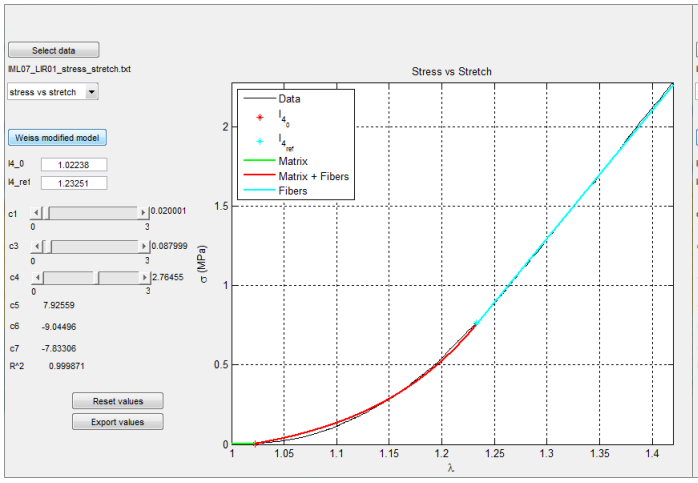

(i) IML07

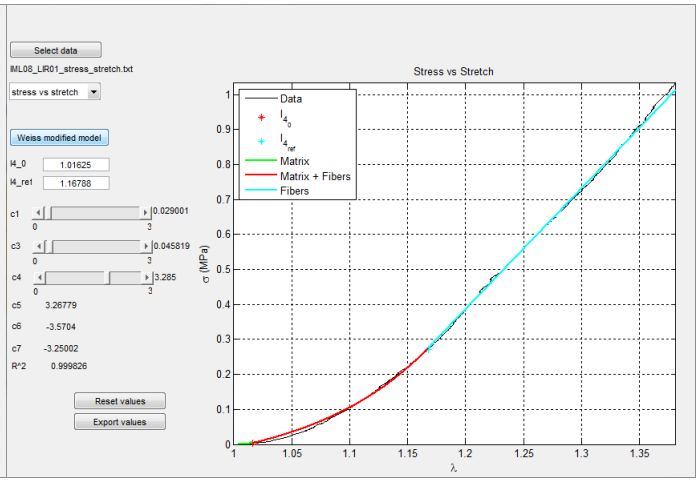

(j) IML08

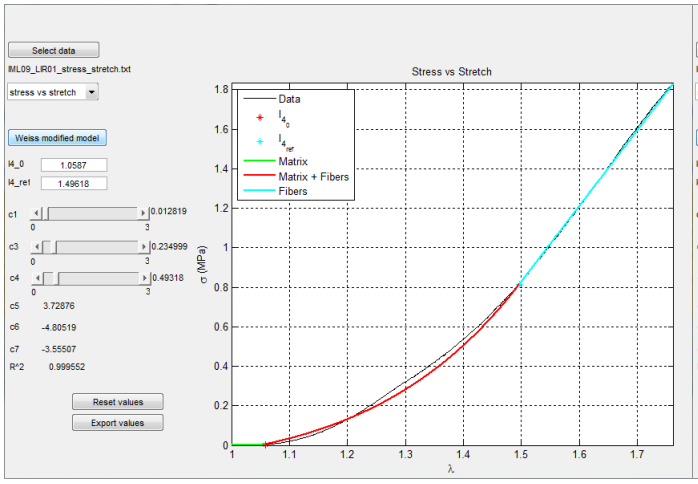

(k) IML09

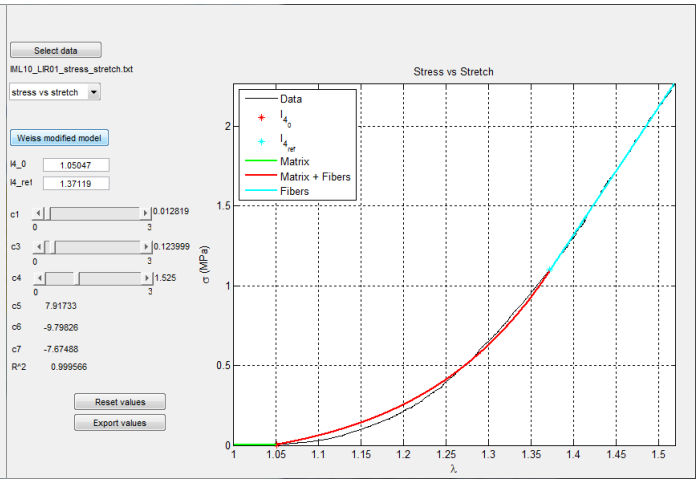

(l) IML10

Figure B.5: Round ligament samples' parameters computed with manual process (2 of 4).

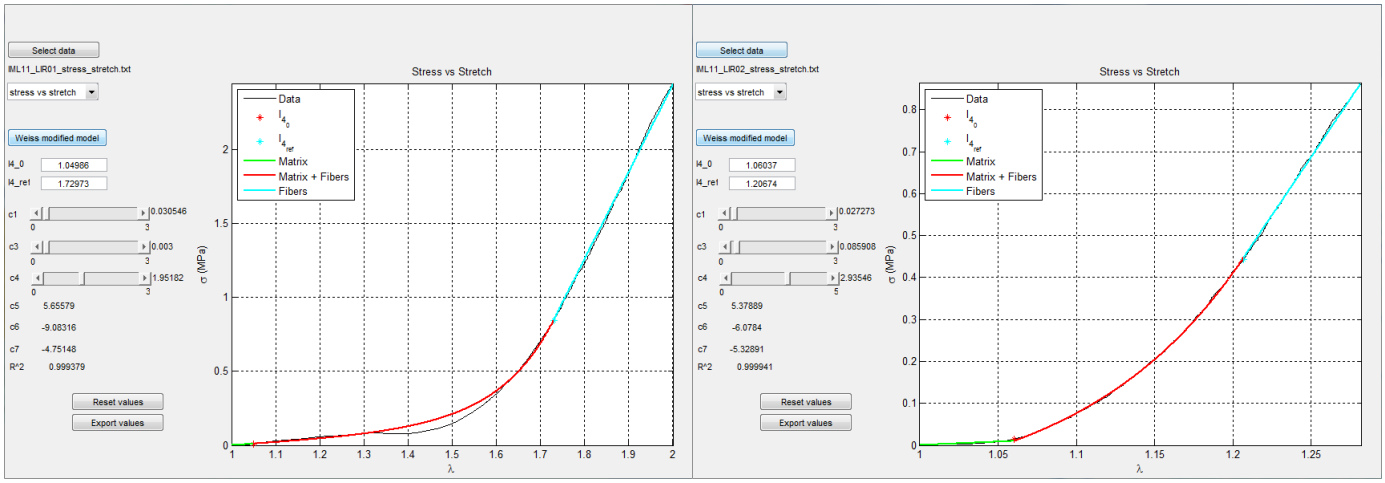

(m) IML11-1

(n) IML11-2

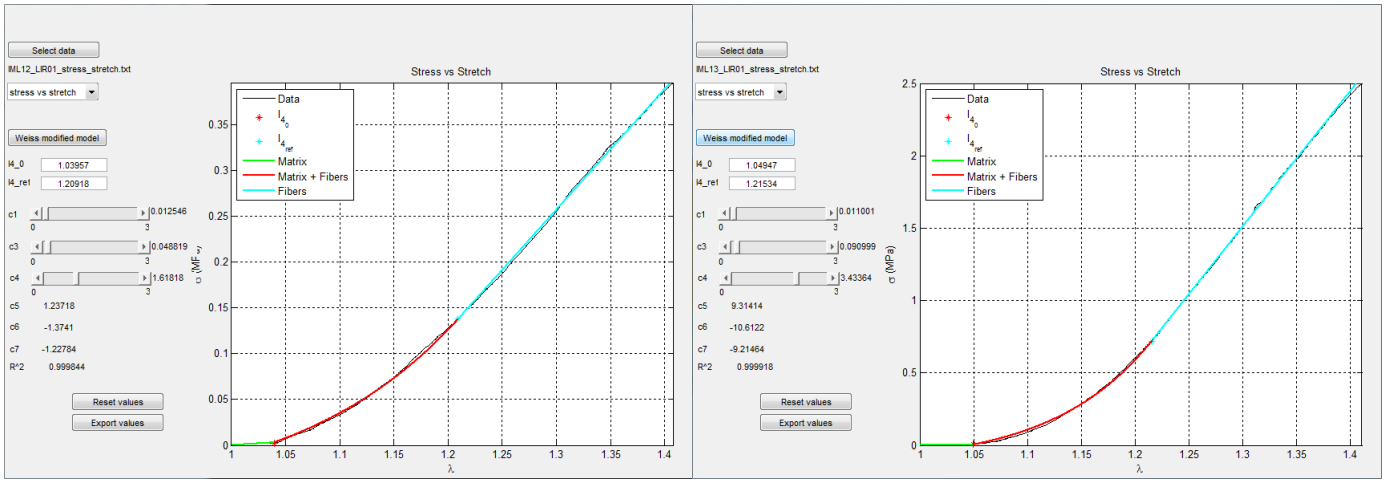

(o) IML12

(p) IML13-1

Figure B.5: Round ligament samples' parameters computed with manual process (3 of 4).

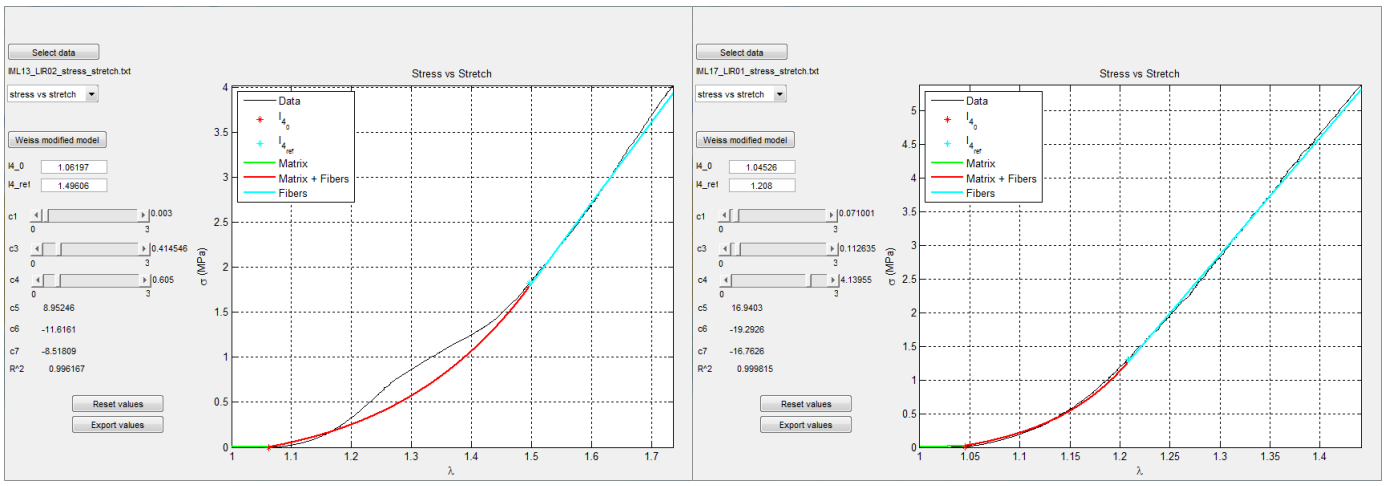

(q) IML13-2 **(r)** IML17-1

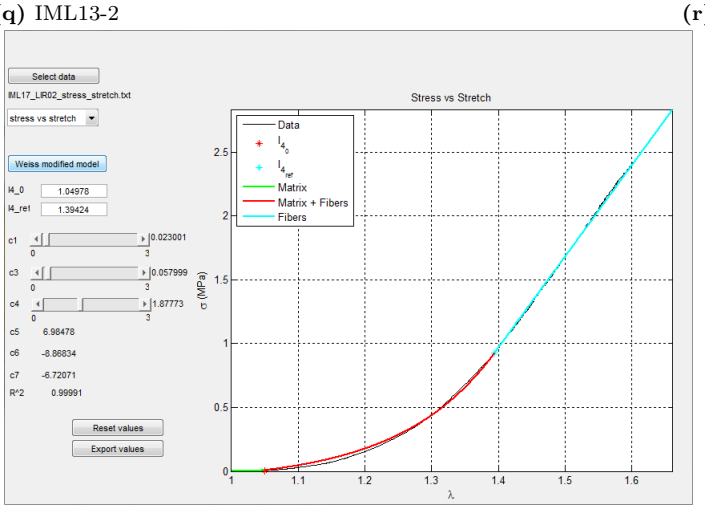

(s) IML17-2

Figure B.5: Round ligament samples' parameters computed with manual process (4 of 4).

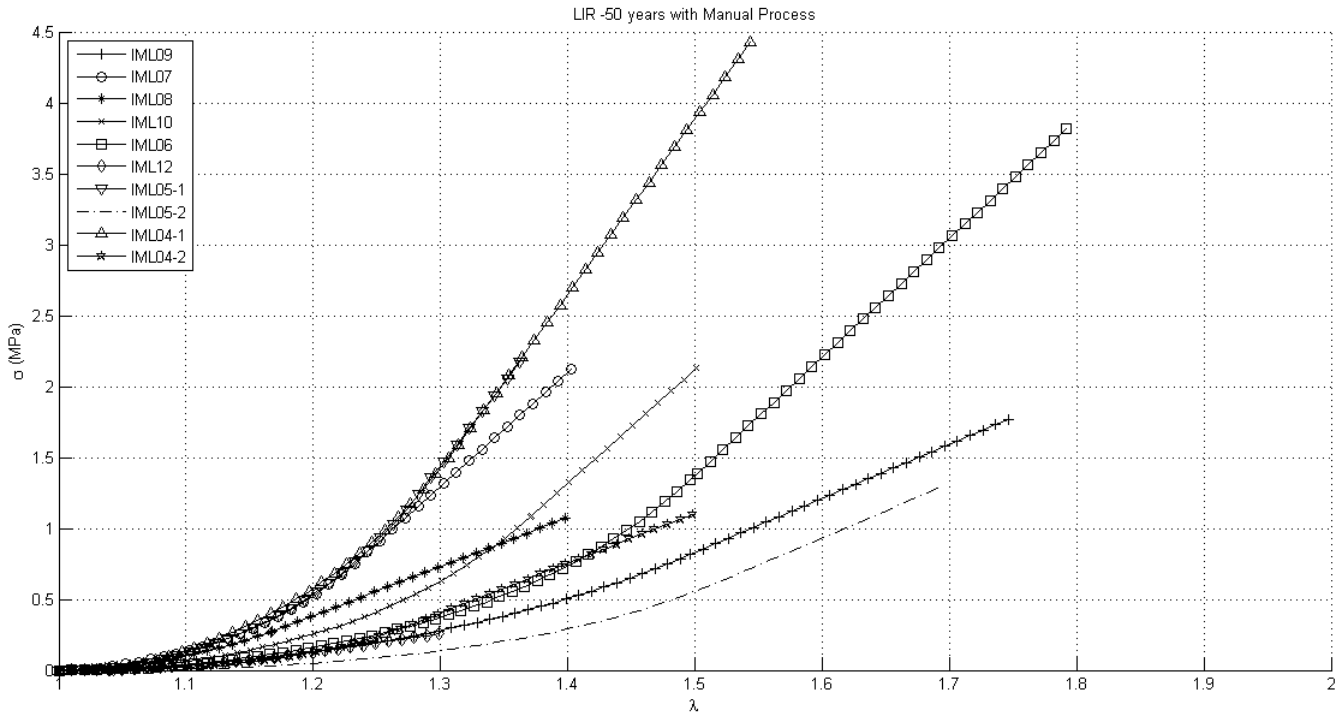

(a) Less than 50 years

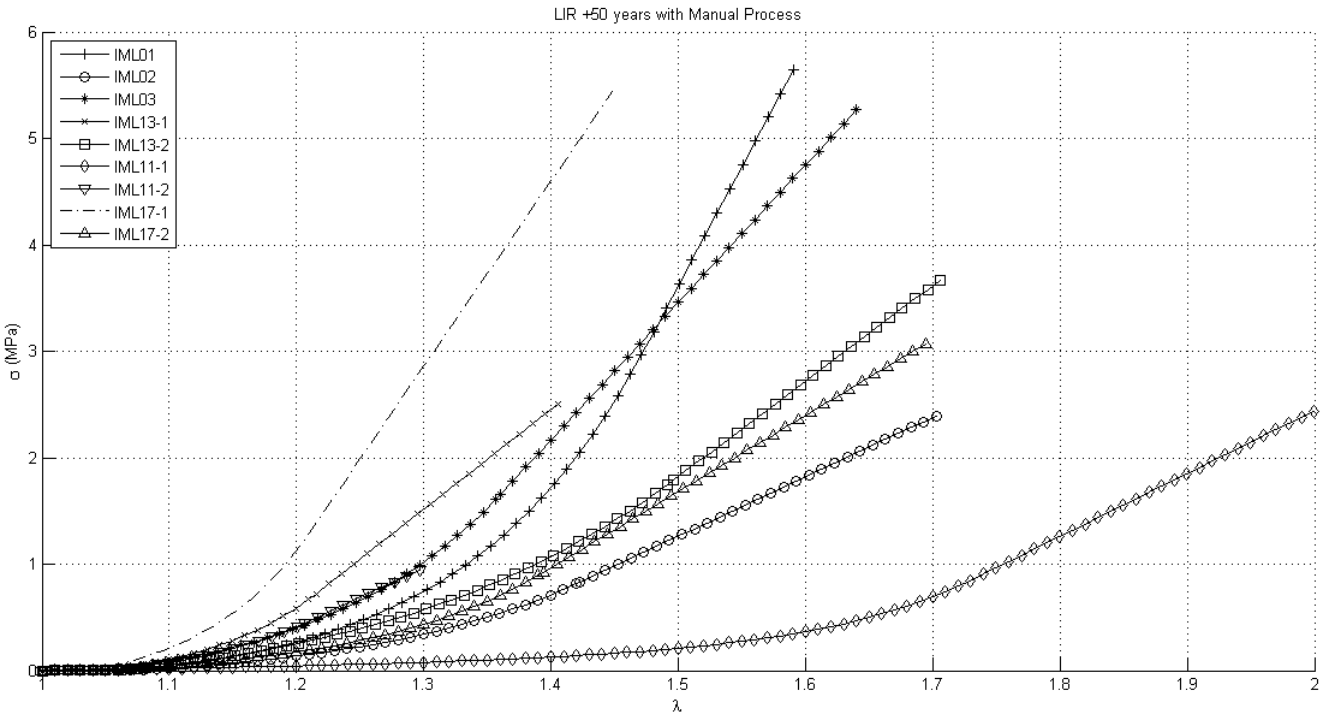

(b) Greater than or equal to 50 years

Figure B.6: Round ligament samples' analytical curves obtained with manual process.

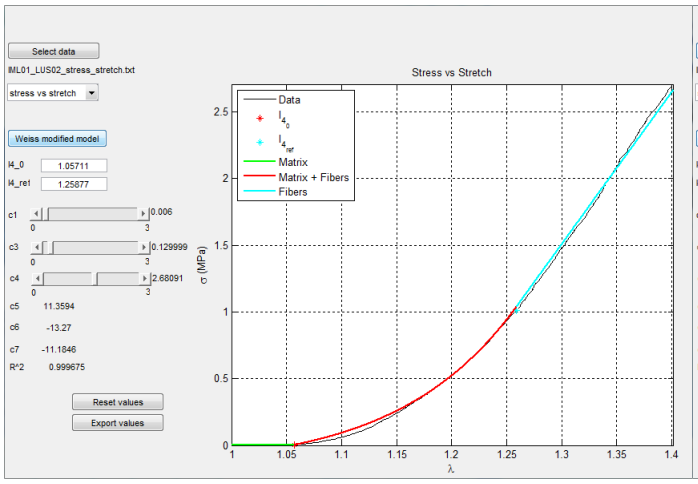

(a) IML01

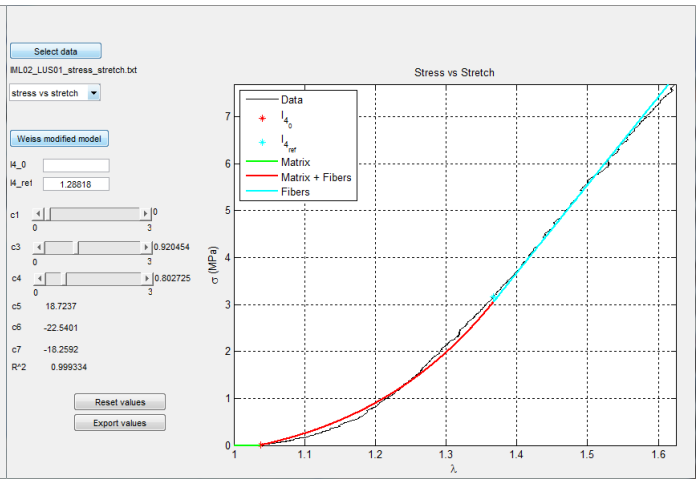

(b) IML02-1

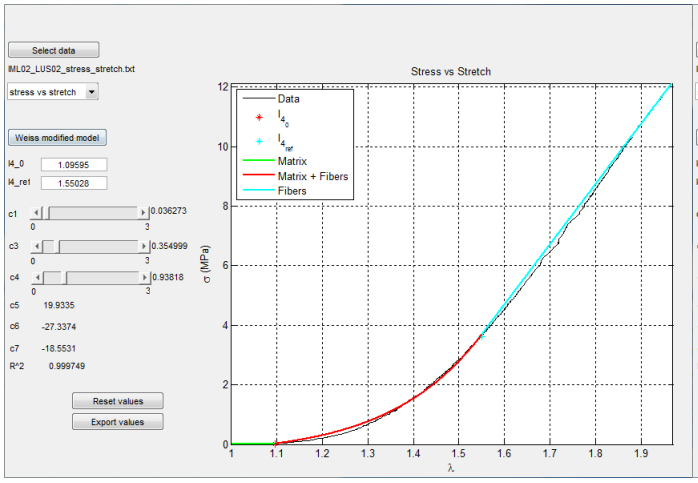

(c) IML02-2

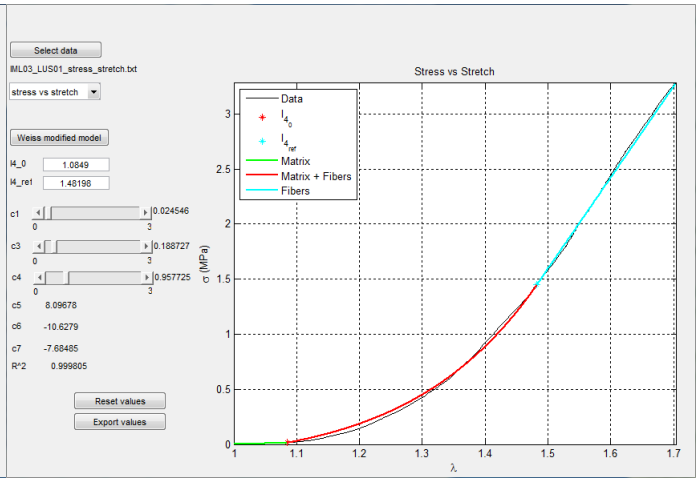

(d) IML03

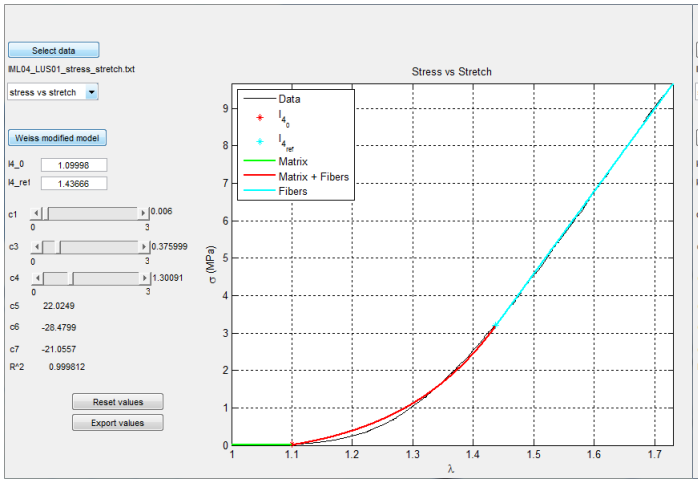

(e) IML04-1

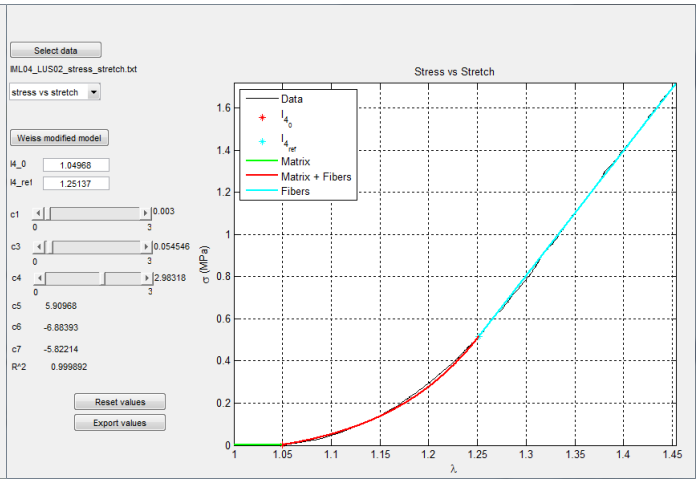

(f) IML04-2

Figure B.7: Uterosacral ligament samples' parameters computed with manual process (1 of 3).

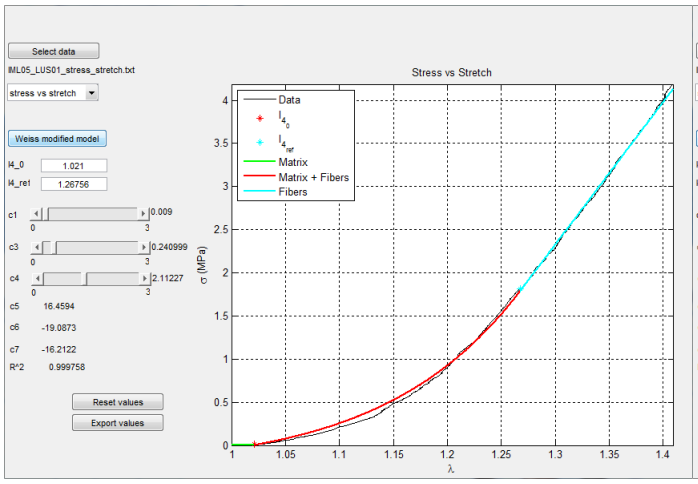

(g) IML05

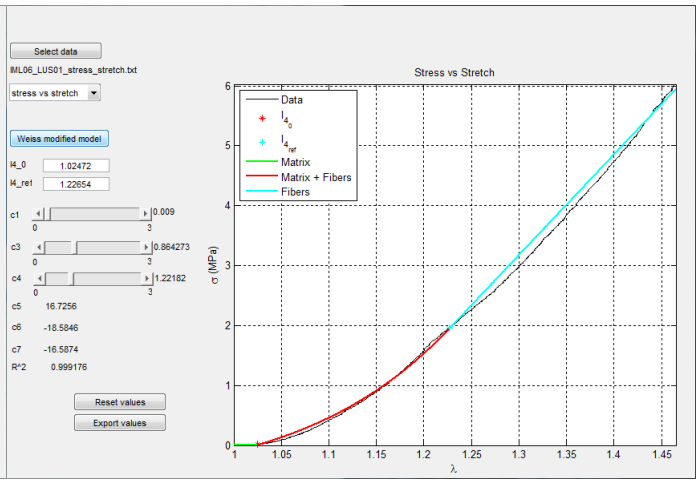

(h) IML06

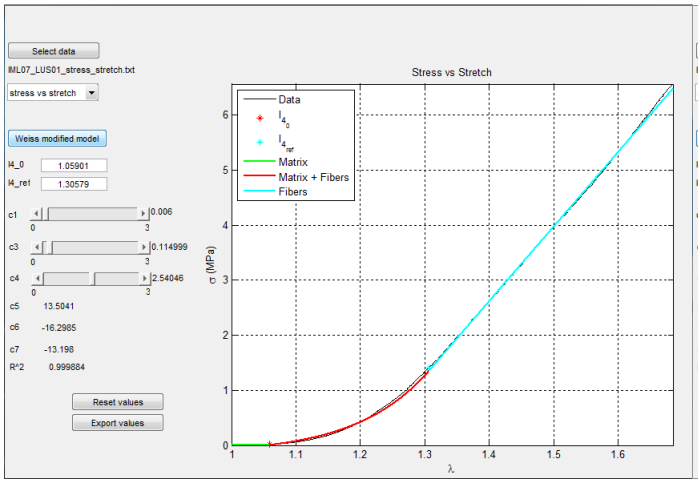

(i) IML07

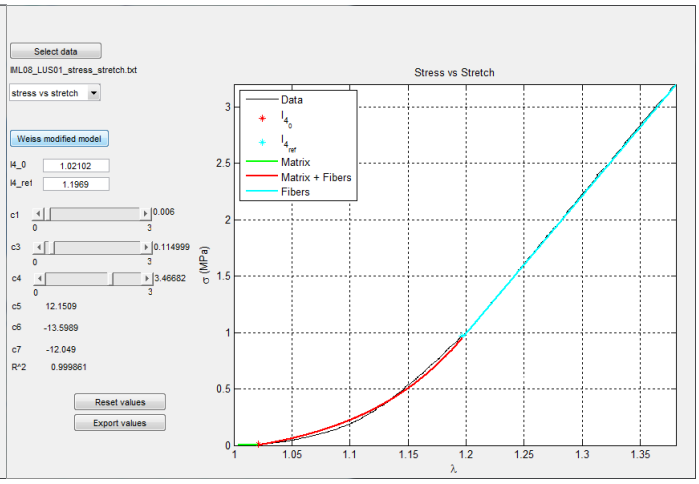

(j) IML08

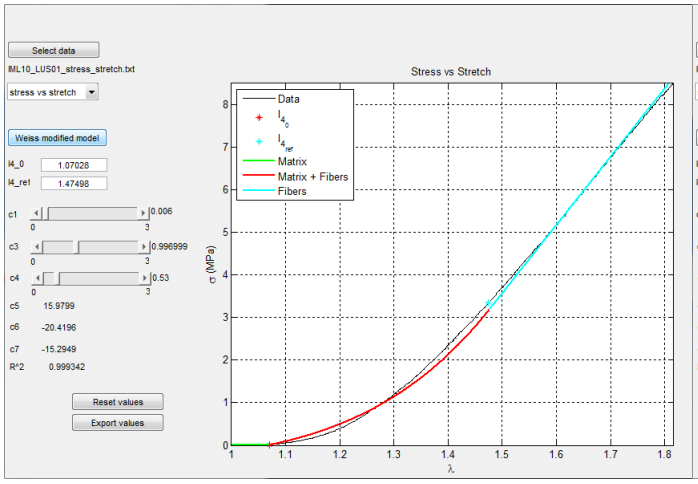

(k) IML10-1

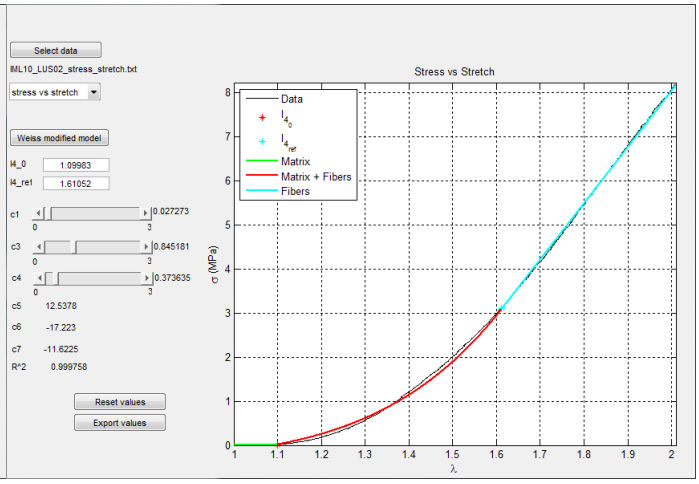

(l) IML10-2

Figure B.7: Uterosacral ligament samples' parameters computed with manual process (2 of 3).

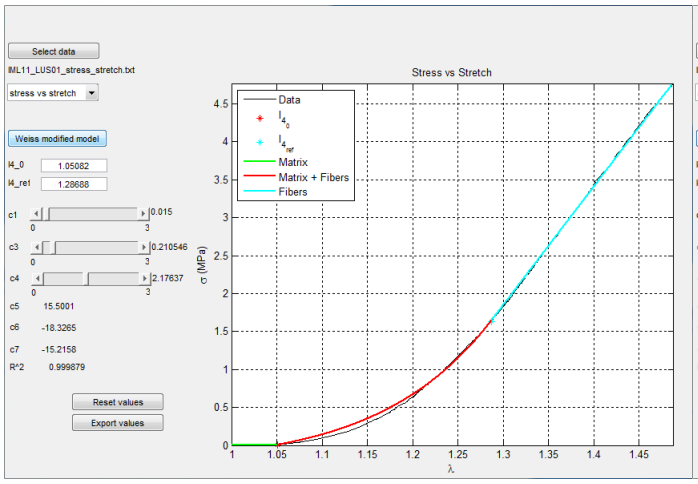

(m) IML11

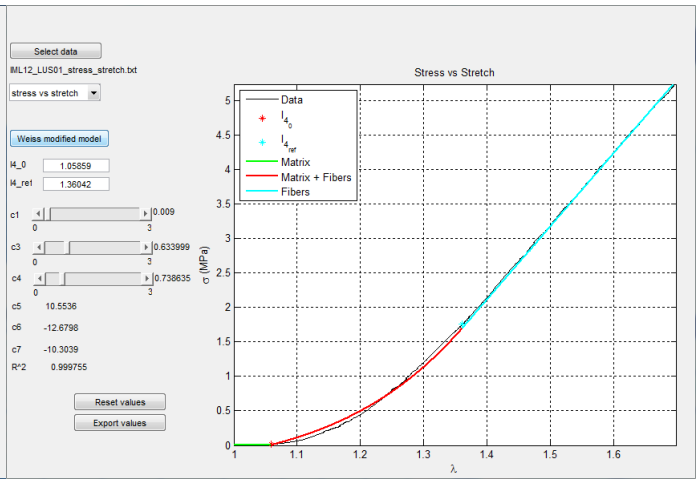

(n) IML12

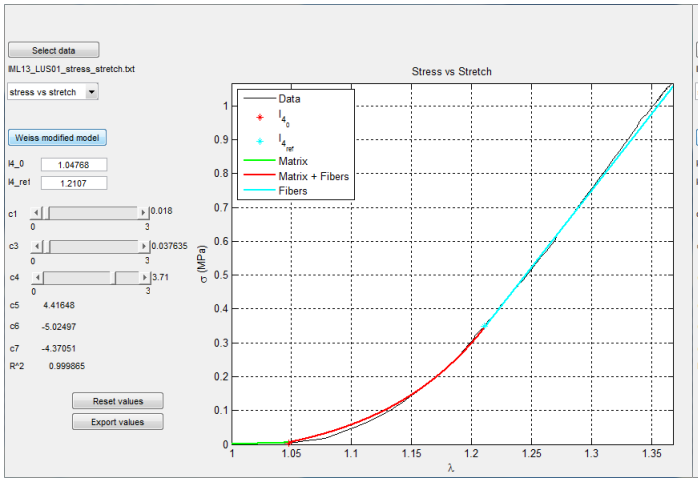

(o) IML13

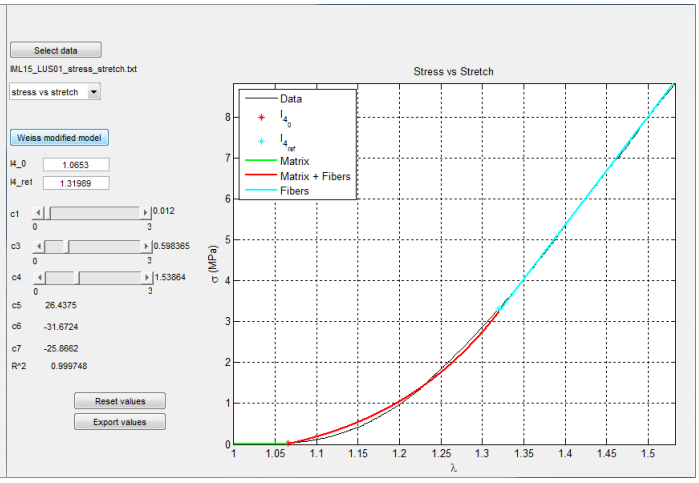

(p) IML15

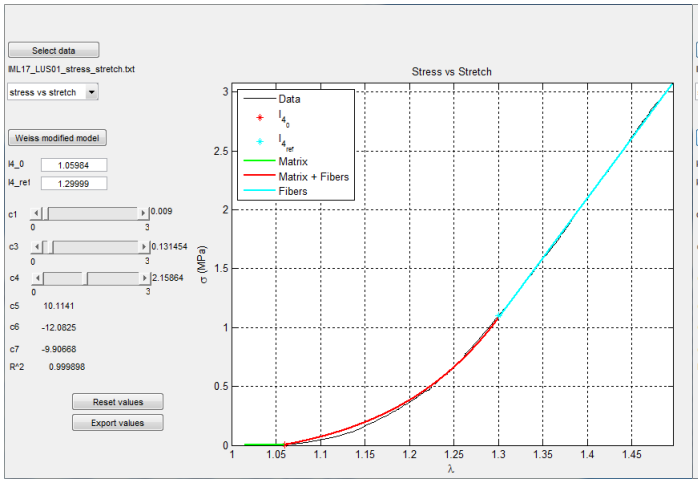

(q) IML17-1

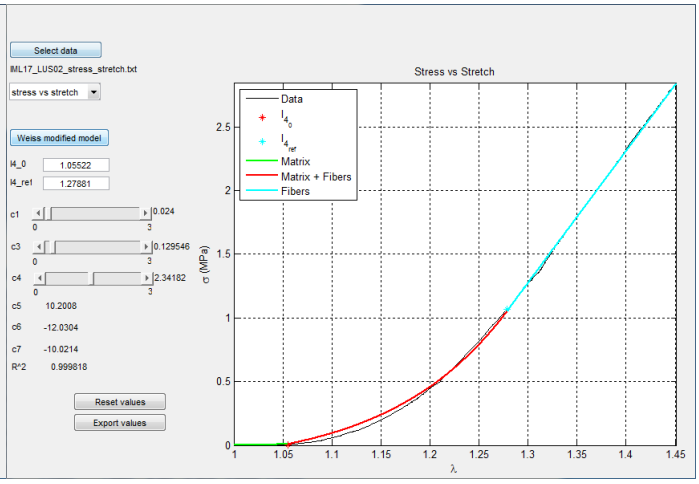

(r) IML17-2

Figure B.7: Uterosacral ligament samples' parameters computed with manual process (3 of 3).

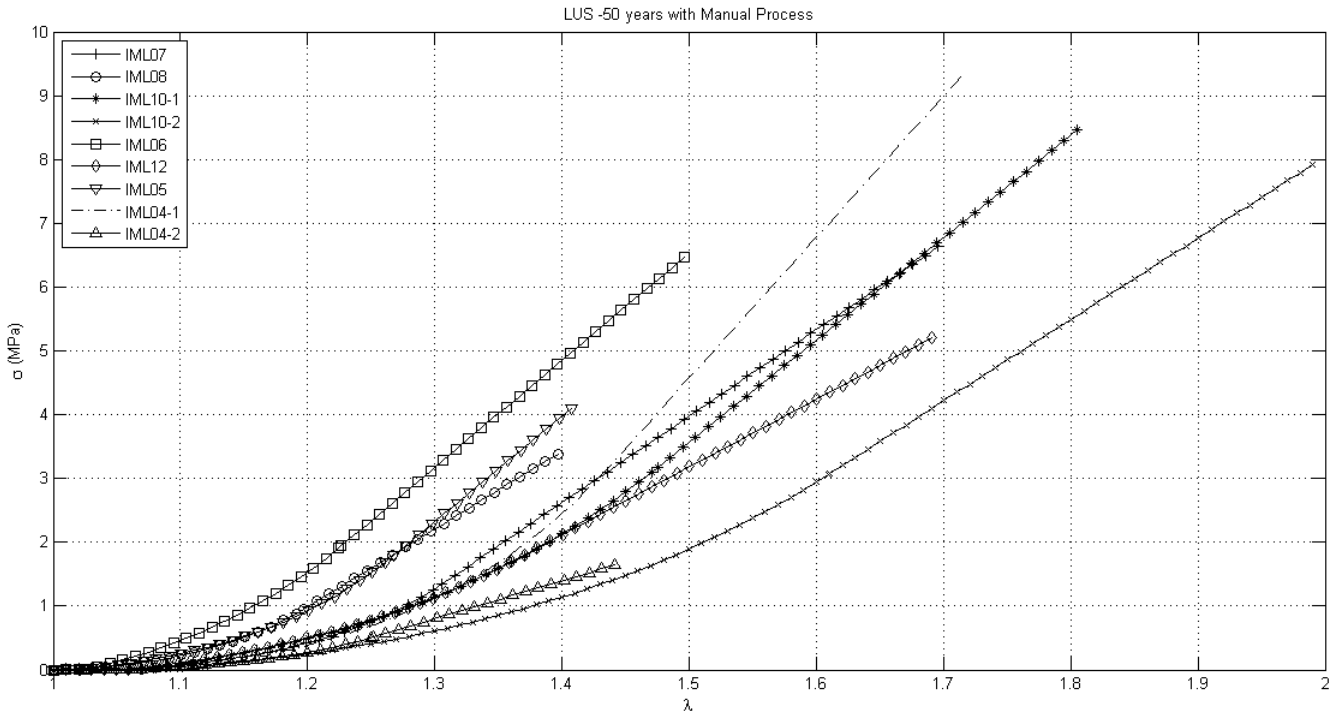

(a) Less than 50 years

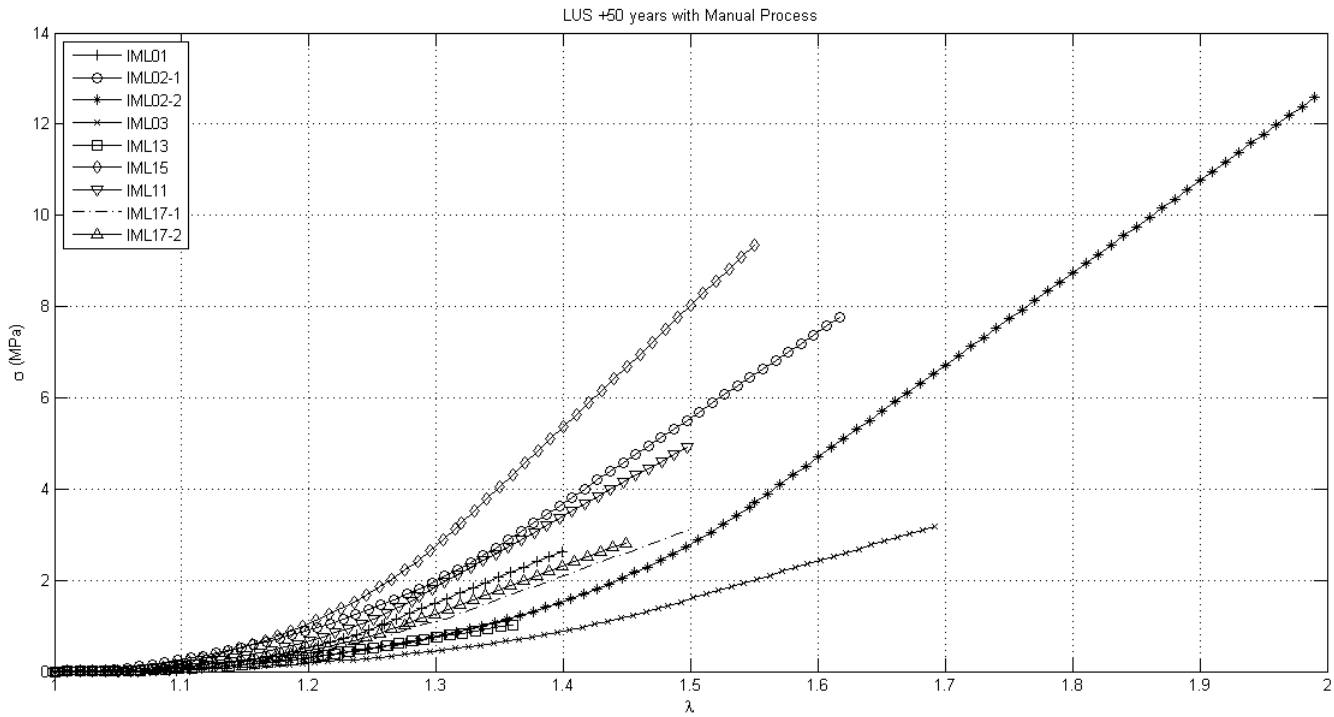

(b) Greater than or equal to 50 years

Figure B.8: Uterosacral ligament samples' analytical curves obtained with manual process.

Appendix C

Age-related Changes of Material Parameters

C.1 Optimization process

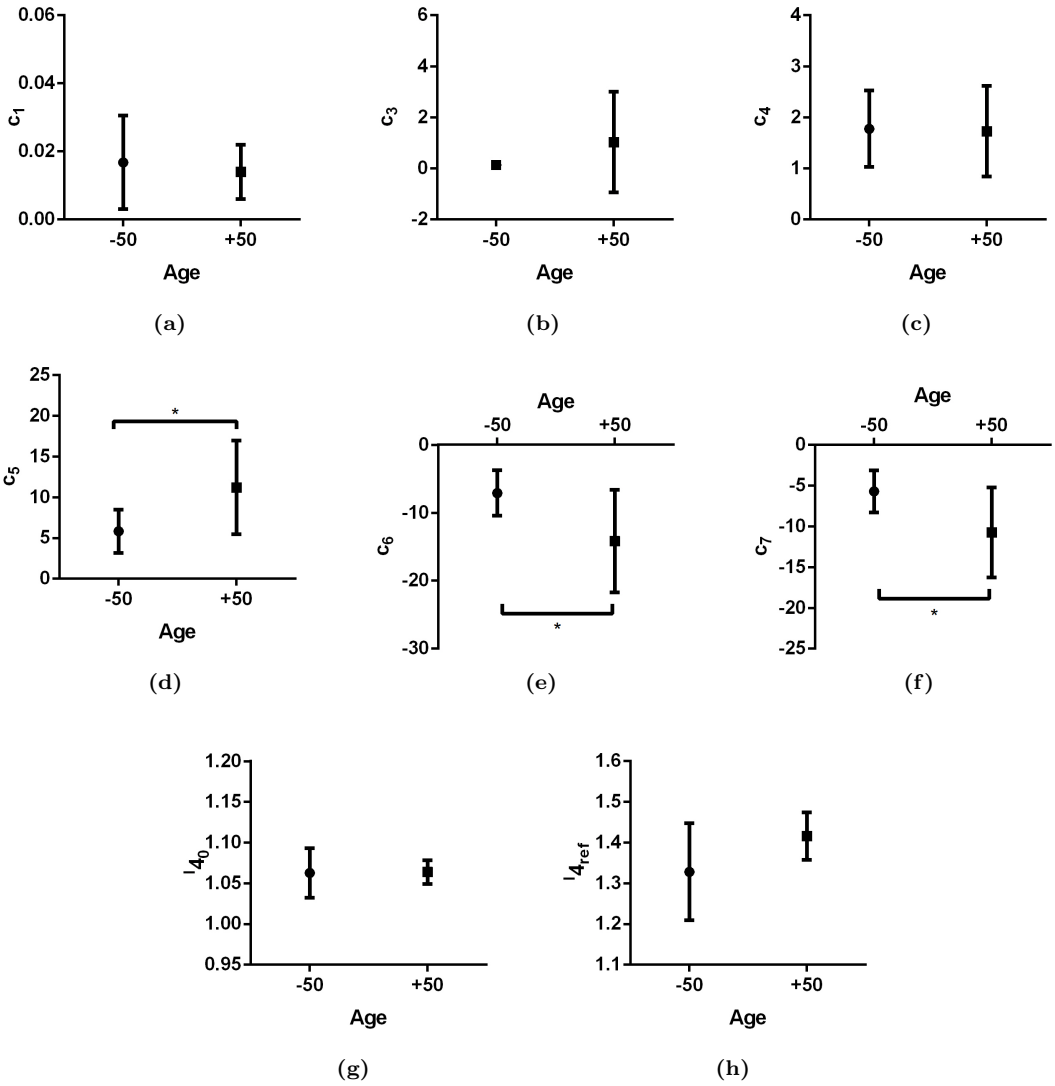

Figure C.1: Material parameters obtained with optimization process for the round ligament samples ((a) c_1, (b) c_3, (c) c_4, (d) c_5 (e) c_6 and (f) c_7) and respective division points of the deformation graphic ((g)I_{4_0} and (h)$I_{4_{ref}}$ stretch values), as a function of age. Statistical analysis was performed using Student's unpaired-samples t-test (p<0.05). (*) implies significant differences. Material constants are in MPa.

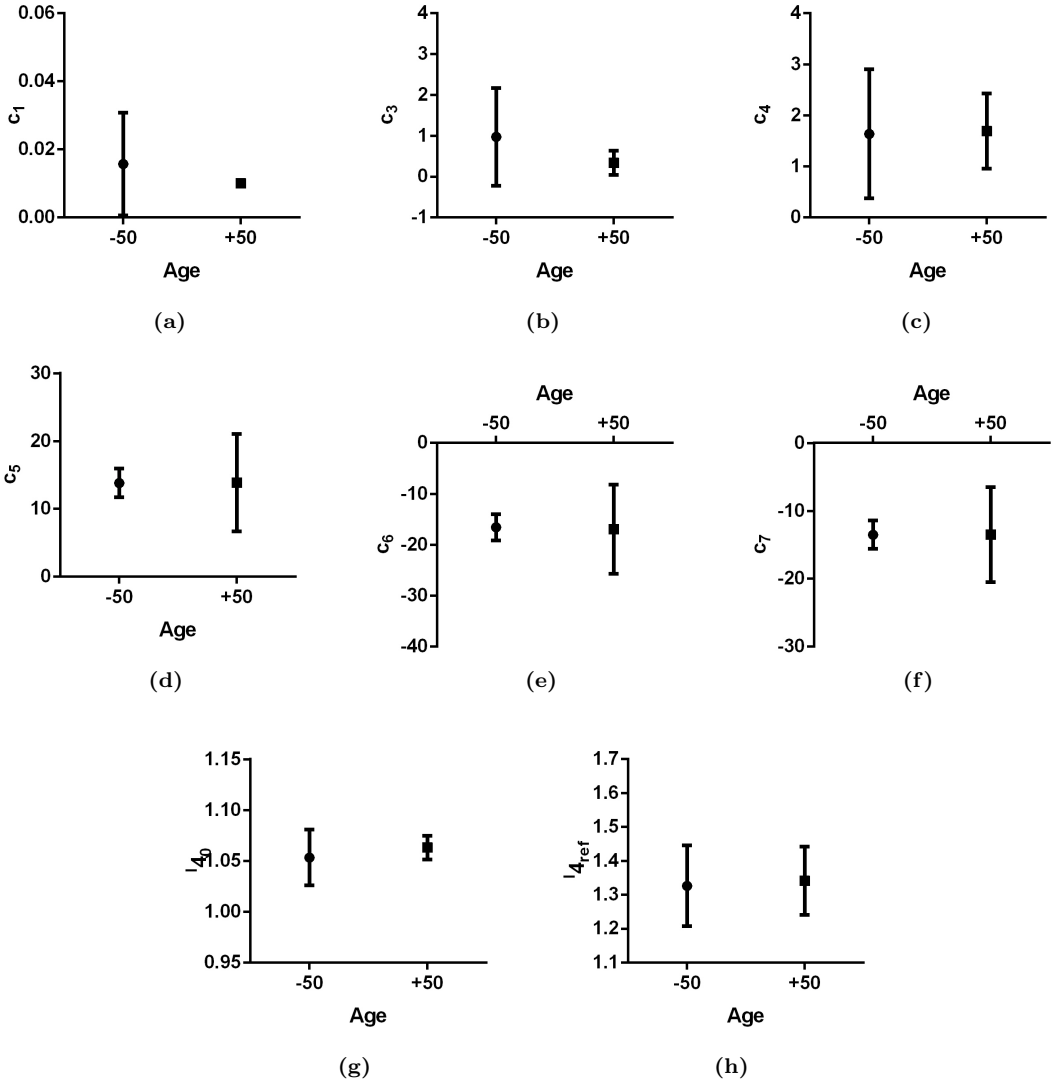

Figure C.2: Material parameters obtained with optimization process for the uterosacral ligament samples ((a) c_1, (b) c_3, (c) c_4, (d) c_5 (e) c_6 and (f) c_7) and respective division points of the deformation graphic ((g)I_{4_0} and (h)$I_{4_{ref}}$ stretch values), as a function of age. Statistical analysis was performed using Student's unpaired-samples t-test (p<0.05). (*) implies significant differences. Material constants are in MPa.

C.2 Manual process

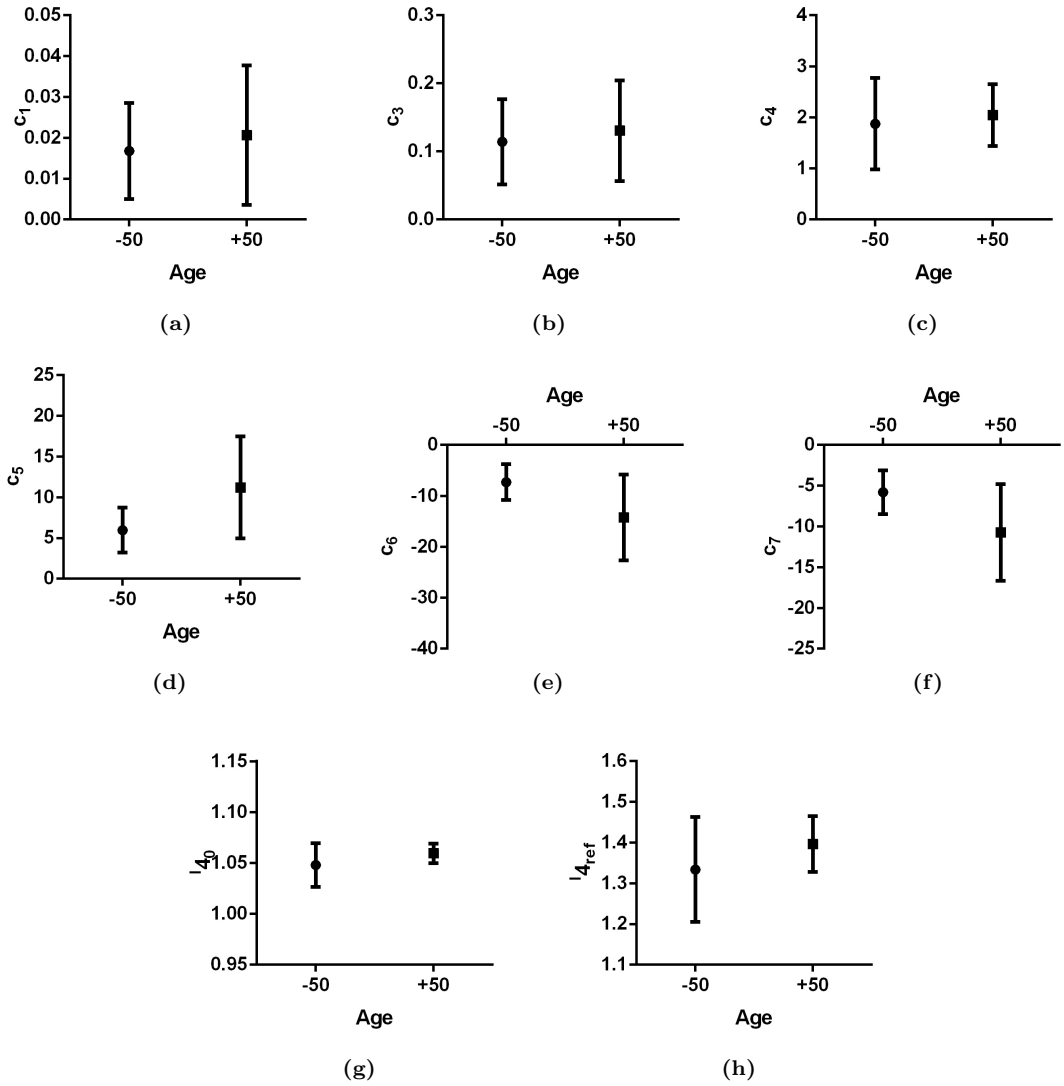

Figure C.3: Material parameters obtained with manual process for the round ligament samples ((a) c_1, (b) c_3, (c) c_4, (d) c_5 (e) c_6 and (f) c_7) and respective division points of the deformation graphic ((g)I_{4_0} and (h)$I_{4_{ref}}$ stretch values), as a function of age. Statistical analysis was performed using Student's unpaired-samples t-test (p<0.05). (*) implies significant differences. Material constants are in MPa.

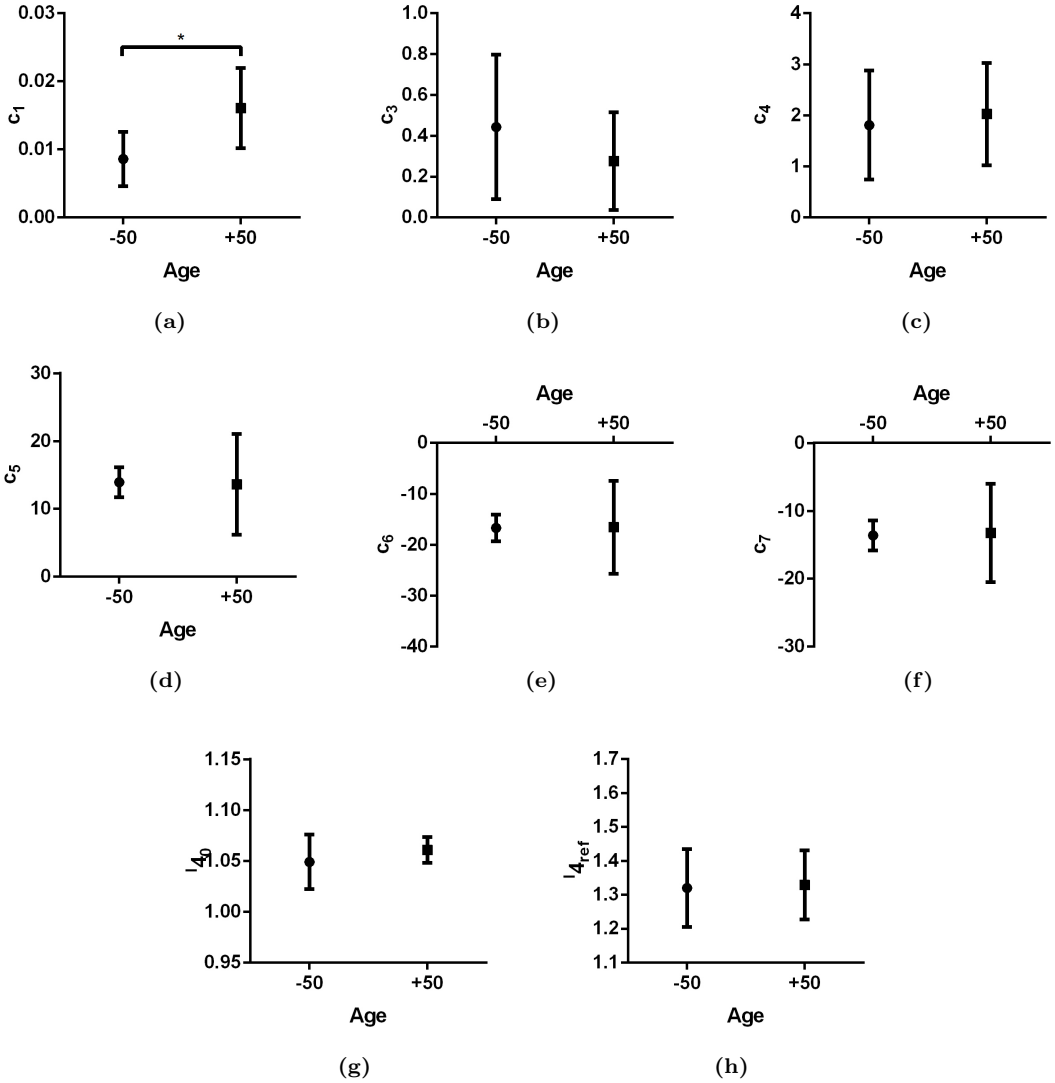

Figure C.4: Material parameters obtained with manual process for the uterosacral ligament samples ((a) c_1, (b) c_3, (c) c_4, (d) c_5 (e) c_6 and (f) c_7) and respective division points of the deformation graphic ((g)I_{4_0} and (h)$I_{4_{ref}}$ stretch values), as a function of age. Statistical analysis was performed using Student's unpaired-samples t-test (p<0.05). (*) implies significant differences. Material constants are in MPa.

Appendix D

Process Comparison

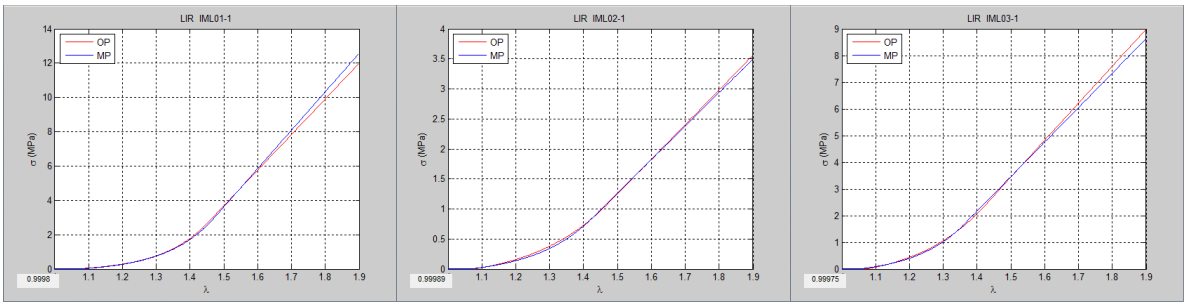

(a) IML01

(b) IML02

(c) IML03

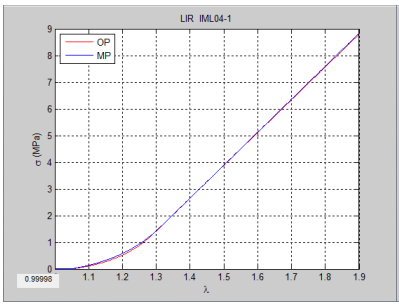

(d) IML04-1

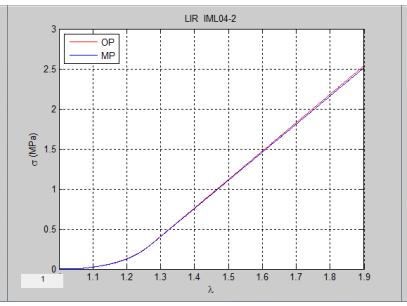

(e) IML04-2

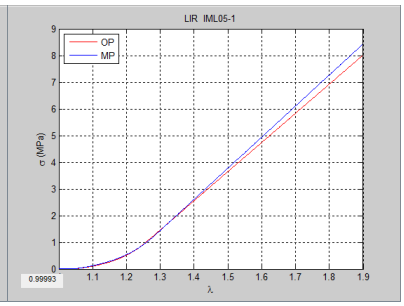

(f) IML05-1

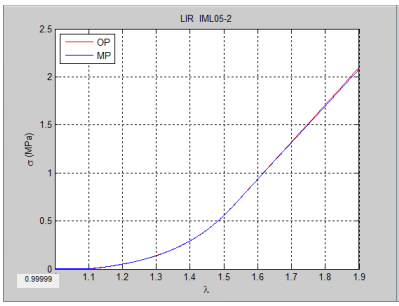

(g) IML05-2

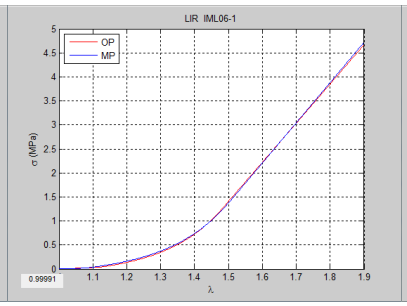

(h) IML06

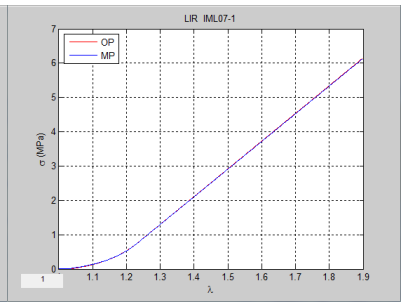

(i) IML07

Figure D.1: Plot of the analytical stress-stretch curve, obtained with both optimization and manual processes, for each of the round ligament samples, and the respective correlation coefficient (1 of 2).

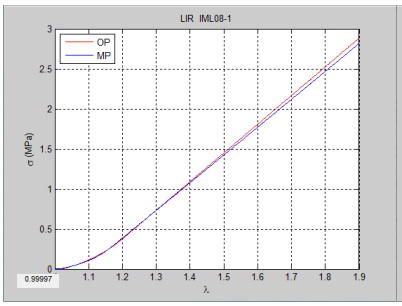

(j) IML08

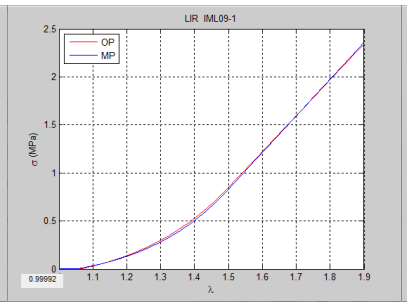

(k) IML09

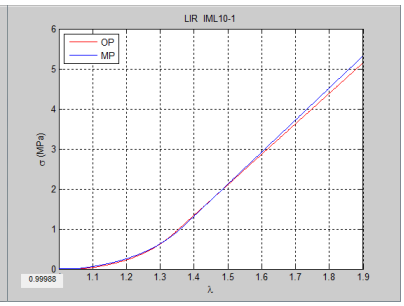

(l) IML10

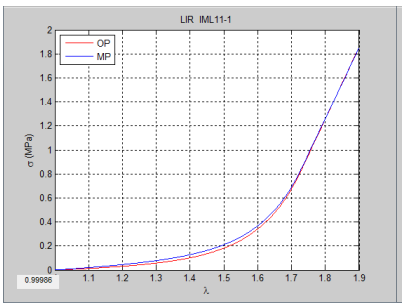

(m) IML11-1

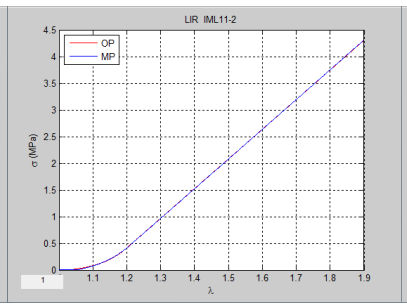

(n) IML11-2

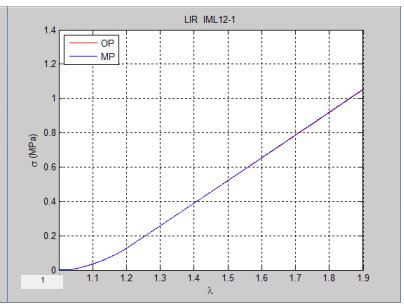

(o) IML12

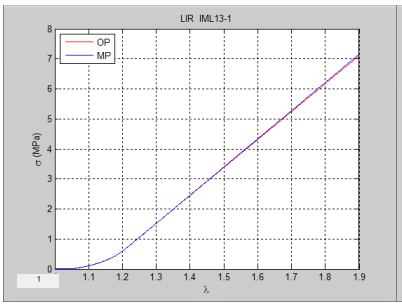

(p) IML13-1

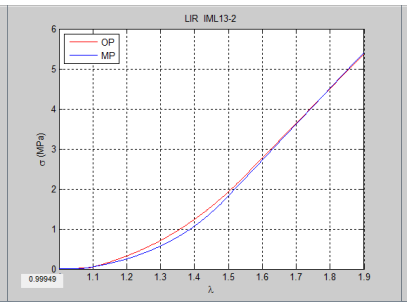

(q) IML13-2

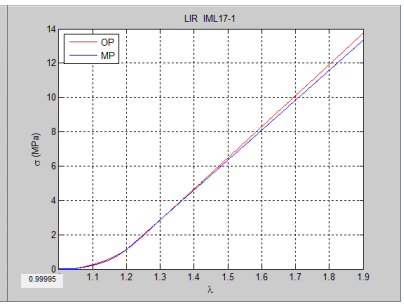

(r) IML17-1

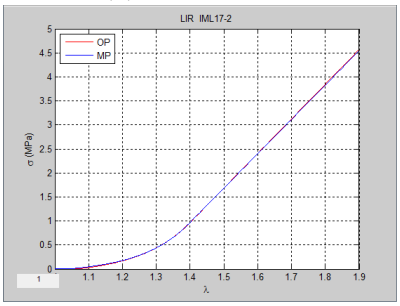

(s) IML17-2

Figure D.1: Plot of the analytical stress-stretch curve, obtained with both optimization and manual processes, for each of the round ligament samples, and the respective correlation coefficient (2 of 2).

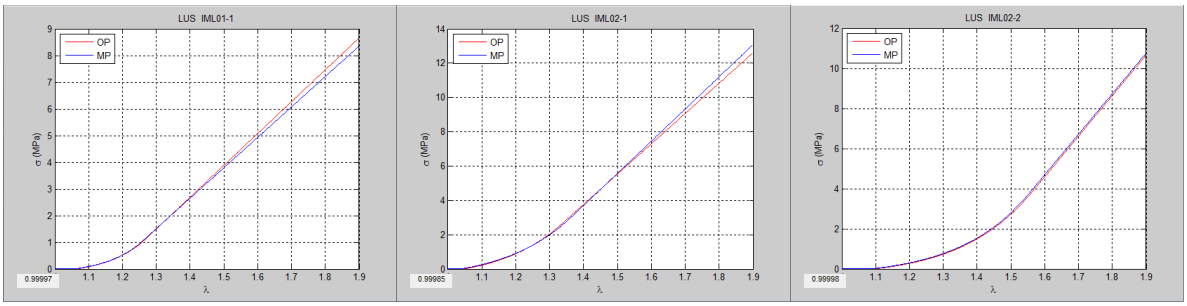

(a) IML01

(b) IML02-1

(c) IML02-2

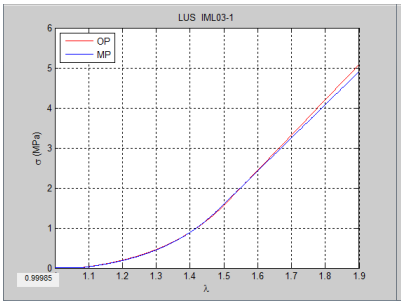

(d) IML03

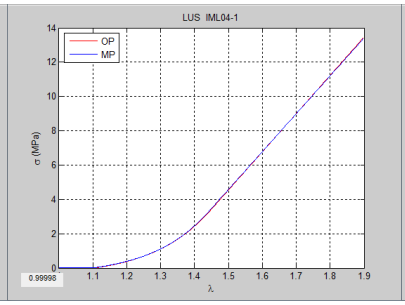

(e) IML04-1

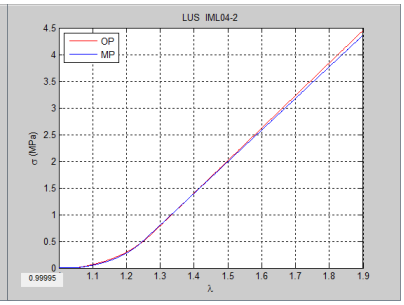

(f) IML04-2

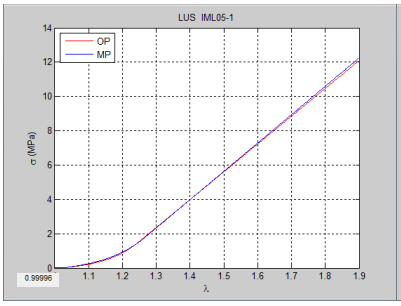

(g) IML05

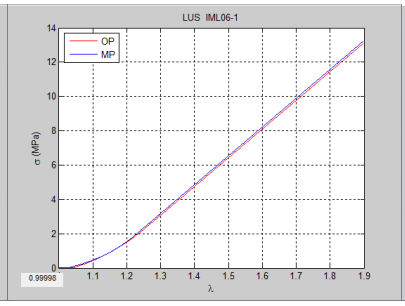

(h) IML06

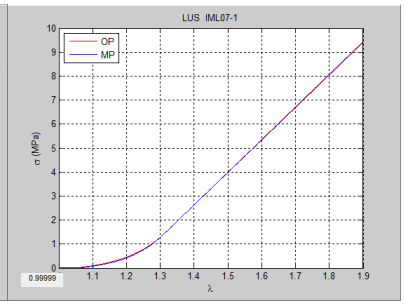

(i) IML07

Figure D.2: Plot of the analytical stress-stretch curve, obtained with both optimization and manual processes, for each of the uterosacral ligament samples, and the respective correlation coefficient (1 of 2).

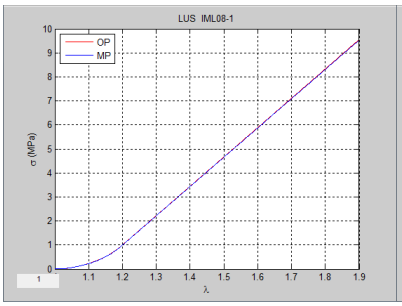

(j) IML08

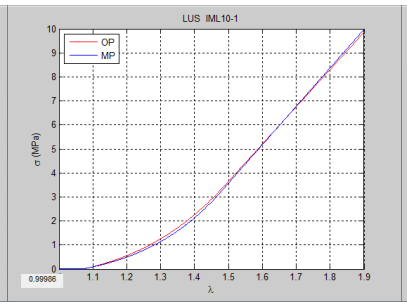

(k) IML10-1

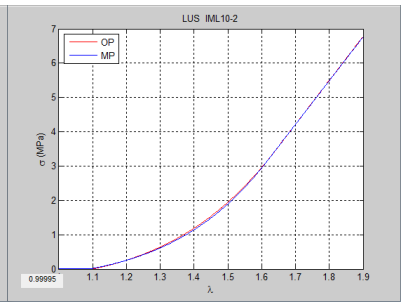

(l) IML10-2

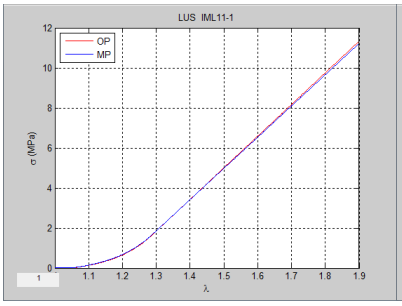

(m) IML11

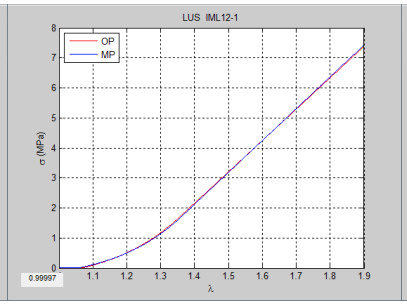

(n) IML12

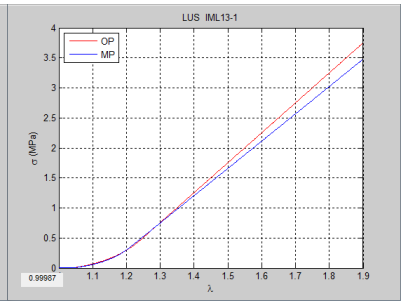

(o) IML13

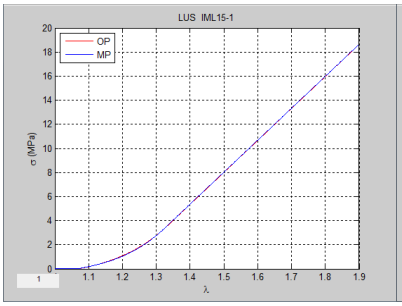

(p) IML15

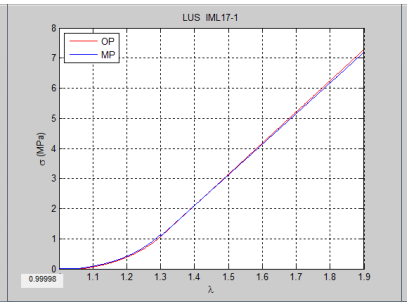

(q) IML17-1

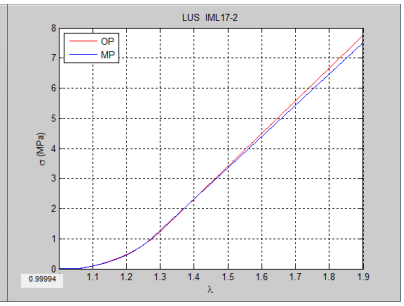

(r) IML17-2

Figure D.2: Plot of the analytical stress-stretch curve, obtained with both optimization and manual processes, for each of the uterosacral ligament samples, and the respective correlation coefficient (2 of 2).

Bibliography

S. D. Abramowitch, A. Feola, Z. Jallah, and P. A. Moalli. Tissue mechanics, animal models, and pelvic organ prolapse: A review. *European Journal of Obstetrics & Gynecology and Reproductive Biology*, 144:S146–S158, May 2009.

J. S. Afonso, P. A. L. S. Martins, M. J. B. C. Girao, R. M. N. Jorge, A. J. M. Ferreira, T. Mascarenhas, A. A. Fernandes, J. Bernardes, E. C. Baracat, G. R. de Lima, and B. Patricio. Mechanical properties of polypropylene mesh used in pelvic floor repair. *International Urogynecology Journal*, (19):375–880, Sept. 2007.

J. A. Ashton-Miller and J. O. L. DeLancey. Functional anatomy of the female pelvic floor. *Annals of the New York Academy Sciences*, 1101, Reproductive Biomechanics:266–296, Apr. 2007.

M. D. Barber. Contemporary views on female pelvic anatomy. *Cleveland Clinic journal of medicine*, 42(4):1–9, Dec. 2005.

E. M. Barros, C. J. Rodrigues, N. R. Rodrigues, R. P. Oliveira, T. E. Barros, and A. J. Rodrigues. Aging of the elastic and collagen fibers in the human cervical interspinous ligaments. *The Spine Journal*, 2(1):57–62, Jan. 2002.

J. R. Berman, S. P. Adhikari, and I. Goldstein. Anatomy and Physiology of Female Sexual Function and Dysfunction. *European Urology*, 38(1):20–29, Jan. 2000.

R. C. Bump and P. A. Norton. EPIDEMIOLOGY AND NATURAL HISTORY OF PELVIC FLOOR DYSFUNCTION. *Obstetrics and Gynecology Clinics of North America*, 25(4):723–746, Dec. 1998.

B. Calvo, E. Peña, P. Martins, T. Mascarenhas, M. Doblaré, R. M. N. Jorge, and A. Ferreira. On modelling damage process in vaginal tissue. *Journal of Biomechanics*, 42(5):642–651, Mar. 2009.

A. Cerami, H. Vlassara, and M. Brownlee. *Glucose and aging*. Jan. 1987.

B. Chen and J. Yeh. Alterations in Connective Tissue Metabolism in Stress Incontinence and Prolapse. *The Journal of Urology*, 186(5):1768–1772, Nov. 2011.

G.-D. Chen. Pelvic Floor Dysfunction in Aging Women. *Taiwanese Journal of Obstetrics and Gynecology*, 46(4):374–378, Dec. 2007.

S. C. Cowin and S. B. Doty. *Tissue Mechanics*. Springer Science & Business Media, Jan. 2007.

M. P. de Araujo, C. C. Takano, M. J. B. C. Girão, and M. G. F. Sartori. Pelvic floor disorders among indigenous women living in Xingu Indian Park, Brazil. *International Urogynecology Journal*, Jan. 2009.

R. Drake, A. Vogl, and A. Mitchell. *Gray's anatomy for students.* Jan. 2009.

R. Droual. Appendicular Skeleton. *Chapter 5 - Bone Development, Growth and Structure.*

M. Emily. Chapter 5 - Adaptations to Anaerobic Training Programs. *Kinesiology, University of New Hampshire*, 2009.

A. Freed and T. Doehring. Elastic model for crimped collagen fibrils. *Journal of Biomechanical Engineering*, 127(4), Feb. 2005.

Y. Fung. Mechanical properties of living tissues. *Biomechanics*, Jan. 1993.

B. Gabriel, D. Denschlag, H. Göbel, C. Fittkow, M. Werner, G. Gitsch, and D. Watermann. Uterosacral ligament in postmenopausal women with or without pelvic organ prolapse. *International Urogynecology Journal*, 16(6):475–479, Dec. 2005.

C. Goepel. Differential elastin and tenascin immunolabeling in the uterosacral ligaments in postmenopausal women with and without pelvic organ prolapse. *Acta Histochemica*, 110(3):204–209, May 2008.

J. Hall. *Guyton and Hall Textbook of Medical Physiology.* Jan. 2010.

S. Herschorn. Female Pelvic Floor Anatomy: The Pelvic Floor, Supporting Structures, and Pelvic Organs. *Reviews in Urology*, 6(Suppl 5):S2–S10, Jan. 2004.

G. Holzapfel. Nonlinear solid mechanics: a continuum approach for engineering science. *Meccanica*, Jan. 2002.

J. Humphrey. *Cardiovascular solid mechanics: cells, tissues, and organs.* Jan. 2002.

T. Iida, K. Abumi, Y. Kotani, and K. Kaneda. Effects of aging and spinal degeneration on mechanical properties of lumbar supraspinous and interspinous ligaments. *The Spine Journal*, 2(2):95–100, Mar. 2002.

P. Kannus, M. Paavola, and L. Józsa. Aging and degeneration of tendons. *Tendon Injuries*, pages 1–7, Jan. 2005.

M. Kerkhof, L. Hendriks, and H. Brölmann. Changes in connective tissue in patients with pelvic organ prolapse—a review of the current literature. *International Urogynecology*, pages 1–14, Jan. 2009.

A. Kökçü, F. Yanik, M. Çetinkaya, T. Alper, B. Kandemir, and E. Malatyalioglu. Histopathological evaluation of the connective tissue of the vaginal fascia and the uterine ligaments in women with and without pelvic relaxation. *Archives of Gynecology and Obstetrics*, 266(2):75–78, Apr. 2002.

W. Lai, D. Rubin, D. Rubin, and E. Krempl. *Introduction to continuum mechanics.* Jan. 2009.

A. Liapis, P. Bakas, A. Pafiti, M. Frangos-Plemenos, N. Arnoyannaki, and G. Creatsas. Changes of collagen type III in female patients with genuine stress incontinence and pelvic floor prolapse. *European Journal of Obstetrics & Gynecology and Reproductive Biology*, 97(1):76–79, July 2001.

L.-K. Liu, W.-J. Lee, C.-L. Liu, L.-Y. Chen, M.-H. Lin, L.-N. Peng, and L.-K. Chen. Age-related skeletal muscle mass loss and physical performance in Taiwan: Implications to diagnostic strategy of sarcopenia in Asia. *Geriatrics & gerontology international*, 13(4):964–71, Oct. 2013.

X. Liu, Y. Zhao, B. Pawlyk, M. Damaser, and T. Li. Failure of Elastic Fiber Homeostasis Leads to Pelvic Floor Disorders. *The American Journal of Pathology*, 168(2):519–528, Feb. 2006.

A. H. MacLennan, A. W. Taylor, D. H. Wilson, and D. Wilson. The prevalence of pelvic floor disorders and their relationship to gender, age, parity and mode of delivery. *BJOG: An International Journal of Obstetrics and Gynaecology*, 107(12):1460–1470, Dec. 2000.

P. Mannella, G. Palla, M. Bellini, and T. Simoncini. The female pelvic floor through midlife and aging. *Maturitas*, Sept. 2013.

P. Martins. Conceitos de Hiperelasticidade e modelos hiperelásticos. *Curso Teórico-Prático de introdução à mecânica não linear dostecidos moles biológicos*, May 2013a.

P. Martins. Caracterização experimental de tecidos moles biológicos e biomateriais. *Curso Teórico-Prático de introdução à mecânica não linear dostecidos moles biológicos*, May 2013b.

P. Martins, E. Pena, E. Peña, B. Calvo, M. Doblaré, T. Mascarenhas, R. N. Jorge, and A. Ferreira. Prediction of nonlinear elastic behaviour of vaginal tissue: experimental results and model formulation. *Computer Methods in Biomechanics and Biomedical Engineering*, 13(3):327–337, June 2010.

P. Martins, A. L. Silva-Lopes, A. M. Fonseca, A. Santos, L. Santos, T. Mascarenhas, R. M. Jorge, and A. M. Ferreira. Strength of round and uterosacral ligaments: a biomechanical study. *Archives of Gynecology and Obstetrics*, pages 1–6, Feb. 2013.

P. A. L. S. Martins, R. M. N. Jorge, and A. J. M. Ferreira. Determination of material parameters for different hyperelastic models. *VIII International Conference on Computational Plasticity*, pages 1–4, Jan. 2005.

P. A. L. S. Martins, R. M. N. Jorge, and A. J. M. Ferreira. A Comparative Study of Several Material Models for Prediction of Hyperelastic Properties: Application to Silicone-Rubber and Soft Tissues. *Strain*, 42(3):135–147, Aug. 2006.

M. Mooney. A theory of large elastic deformation. *Journal of applied physics*, Jan. 1940.

S. Münster, L. M. Jawerth, B. A. Leslie, J. I. Weitz, B. Fabry, and D. A. Weitz. Strain history dependence of the nonlinear stress response of fibrin and collagen networks. In *Proceedings of the National Academy of Sciences*, pages 12197–12202. National Acad Sciences, July 2013.

A. Natali, P. Pavan, E. Carniel, P. Dario, and I. Izzo. Characterization of soft tissue mechanics with aging. *IEEE Engineering in Medicine and Biology Magazine*, 27(4):15–22, July 2008.

I. Nygaard, M. D. Barber, K. L. Burgio, K. Kenton, S. Meikle, J. Schaffer, C. Spino, W. E. Whitehead, J. Wu, D. J. Brody, and f. t. P. F. D. Network. Prevalence of Symptomatic Pelvic Floor Disorders in US Women. *JAMA*, 300(11):1311, Sept. 2008.

R. W. Ogden and P. Chadwick. On the deformation of solid and tubular cylinders of incompressible isotropic elastic material. *Journal of the Mechanics and Physics of Solids*, 20(2):77–90, May 1972.

A. Orlandi and A. Ferlosio. Pelvic Floor Anatomy. *Pelvic Floor Disorders: Surgical Approach*, pages 19–25, Jan. 2014.

P. Petros. *The female pelvic floor: function, dysfunction, and management according to the integral theory.* Jan. 2010.

P. P. Provenzano, R. V, R. Vanderby, and erby. Collagen fibril morphology and organization: Implications for force transmission in ligament and tendon. *Matrix Biology*, 25(2):71–84, Mar. 2006.

V. Raizada and R. K. Mittal. Pelvic Floor Anatomy and Applied Physiology. *Gastroenterology Clinics of North America*, 37(3):493–509, Sept. 2008.

G. Rivaux, C. Rubod, B. Dedet, M. Brieu, and B. Gabriel. Comparative analysis of pelvic ligaments: a biomechanics study. *International Urogynecology Journal*, 24(1):135–139, Jan. 2013.

R. S. Rivlin. Large Elastic Deformations of Isotropic Materials. IV. Further Developments of the General Theory. *Philosophical Transactions of the Royal Society A: Mathematical, Physical and Engineering Sciences*, 241(835):379–397, Oct. 1948.

T. Y. Rosenbaum. REVIEWS: Pelvic Floor Involvement in Male and Female Sexual Dysfunction and the Role of Pelvic Floor Rehabilitation in Treatment: A Literature Review. *The Journal of Sexual Medicine*, 4(1):4–13, Jan. 2007.

G. Santoro, A. Wieczorek, and C. Bartram. *Pelvic Floor Disorders: From Imaging to Clinical Management*. Jan. 2010.

D. Scheiner, C. Betschart, and D. Perucchini. Aging-related changes of the female pelvic floor. *Therapeutische Umschau. Revue thérapeutique*, 67(1):23–6, Jan. 2010.

S. Standring. Gray's anatomy, 40th Edition. *The Anatomical basis of clinical practice*, Jan. 2008.

J. Stoker. Anorectal and pelvic floor anatomy. *Best Practice & Research Clinical Gastroenterology*, 23(4):463–475, Jan. 2009.

K. Strohbehn. Normal Pelvic Floor Anatomy. *Obstetrics and Gynecology Clinics of North America*, 25(4):683–705, Dec. 1998.

A. Tinelli, A. Malvasi, S. Rahimi, R. Negro, D. Vergara, R. Martignago, M. Pellegrino, and C. Cavallotti. Age-related pelvic floor modifications and prolapse risk factors in postmenopausal women. *Menopause*, 17(1):204–212, Jan. 2010.

D. R. Veronda and R. A. Westmann. Mechanical characterization of skin—Finite deformations. *Journal of Biomechanics*, 3(1):111–124, Jan. 1970.

J. A. Weiss, B. N. Maker, and S. Govindjee. Finite element implementation of incompressible, transversely isotropic hyperelasticity. *Computer Methods in Applied Mechanics and Engineering*, 135(1-2):107–128, Aug. 1996.

J. A. Weiss, J. C. Gardiner, B. J. Ellis, T. J. Lujan, and N. S. Phatak. Three-dimensional finite element modeling of ligaments: Technical aspects. *Medical Engineering & Physics*, 27(10):845–861, Dec. 2005.

C. Wester and L. Brubaker. Normal Pelvic Floor Physiology. *Obstetrics and Gynecology Clinics of North America*, 25(4):707–722, Dec. 1998.

S. Woo, M. Aprelena, and J. Hoher. Tissue mechanics of ligaments and tendons. *Biomechanics and ergonomics*, Jan. 1999.

C. A. Woodfield, S. Krishnamoorthy, B. S. Hampton, and J. M. Brody. Imaging Pelvic Floor Disorders: Trend Toward Comprehensive MRI. *American Journal of Roentgenology*, 194, June 2010.

O. H. Yeoh. On the Ogden Strain-Energy Function. *Rubber Chemistry and Technology*, 70(2): 175–182, May 1997.